University of Pardubice

Faculty of Transport Engineering

Use of Ground Penetrating Radar in Condition

Assessment of Railway Ballast

Doctoral Dissertation

2018   Ing. Salih Serkan ARTAGAN

Doctorand:

Ing. Salih Serkan Artagan

Programme of study:

P3710   Technique and Technology in Transport and Communications

Branch of study:

3706V005   Transport Means and Infrastructure

Dissertation Title:

Use of Ground Penetrating Radar in Condition Assessment of Railway Ballast

Supervisor:

 Doc. Ing. Vladimír Doležel, CSc.

Specialist supervisor:

 Ing. Vladislav Borecký, Ph.D.

Dissertation has arisen at the supervising:

Department of Transport Structures

I hereby confirm that:

I have written this dissertation thesis independently. All the reference literature and information used in this work are quoted in the list of reference literature.

I hereby acknowledge that all the rights and duties resulting from Act No. 121/2000 Coll., the Copyright Act, apply to my written work, especially that the University of Pardubice has the right to make a license agreement of use of this written work as a school work pursuant to § 60 section 1 of the Copyright Act. On the condition that the written work shall be used by me or a license shall be provided to another subject for the use hereof, the University of Pardubice shall have the right to require from me a relevant contribution to reimburse the costs incurred for the making of such work including all relevant costs and total overall expenditure and expenses incurred.

I agree with making the work accessible in the University Library.

Dated in Pardubice on 06. 04. 2018

Salih Serkan ARTAGAN

To my daughter,
To my wife,
To my parents,
To my grandmother

ACKNOWLEDGEMENTS

ABSTRACT

Railways are considered as a cost-effective, reliable and safe form of transport. Ensuring the timely maintenance of this transport mode is the prioritized task of the railway operators. Railway ballast is the governing element of track infrastructure, which plays an immense role in the overall track stability. Therefore, assessing the condition of ballast reveals very significant information about the overall track condition. Detecting the level of a phenomenon called ballast fouling, i.e. contamination of ballast within the ballast structure provides beneficial information about the status of the ballast. Ballast fouling occurs when air voids in the ballast are filled with finer materials. It is of crucial importance to diagnose the level and the type of fouling which may jeopardize the all-around safety of the track and its economic life. Another significant threat to track stability is the trapped water within track infrastructure which is mostly due to ballast fouling. Ground Penetrating Radar (GPR), is a powerful non-destructive geophysical diagnosis method providing cost-efficient, time-saving and continuous railway ballast surveys. To that effect, this dissertation addresses evaluation of railway ballast condition by using GPR. Performance compliance tests for the available GPR set have been performed to evaluate the performance of available GPR equipment. Numerous laboratory measurements have been undertaken to analyze ballast fouling condition with two different granite ballast types and three different fouling materials with 2 GHz air-coupled antenna. Strong linear trends have been found between ballast fouling percentage and Relative Dielectric Permittivity (RDP) values with a coefficient of determination greater than 0.9. Moisture content influence on GPR signal was also assessed through laboratory measurements. Relationships between water content and RDP values were determined. Conducted field surveys validated the laboratory measurements where ground truth data and GPR data using the laboratory results were in good agreement. Field survey results were analyzed in terms of antenna types, antenna frequencies ranging from 400MHz to 2GHz, antenna orientation, and type of sleepers under survey. Characteristics of EM signal reflected from limestone railway ballast has been achieved as a function of ballast fouling condition by silty sand, antenna types, antenna frequencies ranging from 1GHz to 2GHz, antenna orientation and presence of sleeper(s)

and rails under controlled laboratory conditions. RDP values of clean and fouled ballast were determined. Overall, all the laboratory and field measurements proved the effectiveness and eligibility of GPR method to diagnose the condition of ballast in terms of fouling level and type, moisture content, and to identify the layering of clean and fouled ballast, hence improving the evaluation and monitoring efficiency of railway infrastructure site investigations. Moreover, sleeper influence on GPR reflected signal was assessed. Optimum type, frequency, and orientation of GPR antennas on GPR railway ballast surveys were determined.

Keywords: Railway Ballast, Ground Penetrating Radar, Ballast Fouling, Relative Dielectric Permittivity, Moisture Content, Railway Sleeper, GPR Antenna Orientation.

ABSTRAKT

Železnice jsou považovány za finančně efektivní, spolehlivý a bezpečný způsob dopravy. Zajištění včasné údržby železniční infrastruktury je prvořadým úkolem správců železniční infrastruktury. Železniční štěrk je důležitým prvkem infrastruktury, který hraje důležitou roli v celkové stabilitě trati. Posouzení stavu štěrku tedy poskytuje velmi důležité informace o celkovém stavu trati. Fenomén nazývaný degradace štěrkového lože, tj. znečištění štěrku, má na stav železničního spodku velký vliv. Znečištění štěrkového lože nastává, když jsou mezery v kamenivu vyplněny jemnějšími materiály. Posouzení míry znečištění štěrkového lože má zásadní význam pro celkovou bezpečnost trati a pro její životnost. Dalším významným ohrožením stability železničního spodku je přítomnost vody, která je způsobena především právě znečištěním štěrkového lože. Georadar je účinná nedestruktivní geofyzikální diagnostická metoda poskytující finančně efektivní, časově úspornou a průběžnou diagnostiku železničního lože. Z tohoto důvodu se tedy práce zabývá hodnocením stavu štěrkového lože právě pomocí georadaru. Za účelem zjištění parametrů dostupné sestavy georadaru byly zpracovány testy výkonnosti georadarových systémů. Pro zjištění stupně znečištění štěrkového lože dvou typů základního kameniva třemi různými znečišťujícími materiály byla za pomoci 2GHz antény provedena četná laboratorní měření. Byla zjištěna vysoká závislost mezi znečištěním štěrku a hodnotami jeho relativní permitivity s koeficientem determinace větším než 0,9. Dalšími laboratorními měřeními byl také hodnocen vliv vlhkosti na vlastnosti odraženého signálu. Byl stanoven vztah mezi obsahem vody a hodnotami relativní permitivity. Hodnoty získané při měřeních in-situ se shodovaly s hodnotami získanými při laboratorních experimentech. Výsledky průzkumu v terénu byly analyzovány z hlediska typu antény, frekvence antény (rozmezí 400MHz až 2GHz), orientace antény a typu pražců. Na základě stupně znečištění železničního štěrku jemným pískem, typů antén, použitých frekvencí, orientací antén a vlivů pražců a kolejnic byly pozorovány vlivy na zaznamenaný signál. Byly určeny hodnoty relativní permitivity pro čistý a znečištěný železniční štěrk. Celkově se ve všech laboratorních a terénních měřeních prokázala spolehlivost a způsobilost georadaru pro diagnostiku stavu železničního štěrku z hlediska úrovně a typu znečištění, vlhkosti a tloušťky vrstev čistého i

znečištěného štěrku, a tedy i zvýšení efektivity při monitorování a hodnocení železniční infrastruktury. Navíc byl určen vliv pražců a vliv frekvence a orientace antén na odraz signálu při provádění diagnostiky železničních tratí georadarem.

Klíčová slova: železniční štěrk, georadar, degradace železničního lože, relativní permitivita, vlhkost, železniční pražec, orientace antény.

TABLE OF CONTENTS

LIST OF FIGURES

XVIII

XX

XXIII

LIST OF TABLES

XXV

NOMENCLATURE

List of Abbreviations in alphabetical order

ASTM	The American Society for testing and materials
BRRC	Belgian Road Research Center
CMP	Common mid-point
COST	Cooperation in science and technology
CRIM	Complex refractive index model
EM	Electromagnetic
FTS	Faculty of technical sciences
GPR	Ground penetrating radar
GSSI	Geophysical survey systems
HDPE	High-density polyethylene
IBC	International bulk container
IDS	Ingegneria Dei Sistemi S.p.A.
KHM	Known height method
LNEC	Laborario Nacional de Engenharia Civil
NMO	Normal Moveout
RDP	Relative dielectric permeability
SRM	Surface reflection method
STSM	Short-term scientific mission
SŽDC	Správa Železniční Dopravní Cesty
TCDD	Republic of Turkey General Directorate of State Railways Administration
TWT	Two-way travel time
TW	Time window

List of Symbols in order of appearance within the text

$F_{I\text{-}SW}$	Fouling index proposed by Selig and Waters [9]
$F_{I\text{-}I}$	Fouling index proposed by Ionescu [24]
$P_{0.075}$	Percentage of material passing the sieve size 0.075 mm
$P_{4.75}$	Percentage of material passing the sieve size 4.75 mm
P_{14}	Percentage of material passing the sieve size 14mm
v_r	Relative speed
c	Speed of light
ε_r	RDP
d	The depth of the object or stratigraphic layer of interest
L	Size of the square metal reflector
λ_c	The wavelength at the central frequency
f_c	Central frequency
A_{mp}	The amplitude of metal plate
A_n	The average peak-to-peak amplitude of the noise
$h_{1,2,3}$	The height of antenna from surface
SS	Signal stability
A_{max}	Maximum peak-to-peak amplitude of the metal plate reflection
A_{min}	Minimum peak-to-peak amplitude of the metal plate reflection
A_{avg}	Average peak-to-peak amplitude of the metal plate reflection
$T_{21,31}$	Absolute time difference
$\Delta t_{1,2,3}$	Time delay corresponding to $h_{1,2,3}$
$C_{21,\,31}$	Speed factor
M_q	Sliding-average amplitude
A_1	Peak-to-peak amplitude of the first trace

$M_{max, min}$	Maximum and minimum of M_q
ε_a	RDP value of ballast layer
A_s	Amplitude from the ballast surface
A_m	Amplitude from the metal plate
ε_T	RDP of the mixture
$\varepsilon_{A,i}$	RDP of component i
A_i	Volumetric percentage of component i
α	Geometric factor
w	The water content in percentage
m_w	Mass of wet sample and container
m_d	Mass of oven-dry sample and container
m_c	Mass of container

1 INTRODUCTION

Railways are regarded as the most environment-friendly, cost-effective type of transportation with its more reliable and better-organized nature compared to other modes of transports [1]. Moreover, higher capacity, suitability for bulky and heavy goods, high speed over long distances and relative safety compared to other transportation modes are the basic advantages of railway transportation at the first glance [1,2]. There is a growing body of literature that recognizes the significance of environment-friendly nature of railways when particularly, the global warming issues caused by the CO_2 emissions of the highway vehicles are considered. A striking statistic was reported in [3] which reveals that in 2014, the transport as a whole was liable for 23% of the total CO_2 emissions from fuel combustion, where road transport was responsible for 20%. Those reasons boosted the demand for freight and passenger travel on railways worldwide. Continuously and globally increasing freight tonnage, traffic speeds and frequency of trains continuously have led to raised wear and shorter economic life for all track components in superstructure and substructure [4].

Therefore, maintaining the economic, safe, comfortable and fast transportation conditions on railways is of crucial importance to the railway operator organizations. To accomplish this aim, timely diagnosis and maintenance of track structure with minimum traffic interruptions and slow orders should be addressed.

As can be seen in Figure 1.1 below, typical railway structure can be categorized into two main groups as infrastructure (substructure) and superstructure, where infrastructure is composed of ballast, sub-ballast and subgrade while superstructure comprises rails, sleepers (ties) and other fastening accessories [5].

The status of railway infrastructure has a substantial impact on track performance. Track infrastructure in poor condition not only may generate an immense rate of track geometry deterioration but also lead to higher degrees of wear or even failures of rails, sleepers, fasteners, etc. [6]. Maintenance of railway infrastructure requires huge budgets with numerous challenging organizational and planning problems. However, more of the research has been focused on train traffic operations compared to infrastructure maintenance operations research area [7]. Researches on strategical

decision making on the time and cost schedule of track infrastructure maintenance are of vital importance. An efficient and overall diagnosis assists prioritizing the maintenance areas.

Currently available customary methods of track infrastructure diagnostics for maintenance such as selective drilling and ballast sampling do not provide continuous information and there exists the possibility to miss out the potentially degraded sections in between two selected trench locations. Besides, the whole procedure in traditional methods is destructive, requires labor and takes a considerable amount of time [1,5,8].
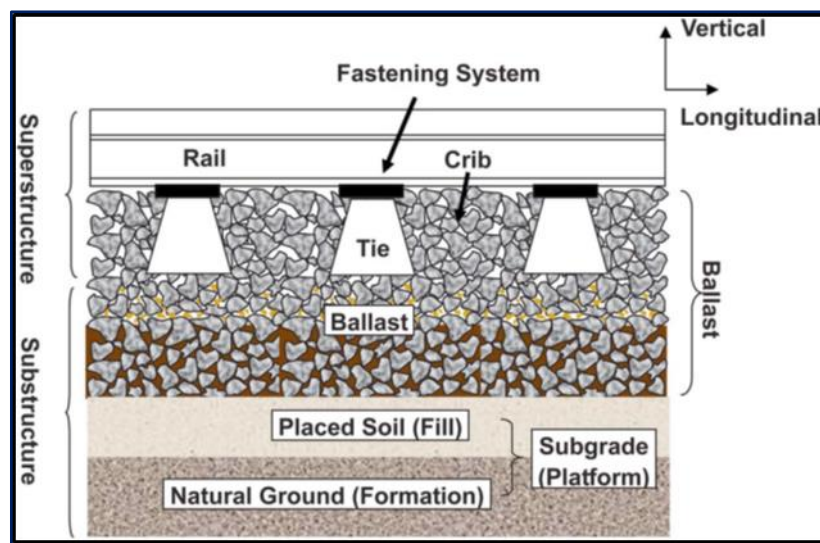
Figure 1.1. Track Structure adapted from [5,9]

It is noteworthy that high-quality ballast has a pivotal role in track structure and overall stability [10] since ballast has the following fundamental functions some of which are resisting vertical, longitudinal and lateral stresses applied to sleepers, preserving the track position and enabling drainage of water from the track platform [5,10,11].

Therefore, appropriately maintaining the ballast layer is the most essential subject in avoiding the gradual worsening of the track bed and subsequently the deformation of the tracks. An ignorance in minor drainage complications together with an overlook in fouling levels in the ballast body may give rise to severe maintenance troubles and induce lower safe speeds and raise the probability of derailments [10]. In other words,

ballast fouling (contamination) may disable the ballast body of the track to fulfill the above-mentioned expected functions and risk the overall safety of the track [5].

Taking into account the destructive character, elapsed time, discontinuity of surveys, limited coverage of surveys, traffic obstructions and low-speed limitations encountered during the traditional railway diagnosis works, the rail industry has been seeking for time saving and cost-effective diagnosis procedures. In this respect, GPR has excited the great interest of researchers and practitioners in pinpointing railway infrastructure problems before it becomes too late to fix them (especially railway ballast evaluation) as a noninvasive geophysical detection method overcoming the restrictions of the traditional methods [1,12].

To that effect, this dissertation addresses evaluation of railway ballast condition by using Ground Penetrating Radar.

1.1   Railway Structure and Components

Typical railway structure can be divided into two basic categories as infrastructure (substructure) and superstructure, where infrastructure comprises ballast, sub-ballast and subgrade while superstructure is composed of rails, sleepers (ties) and other fastening accessories [4]. Figure 1.2 and Figure 1.3 below illustrate respectively, the longitudinal and vertical cross-sections of a typical railway structure.
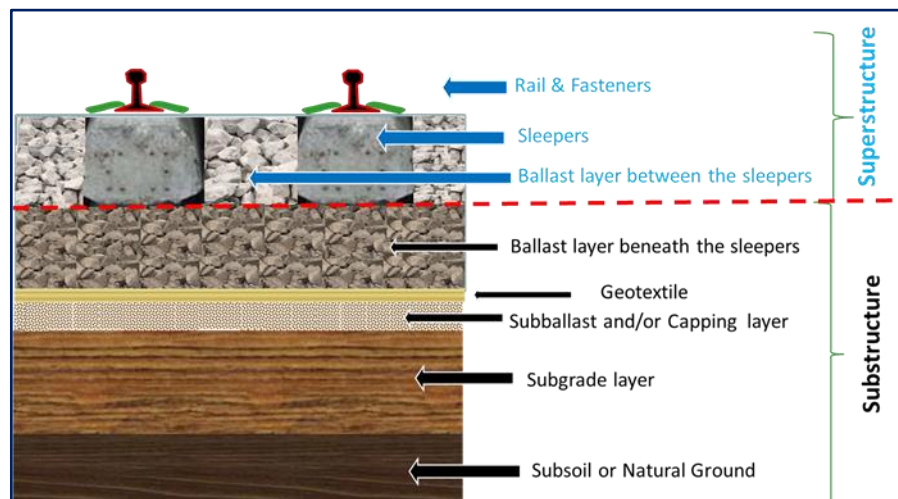
Figure 1.2. The longitudinal cross-section of railway structure

31
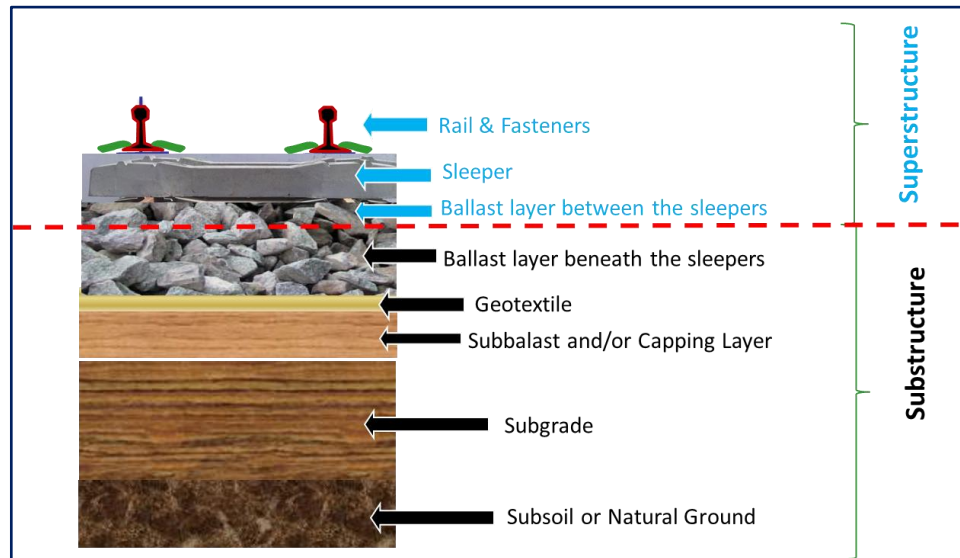
Figure 1.3. Vertical cross-section of railway structure

1.1.1 Railway Superstructure Components

1.1.1.1 Rails:

Rails are two longitudinal and parallel steel elements placed on top of, and perpendicular to, the sleepers. They are typical of the form of an asymmetrical I-section. Rails are composed of head, web, and foot as depicted in Figure 1.4. The rails may also provide the secondary task of completing a low voltage circuit that operates the network's signals [9]. Bullhead rail was the standard from the mid-19th until the mid-20th century in Britain. Flat bottomed rail is the governing rail profile in worldwide use [13].
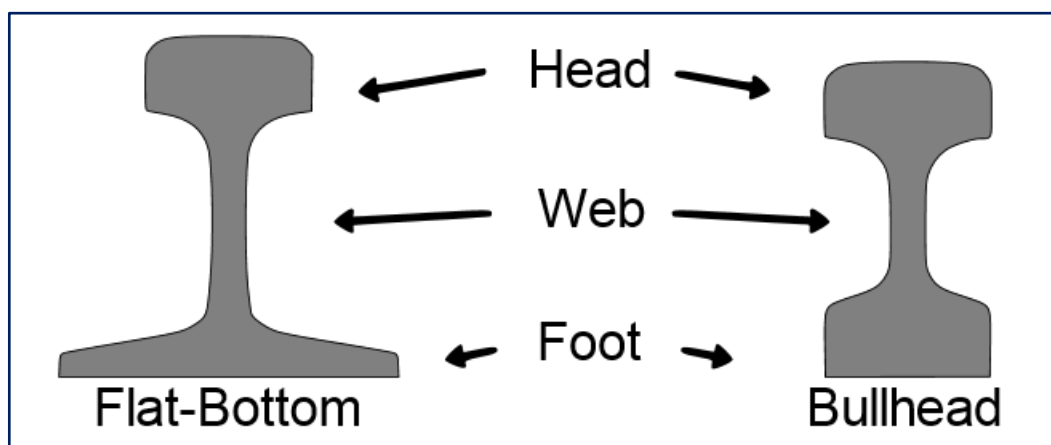
Figure 1.4. Cross-sections of flat-bottomed rail and bullhead rail [13]

1.1.1.2   Sleepers (Ties):

Railway sleepers are traditionally made of wood, however pre-stressed concrete railway sleepers are now in wider usage, particularly in Europe and Asia. Steel ties are common on secondary lines in the UK. Plastic composite sleepers are also seldom employed [14]. Figure 1.5 a, b and c below depict respectively, the concrete, steel and wooden sleepers.

Figure 1.5. Sleeper types according to the material it is made of a) reinforced concrete, b) steel, c) wooden

The basic function of railway sleepers (or "ties" in the US) is the distribution of traffic loading from the rails uniformly to the ballast, sub-ballast and sub-grade, and to keep the alignment of the rail under train loads and weathering effects. Sleepers are usually placed perpendicular to the rail and provide the structure to which the rails are attached. They also ensure the rail gauge: i.e. the constant distance between the rails [15].

1.1.1.3   Fastenings:

Rail fastening systems are employed to attach the rail to the sleeper to confront the various forces which may cause the rail to move, deform, deviate, or fail due to train loading or other conditions. The kind of fastening system selected depends on the type of sleeper material [15].

1.1.2   Railway Infrastructure Components

1.1.2.1   Subgrade:

Subgrade is the foundation layer of the railway track which enables a suitable and stable base on which all other layers can be constructed. The dynamic loading from trafficking can penetrate up to five meters and this would be some way into the sub-grade layer; therefore, it is important that the strength and durability of the sub-grade are sufficient [9].

1.1.2.2   Sub-ballast and Geotextiles:

Sub-ballast is regarded generally a good performing layer and it has been constructed in new and reconstructed tracks [16]. In Turkey, sub-ballast layers are constructed in between subgrade and ballast layer for high-speed railway lines. This layer is usually made of sand or gravel with the aim to block the migration of finer material from the subgrade into the ballast and lessen the forces transferred to subgrade [15]. However, poor performing results were reported commonly for the sub-ballast layer to fulfill those functions [15,16]. In order to overcome this problem, geotextiles are used to separate granular layers for railway permanent way. Geotextiles are permeable to filter water but prevent particles from mixing with other layers. Moreover, they assist ballast stiffen, thus spreading the vertical loads through sleepers more evenly [17].

1.1.2.3 Ballast:

Railway ballast is the component of track infrastructure into which sleepers are laid. Ballast is filled between, beneath, and around the sleepers. The area of ballast between two sleepers is called as a crib. Ballast has the following functions [18]

- to confront and distribute vertical, longitudinal and lateral stresses from trafficking applied to sleepers
- to keep the track position
- to enable drainage of water from the track platform
- to accommodate continuous voids in the material around the sleepers to hinder capillary action, minimizing the influences from frost heave.
- to block vegetation
- to provide flexibility and ensure damping for the track
- to enable maintenance actions where surface irregularities can be fixed through ballast tamping or adjusting the sleeper position to re-align the track.

For the requirements of a high-quality ballast, EN 13450:2002/AC:2004 standard [19] is the governing document at the European level, which requires an intensive set of data about the geometric, mechanical and mechanical and physical properties that the railway ballast layer should possess in the track bed [20]. Overall, the ballast of high-quality should be strong, durable, simple to clean, resistant to degradation, workable, easily available, and fairly inexpensive to procure [18]. Railway ballasts are generally produced from natural deposits of limestone, dolomite, granite, and basalt.

Ballast grading is one of the indicators of good ballast since it is widely accepted that ballast should be in between threshold values of 28 mm and 50 mm in diameter. Finer particles prevent the drainage ability of the ballast whereas larger aggregates will lead to uneven distribution of the dynamic loads [15]. Table 1.1 below present the UK/ Europe, Australia and USA grading. The selection process of ballast grading to be used in a railway depends on factors such as train axle loads, route tonnages and subgrade conditions [21].

Table 1.1.Ballast Grading Standards [21]

Sieve size		% Passing (by mass)				
		UK / Europe	Australia		USA	
inches	mm	EN13450	QR	ARTC	AREMA24	AREMA4
2.480	63.0	100	100	100	90 - 100	
2.087	53.0		95 - 100	85 - 100		
1.969	50.0	97 - 100				100
1.476	37.5	35 - 65	35 - 70	20 - 65	25 - 60	90 - 100
1.102	28.0	0 - 20				
1.043	26.5		0 - 15	0 - 20		
0.984	25.0					20 - 55
0.787	20.0					0 - 15
0.748	19.0			0 - 5	0 - 10	
0.551	14.0	0 - 2				
0.520	13.2			0 - 2		
0.500	12.7				0 - 5	
0.374	9.5		0 - 5			0 - 5
0.187	4.8			0 - 1		
0.046	1.18	0 - 0.8				
0.003	0.08		0 - 0.7	0 - 1		

1.1.3 Ballast Deformation

Upon cyclic loading of trains and through weathering processes, ballast deteriorates by time. Among many mechanisms, which lead to ballast deterioration, ballast fouling and moisture retention within ballast will be focused within the scope of this research. Ballast fouling, i.e. contamination of ballast takes place when voids in the ballast are filled because of ballast breakdown and infiltration of other materials from the ballast surface or infiltration from the base of the ballast layer [22]. According to Selig and Waters, reasons of ballast fouling could be divided into five categories, namely, ballast breakdown (76%), underlying granular layer infiltration (13%), ballast surface infiltration (7%), subgrade infiltration (3%) and sleeper wear (1%) [5,9]. Detailed problems caused by ballast fouling could be found in [23]. Schematic representation of ballast fouling is illustrated in Figure 1.6.
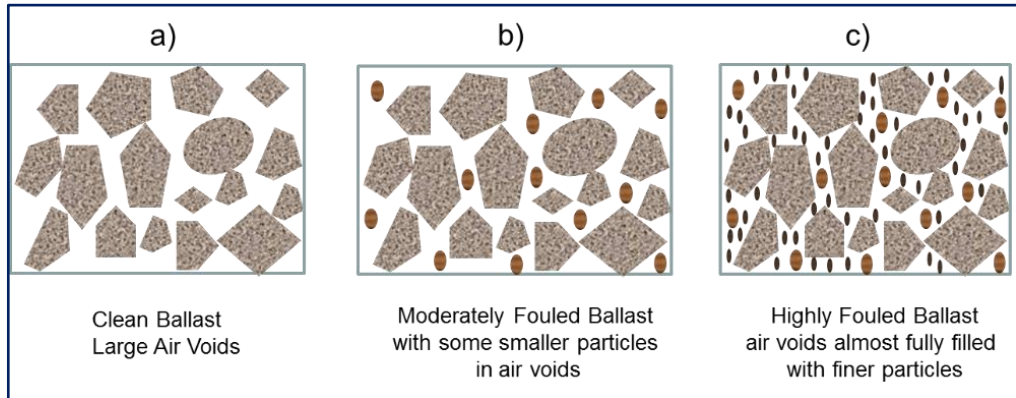
Figure 1.6. Schematization of ballast fouling mechanism from clean to highly fouled ballast: a) clean, b) moderately fouled, c) highly fouled ballast

Recently, a considerable literature has grown up around the theme of quantification of ballast fouling. The Fouling Index concept developed by Selig and Waters [9] use the ballast material passing through two sieve sizes 0.075 mm and 4.75 mm, and sums the percentage passing each sieve to determine the fouling index by equation (1).

$$F_{I-SW} = P_{0.075} + P_{4.75} \qquad (1)$$

where F_{I-SW} is fouling index proposed by Selig and Waters [9], $P_{0.075}$ is the percentage of material passing the sieve size 0.075 mm and $P_{4.75}$ is the percentage of material passing the sieve size 4.75 mm. There is also a similar index by Ionescu [24], where the sieve size of 4.75 mm is replaced by 14 mm sieve as that fits more to the Australian standards. Ionescu [24] fouling index is given in equation (2) [15].

$$F_{I-I} = P_{0.075} + P_{14} \qquad (2)$$

where F_{I-I} is fouling index proposed by Ionescu, P_{14} is the percentage of material passing the sieve size 14mm. Table 1.2 demonstrates the categories of ballast according to the fouling condition [9].

Anbazhagan et al. [25] list the alternative fouling indices developed by other researchers like fouling indices above such as percentage of fouling, D-bar method, effective degree of fouling, percentage void contamination and relative ballast fouling ratio in a comparative way.

Table 1.2 Categories of Fouling [9]

Category of Ballast Condition	Abbreviation	Fouling Index
Clean	C	<1
Moderately Clean	MC	1-10
Moderately Fouled	MF	10-20
Fouled	F	20-40
Highly Fouled	HF	>40

Unless the track is drained adequately, water accumulation will begin in the track body, which will, in turn, lead to a reduction in shear strength and stiffness of ballast as well as increasing the rate of deterioration and fouling process [26].

Influence of water on fouled ballast is much greater than it is on clean ballast since air voids present in clean ballast allow drainage of water while in fouled ballast finer particles replacing air voids adversely affect the drainage capability.

Early diagnosis of ballast fouling and trapped water within the ballast is therefore vitally important.

1.1.4 Current Diagnosis Methods for Maintenance Strategy

Currently, the majority of track infrastructure inspection processes is carried out by means of traditional methods, which are visual inspection by an experienced railway engineer and/or opening selective trenches at the locations where potential deterioration is likely to occur [5,9,11]. Portable ballast samplers is also a way of inspection [27].

For track superstructure diagnosis, many modern vehicles are running at normal traffic speeds to measure mainly the track geometry [15,28]

In the specific example of Turkish railways, the ultrasonic measurement technique is used as a non-destructive method for detection of track defects. Besides, non-destructive rail inspection cars traveling at a speed of 80 km/h have been purchased by Republic of Turkey General Directorate of State Railways Administration (TCDD) in order to measure track and examine the vehicles in the inventory [29]. These cars can conduct track geometry, rail profile and rail corrugation inspections together with

vehicle measurement systems such as vehicle identification, wheel profile measurement, wheel surface defects and wheel flatness detection, brake shoe, lining, and disc wear detection, and axle box detector [29]. However, there is not a widespread and routine non-destructive inspection methodology for investigation of track substructure i.e. ballast, sub-ballast and subgrade for Turkish railways, yet.

In his Ph.D. thesis, De Bold [15] identifies the potential non-destructive methods for ballast assessment such as falling weight deflectometer, sonic echo, impulse response, impedance logging, cross-hole sonic logging, parallel seismic, ultrasonic pulse velocity, ultrasonic echo, impact echo, spectral analysis of surface waves and GPR [15]. A set of diagnosis methodologies, ranging from the traditional to the most innovative ones available, with a special focus on GPR, is elaborated in a review study by Bianchini Ciampoli et al. [30].

Advantages of GPR are stated in [31] as the provision of significant, dense and accurate data and higher resolution in comparison with other non-destructive geophysical technologies such as seismic, transient electromagnetic, electrical and magnetic approaches. Considering these advantages GPR method is used in this research.

1.2 Structure of the Thesis

The remainder of this thesis is organized as follows. The objectives of the dissertation are elaborated in Chapter 2. In the next chapter, the historical development of GPR will be explained. Then GPR basic principles together with the pros and cons of the method will be introduced. Major fields of GPR applications, typical GPR equipment and accessories will be introduced. Then the transport infrastructure surveys with GPR will be mentioned in the last section of Chapter 3. Chapter 4 focuses on the state of the art research on the use of GPR on railway infrastructure. In Chapter 5, used equipment, hardware and software will be described. Chapter 6 comprises all the experimental work both in the laboratory and in the field. First Section of Chapter 6 evaluates the GPR system performance compliance tests for the available GPR equipment. Next section targets to obtain the variations in RDP values of granite ballast under various fouling levels. In Section 3 of Chapter 6, the focus is on experimental

assessment of the moisture influence in the clean and fouled coarse granite ballast on the GPR signal characteristics under controlled laboratory environment. In the 4th Section of Chapter 6, field track survey with 2 sets of GPR with antenna frequencies ranging from 400MHz to 2GHz along the railway next to Rozhovice Station is presented. The field surveys were undertaken within the scope of co-operation with Správa Železniční Dopravní Cesty (SŽDC). In the last section of Chapter 6, laboratory experiments realized at the laboratory of Engineering Department of University Roma Tre will be explained, where the EM response of limestone ballast material was evaluated under different configurations of laboratory experiments. In Chapter 7 results and discussion of results will be presented. Chapter 8 will include the overall conclusions, contribution of the dissertation and future perspectives. References will be given next. Then publications of the Ph.D. student on the dissertation subject will be presented. Lastly, appendices will take place.

2 DISSERTATION OBJECTIVES

The main aim of this dissertation is to elaborate the implementation of non-destructive GPR methodology in railway track bed surveys (particularly ballast), through both laboratory and field experiments.

Research objectives, in general, are set as:

- to assess electromagnetic (EM) characteristics of reflected GPR signal from the ballast
- to obtain variations of RDP values versus ballast fouling and RDP values versus moisture content under clean and fouled conditions in the laboratory environment as a function of different types, frequencies, and orientations of GPR antennas and presence of sleepers and rails
- to perform GPR field surveys along a railway segment having different types of sleepers as a function of various types, frequencies and orientations of GPR antennas
- to validate the laboratory results with theoretical and practical results
- to compare the results of collected GPR data with different sets of GPR equipment on the same railway segment (in terms of brands – GPR sets owned by Department of Transport Structures of Faculty of Transport Engineering University of Pardubice and GPR set owned by SŽDC

To that effect, it was aimed at gaining the required experience, knowledge and competence with the available GPR software and hardware in order to conduct the experiments, interpret and analyze the results and understand capabilities and the limitations of the GPR methodology.

Specific objectives of the dissertation as per the sections in Chapter 6 "Laboratory and Field Experiments & Results & Discussion of Results" are as follows:

1) In Section 6.1:

to assess the performance of available GPR equipment through GPR system performance compliance tests

2) In Section 6.2:

to comprehend the EM response of clean and fouled ballast materials. In order to achieve this aim, the following objectives are set:

- to calculate the RDP of ballast under dry clean and dry fouled conditions by means of various estimation methodologies (by gradually increasing the volume of fouling material incorporated into the ballast material)
- to form a basis for the estimation of the level and type of ballast fouling by correlating the calculated RDP values from GPR acquisitions with fouling percentages based on the ballast materials and fouling agents used in the laboratory experiments, hence improve the assessment and monitoring efficiency of railway site investigations on the condition that similar ballast types used in these experiments are fouled by similar fouling agents in real track conditions.

3) In Section 6.3:

to evaluate the influence of moisture (water) in the clean and fouled coarse granite ballast on the GPR signal characteristics. In order to achieve this aim, the following objectives are set:

- to calculate the RDP of ballast under wet clean and wet fouled conditions by means of different estimation methodologies (by gradually increasing the volume of fouling material and water to be added into the ballast material)

- to construct a baseline for the prediction of the RDP values of wet clean and wet fouled ballast by comparing the RDP values with the added volumetric percentage of water for a specific fouling level.

4) In Section 6.4:

to analyze and comprehend the performance of GPR surveys on different types of sleepers with various nominal frequencies, types, and orientations of the antennas along a real railway track. In order to achieve this aim, the objective is set:

- to find out an agreement between the GPR data collected from a 138-m long railway segment nearby Rozhovice railway station and the ground truth data taken from 11 trenches (9 on the track axis, 2 on the shoulders) dug on the same railway segment including the road level crossing P4992

5) In Section 6.5:

to evaluate the EM response of limestone ballast material under different configurations of laboratory experiments. Based on numerous different configurations, the main aim is to comprehend how and to what extent GPR signal is influenced by the clean and fouled configurations of ballast material with and without the reinforced concrete sleepers and rails by using 4 different air-coupled antennas in two different antenna orientations. A secondary goal is to determine the variation of RDP values of ballast material caused by fouling.

Overall, through all the laboratory and field measurements the final aim is to test the reliability and eligibility of GPR method to diagnose the condition of ballast in terms of fouling level and type, moisture content, and to identify the layering of clean and fouled ballast, hence improving the evaluation and monitoring efficiency of railway infrastructure site investigations.

3 GPR HISTORY, BASIC PRINCIPLES, EQUIPMENT AND APPLICATION FIELDS

In this chapter, historical development and use of GPR will be handled. GPR basic principles and fundamentals, equipment and the steadily increasing use of GPR on many application fields will be elaborated.

3.1 GPR History

Research into GPR has a rather long history. In order to thoroughly comprehend GPR history, one needs to delve into the historical development of "Radar". In doing so, it is noteworthy to firstly mention James Clerk Maxwell and Heinrich Hertz, both of whom had substantial researches in the second half of the 19th century.

Maxwell [32] was the first to hypothesize the presence of EM waves in 1861 [15]. Then Hertz [33] established simple transmitter and receiver validating Maxwell's theory [15].

In 1897, the Italian inventor Guglielmo Marconi [34] registered the first long distance transmission of EM waves which was also regarded as the invention of the radio [15].

In 1904, Hülsmeyer [35] has demonstrated the detection of remote metal objects by the use of EM waves, in the specific presentations of the anti-ship colliding system [15,36].

Six years later, in 1910 Leimbach and Löwy [37] buried dipole antennas in a set of vertical boreholes and the magnitude of signals were compared when sequential dipole pairs were used to receive and transmit [15,36].

In 1917, Nikola Tesla [38] stated initial principles concerning the frequency and power levels for the first primitive radar units and foreseen that distance and speed can be measured [15].

In order to detect objects placed underground, radar waves were firstly used by Hülsenbeck [39] in 1926. He stated that any change in dielectricity causes reflections which are likely to be a more advantageous method compared to seismic methods [36].

This was the first application when EM waves were purposely radiated trough solids [40]. Three years later, in 1929, GPR was firstly used in order to determine the thickness of the glacier in Austria by Stern [41,15].

Both the pre-World War II period [15] and the war itself [40] have boosted the rapid development of radar owing to its efficient use in detecting and tracking military units like fighter aircrafts.

The term RADAR was devised as an acronym for RAdio Detection And Ranging in 1940 by the United States Navy. Then the term radar has turned out to be a common noun in English and other languages by losing all capitalization [42].

GPR technology was ignored about until 1950s [15,40,43] when a US Air Force plane, trying to land, crashed into the ice in Greenland because of misreading the altitude given by its radar system. Airborne radar analysts detected the bedrock beneath the ice, however, they interpreted it as the ground surface (since at that time it was not expected that the radar could "see" through ice) which caused the plane to crash. This realization of comprehension which radar could penetrate ice resulted in a diverse number of surveys testing the capability of radar to probe into the subsurface in order to identify stratigraphic interfaces, to map soil properties and to detect the groundwater table [40,43].

In 1956, the interference between direct air transmitted signals and signals reflected from the water table was used by El Said [44] in order to estimate the depth of water table [15,45].

In the early 1960s, probing in ice in polar regions and on glaciers continued as reported by Annan [45]. The Scott Polar Research Institute at Cambridge [46] and the Geophysical and Polar Research Center at the University of Wisconsin [47,48] conducted researches in ice sounding. Substantial depths in ice [49,50] were penetrated as also mentioned by Daniels [36].

In 1967, a GPR system was used on lunar investigations within the scope of the Apollo 17 mission (within Surface Electrical Properties Experiment) [51,52]. In Figure 3.1, the GPR system developed by National Aeronautics and Space Administration (NASA) can be seen.
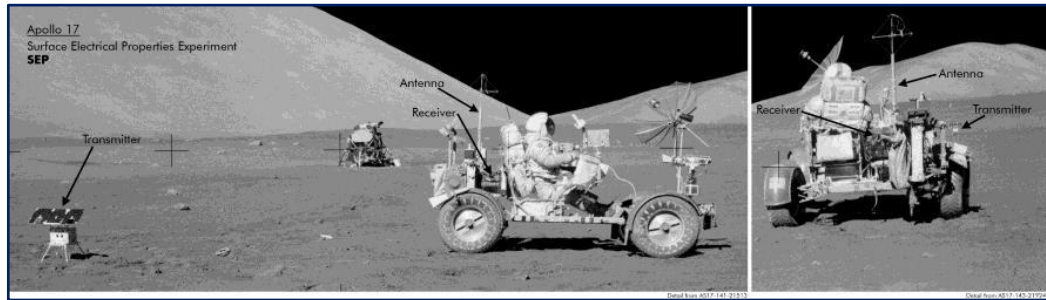
Figure 3.1 GPR equipment on the Moon [53]

During the Vietnam War, a radar system called "Combat Radar" was fostered by US Army in order to determine the locations of mines, tunnels, and bunkers. This system, in turn, paved the way for the development of GPR system for diagnosing and mapping subsurface geological properties in the following years [40].

Morey and others formed Geophysical Survey Systems Inc. (GSSI) [45], which resulted in a boost in applications and research [15].

Since the seventies, GPR was employed in many applications such as determining the thickness of the ice, detection of utilities and profiling the bottom of lakes and rivers. Besides, GPR was used for example in the mining industry, identification of sites for nuclear waste storing and archeology [52].

Potential of conducting archeological surveys with GPR prospecting had also attracted archeological community [43]. A detailed account of the history of GPR use in archeology is given by Conyers [43].

Between 1980 and 1985, the optimistic approach to the potential of GPR was masked due to the fact that many environments were not suitable for GPR, whereas, after 1985, the advantages and limitations were realized better [45].

In the period of early nineties, the breakthrough progress in GPR technology realized when several commercial companies had a rapid growth. On the other hand, GPR conferences organized once in two years gathered people and resulted in valuable proceedings to the new users [45].

To conclude, since nineties GPR has a steadily increasing attraction in many fields of applications such as detection of pipe and cables, archeology, voids detection,

tunnels and mineshafts, remote sensing by satellite and diagnostics & quality evaluation in transport infrastructures [36].

3.2 GPR Basic Principles

GPR is a probing technique, which uses discrete pulses of EM energy in order to detect variations of electrical properties of the subsurface [54,55] with a dominating frequency range from 10MHz to 2.5GHz to reveal the positions and sizes of electrically dissimilar layers and objects [56].

GPR has been in use for about 5 decades and it has proven itself as a strong geophysical method in order to diagnose and monitor the subsurface structural and material aspects [57,58]. Especially with the recent improvements of the hardware and software technology, there has lately been a boost in both applications and researchers getting involved in the method [57]. GPR method is basically composed of GPR antenna transmission of a radio frequency (EM energy) into the ground or another medium via short EM pulse. Part of the transmitted EM energy is reflected by differences in material relative permittivity and electrical conductivity at material interfaces. Such dissimilarities or so-called anomalies appear in the form of changes in soil layers, groundwater surfaces, or buried objects [58].

The physics of EM fields are described mathematically by Maxwell's equations, whereas constitutive equations quantify material properties. Combining the two enables the quantitative description of GPR signals [59]. Maxwell's equations together with constitutive relationships are not typed in here, however, they can both be easily seen in many sources such as in the book by Jol [59].

The transmission and reflection of EM pulses are governed by the magnetism of the material, relative dielectric permittivity (RDP) and the electrical conductivity.

The magnetic susceptibility of a soil or road material is assumed to have no effect on GPR signal propagation [56].

RDP (or also known as dielectric constant) and the conductivity of a material are the major material properties which influence the transmission and reflection of the EM wave. A material's RDP can be defined as the amount of electrostatic energy stored per

unit volume for a unit potential gradient. Table 3.1 below demonstrates RDP values of common earth materials measured at 100MHz [60].

Table 3.1 RDP values for common earth materials [60]

Bulk RDP values of common earth materials (measured at 100MHz).		
Material	**Davis and Annan** [61]	**Daniels** [36]
	RDP	RDP
Air	1	1
Distilled water		80
Fresh water	80	81
Sea water		80
Fresh water ice	3–4	4
Sea water ice		4–8
Snow		8–12
Permafrost		4–8
Sand, dry	3–5	4–6
Sand, wet	20–30	10–30
Sandstone, dry		2–3
Sandstone, wet		5–10
Limestone	4–8	
Limestone, dry		7
Limestone, wet		8
Shales	5–15	
Shale, wet		6–9
Silts	5–30	
Clays	5–40	
Clay, dry		2–6
Clay, wet		15–40
Soil, sandy dry		4–6
Soil, sandy wet		15–30
Soil, loamy dry		4–6
Soil, loamy wet		10–20
Soil, clayey dry		4–6
Soil, clayey wet		10–15
Coal, dry		4
Coal, wet		8
Granite	4–6	
Granite, dry		5
Granite, wet		7
Salt, dry	5–6	4–7

Electrical conductivity is a measure of the ease with which an electrical current can flow through a material [15].

The travel time of the GPR signal is the sole direct measurement acquired in the field. The signal velocity, however, is variable and dependent on the physical properties of the materials among which RDP is the most significant one. Once RDP is known, the relative EM wave velocity can be computed from equation (3):

$$v_r = \frac{c}{\sqrt{\varepsilon_r}} \tag{3}$$

where v_r is relative relative EM wave velocity, c is the speed of light, ε_r is RDP [36]. Once EM wave velocity is known, the depth of object or interface can be computed from equation (4):

$$d = v_r \cdot \frac{twt}{2} \tag{4}$$

where d is the depth of the object or stratigraphic layer of interest and twt is the two-way radar travel time to and from the target [36].

The amplitude and return time of signal reflections are picked up by a receiving antenna while the transmitted wave penetrates the medium and the antennas move along the surface of the medium. The recorded raw data is then processed by a commercial software package to produce an image (radargram) of the subsurface profile where the wave reflections are shown as functions of the wave travel time. The wave travel time is then converted to penetration depth from equation (4) on the basis of EM wave velocity calculated from equation (3) given above [58]. The reflected signal includes information on the medium in the form of return time, amplitude, shape, and polarity of the received signal, and this enables the chance to research new ways of data analysis with regard to the material of interest [15]. Changes in the condition and composition of the material will lead to variations in the received signal. Therefore, changes in the return time, amplitude, shape, and polarity of the received signal will reveal information on the medium, the distance of the reflector, signal velocity through the medium, and

attenuation characteristics. From these elements, deductions about the test element's material properties can be made [15].

GPR can be considered as the EM equivalent of seismic reflection and its implementations are unlimited, however, the one of the most significant problem is the interpretation of GPR information into beneficial quantitative information for end users. GPR sections usually will be collected where there is much more information than required which hinder the more straightforward understanding of the conditions at a site [57]. A GPR operator should have a good comprehension of the basic principles of the technique [36], and if needed, before executing surveys in the field, training and/or participation in a survey with an experienced user are required [54].

In GPR glossary, single waveform versus time is called as A-scan. Adjacent A-scans are combined to build a radargram also known as B-scan [54]. In a B-scan, each row represents one sample point (pulse) on a column which represents each individual trace. The value of the matrix element is the voltage amplitude for a given trace and the sample. Assigning color bar to voltage amplitudes can display matrix as the image [62]. In Figure 3.2, typical A-scan and B-scan are presented.
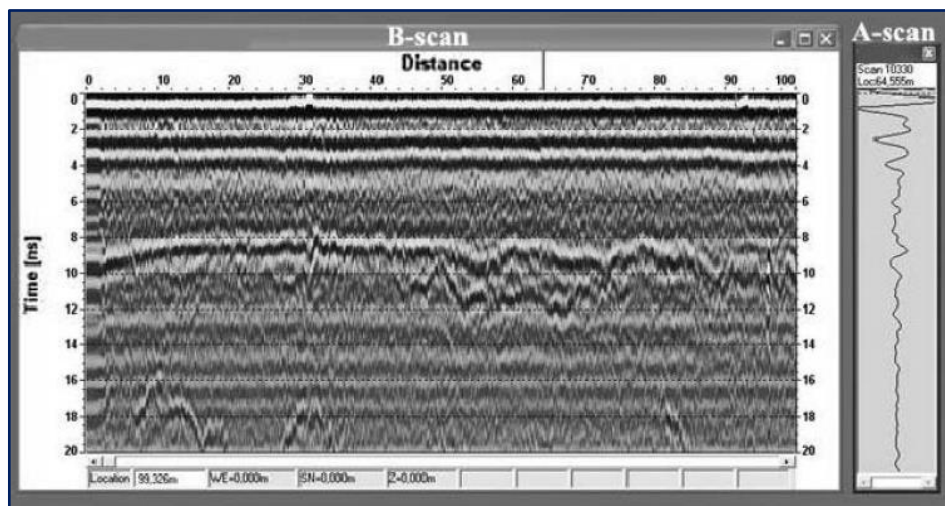
Figure 3.2 Typical A-scan and B-Scan (Radargram) [63]

As indicated in [54], antenna frequency selection is very important since there is a compromise between the desired resolution and the achievable depth of penetration. As a rule of thumb, it is better to prioritize the depth of penetration instead of resolution, in order to ensure that the layer or object beneath is within the reach of GPR, since high

50

resolution would be totally useless when the target cannot be detected at all [64]. Table 3.2 shows penetration depths for various GSSI antennas of different frequencies together with the time windows (travel times ranges in ns) and typical applications used [31].

Table 3.2. Depth of penetration values for various GSSI antennas of different frequencies together with the time windows ranges in ns and typical applications used adapted from [31].

Center frequency (MHz)	Depth of penetration (m)	Travel time (ns)	Typical applications
2600	0.4	8–15	Thickness and condition assessment for shallow depths
1600	0.5	10–15	
900	1.0	10–25	Subbase evaluation and layer condition assessment
400	4.0	20–100	Void detection, utilities, thick concrete structures, subgrade evaluations
270	6.0	50–200	Geotechnics
2000 HORN	0.75	8–15	Pavement thickness and road condition assessment
1000 HORN	0.9	10–20	Pavement and bridge deck evaluations

Therefore, it is of crucial importance to design a survey in accordance with the objectives and the requirements of that survey in order to conduct an efficient GPR imaging.

Miscellaneous parameters such as vertical frequency, temporal sampling interval, time window, and step size (horizontal resolution) etc., are required to be set when designing a single fold, fixed-offset reflection survey, which is the most common mode of GPR data collection [54]. The criteria for setting such parameters for a good survey design are detailed in [54]. Figure 3.3 illustrates a fixed offset profiling, where T denotes for Transmitter of the antenna and R is used for the Receiver of the antenna.

GPR methodology possesses many advantages such as the provision of dense and accurate data and higher resolution in comparison with other non-destructive geophysical technologies whereas basic performance restrictions of the method appear in surveying high-conductivity materials, such as salt-contaminated soils and clay, and in heterogeneous conditions leading to complicated EM scattering phenomena [31]. Leng and Al-Qadi [65] emphasize an important point to be kept in mind that despite

the many advantages of GPR technique, users should be aware of the limitations of it so that the benefits thereof would not be oversold. Olhoeft [51] draws the attention to the growing number of factors such as internet access, HDTV, cell phones, and so forth, which are likely to produce noise during a GPR survey.
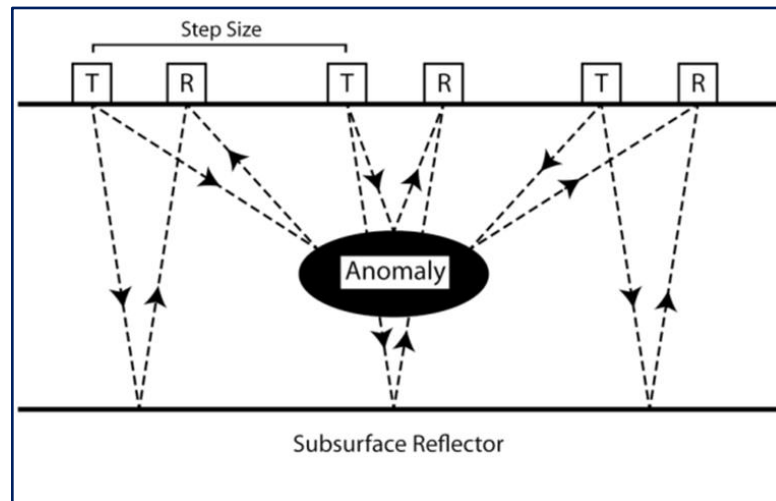
Figure 3.3. Fixed offset profiling [54]

Loulizi [40] pinpoints the gap between the electrical and civil engineering disciplines in view of GPR technology. He emphasizes that electrical engineers design and build antennas without a thorough understanding the needs and goals of civil engineers who are GPR end users whereas civil engineers usually employ the system with very little knowledge of how the system is functioning. To solve his problem joint workshops including many disciplines (antenna producers, end users, stakeholders) related to GPR could come together and produce guidelines and standards. The list of existing standards and specifications on the GPR use on many fields of application are listed in [66].

It can be concluded that GPR has a great potential as a non-destructive inspection tool with many advantages such as continuity of surveys, non-destructive nature, high and fast coverage, limited traffic disturbance in case of transport infrastructure surveys. Therefore, its advantages should be maximized in the wide range of applications keeping the above-mentioned limitations of the technique in mind.

3.3 GPR Equipment and Accessories

A typical GPR set (Figure 3.4) can be composed of i) ground coupled and/or air coupled antennas, ii) GPR control unit and PC iii) encoder (odometer) iv) cables and power supply and/or batteries v) auxiliary equipment such as GPS, video recorder, drilling unit etc. [56].
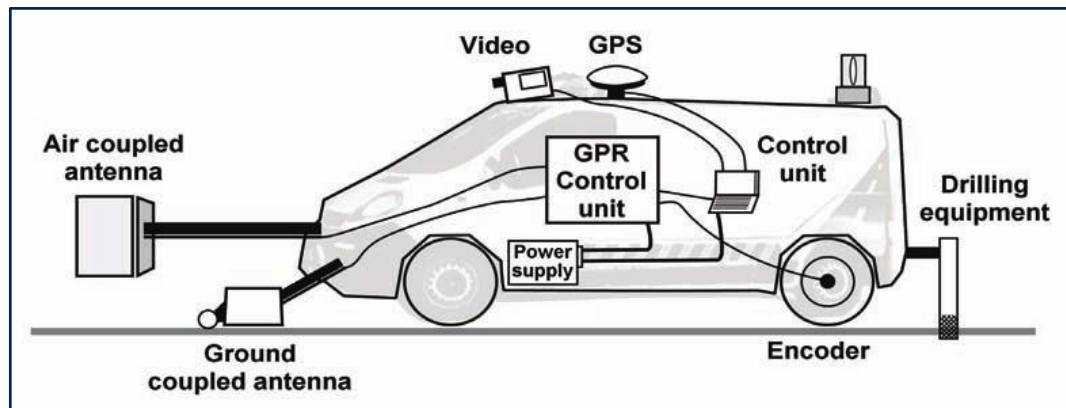
Figure 3.4 A typical GPR set with accessories [56]

3.4 Application Fields of GPR

GPR has been used in a great many fields ranging from detection of ice glaciers' thickness to mine detection and from forensic investigations to archeological works. Major fields of applications of GPR is given by Daniels [36] some of which are listed below:

- archaeological investigations
- borehole inspection
- geophysical inspections (contaminated land investigation and snow, ice and glacier inspections)
- forensic investigations
- planetary exploration
- detection of buried mines (anti-personnel and anti-tank)
- utility detection (pipes and cables)

- transport infrastructure and civil engineering surveys (bridge deck analysis, rail track and bed inspection, road condition surveys, tunnel linings)
- structural assessment (building condition assessment, evaluation of reinforced concrete, wall condition)
- medical imaging
- remote sensing from aircraft and satellites
- timber condition

3.5 GPR use in Transport Structures

Surveys in traffic infrastructure, which include the feasibility of radar in tunnels and bridge decks, moisture detection in construction materials, detection of voids under concrete highways, date back to early 1970s [56]. Since then GPR has been used in a variety of traffic infrastructure inspections such as pavement layer thickness measurements, detection of voids, bridge delamination, measurements of depth to steel dowels, detection of buried objects and utilities, asphalt stripping and scour around bridge piers [56].

Borecky [66] elaborates the combined use of GPR and another non-destructive method, Falling Weight Deflectometer (FWD).

A very detailed list of applications of GPR use in pavement diagnosis is given in [31] as divided into the categories of common and research applications.

In airports, GPR is also found useful due to its capability to handle a large amount of data rapidly. Especially multichannel 3D GPR technique allows speedy and economical coverage of the large areas of runways and taxiways in order to detect segregations, cracks, damaged areas and pipes and cables [56].

Maser (1996) also gives the basic applications of GPR with the emphasis on transport infrastructures [67].

GPR technique reveals important aspects of structures and soils and provides data about electrical properties which may subsequently be correlated to mechanical

properties and performance of materials which is quite significant in transport structures [56].

Next chapter focuses on the GPR use in railway track infrastructure diagnostics.

4 STATE OF THE ART RESEARCH ON USE OF GPR ON RAILWAY INFRASTRUCTURE

As expressed in [68] first GPR applications in railway engineering date back to the eighties. Initial work was limited to ground-coupled antennas operating with center frequencies below 500MHz. It is noted that railway industry has begun to make use of GPR technology in mid-nineties in Europe (mainly in Switzerland, UK, Finland), and North America [56].

Basically, GPR has been used in a wide range of applications for railway infrastructure such as determination of layer thicknesses [69], investigation of embankment stability [70,71], localization of trapped water areas [12], indirect estimation of track modulus from GPR [72], detection of permafrost sections [73–76].

Noteworthy developments have recently been recorded in the implementation of GPR technique for track substructure investigation and evaluation. Miscellaneous GPR commercial sets specific to railways have evolved both in terms of measuring instruments and data processing & interpretation software [6]. The advancements in the technology that GPR reached has brought forward even the chance to compare the commercially available GPR systems to decide the most suitable one to the specific application among many sets. Thompson II and Carr [58] have assessed six commercial GPR systems with different central frequencies to visualize the track bed condition, whereas Maturana et al. [77] compared three different proprietary GPR systems in terms of the data quality.

The reoccurrence of the GPR measurements over time enables to predict the deterioration rate of the track substructure (especially ballast) and to monitor the effectiveness of the maintenance procedures, which will facilitate to effectively schedule the required maintenance works in short, medium and long-term bases with notable cost and time savings [77].

In Figure 4.1, there is a schematic view of GPR profile generation over ballasted track substructure [78].
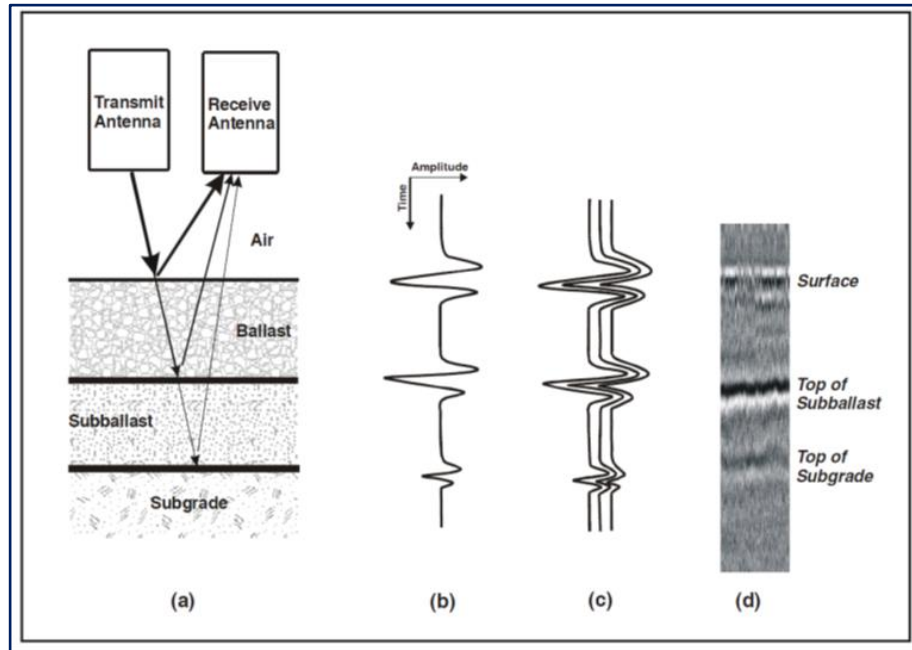
Figure 4.1. The generation of a GPR profile with an air-coupled antenna over track bed. a) The transmitted energy is reflected off the boundaries in the substructure, b) A single trace composed of the reflection amplitudes for the reflections in (a), c) Multiple scans are generated in quick succession, d) Adjacent scans are combined to build a B-scan [78].

Gallagher et al. [79] employed GPR in order to characterize the level of ballast degradation and detect the interface between ballast and subgrade. Jack and Jackson [27] qualitatively detected the condition changes within the ballast layer to categorize the GPR profile into sections based on those condition changes.

In an intensive study in Switzerland, use of GPR not only proved very beneficial compared to traditional methods in ballast condition assessment leading to minimization of the number of trenches required but also diagnosed reliably the regions where subsoil material penetrated into ballast [8].

In many studies, GPR data could be satisfactorily used in the categorization of ballast quality and thicknesses determination. De Bold [15], in his Ph.D. thesis, has attested that GPR could be utilized in ballast characterization and found a high correlation between Ionescu fouling index and the scanned area by GPR. He also added that the best results were attained with the 500MHz antenna.

In a study which set out to test GPR capabilities to inspect continuous large sections of trackbed with adequate resolution and sampling rates and subsequently

enable the optimized maintenance works, it was expressed that GPR pulses in ballast are affected by [77]

- the attenuation in high frequencies
- the existence of reflectors inside the ballast
- loss of reflector at the base of ballast
- the decrease in the signal velocity, which can either stem from a change in ground composition, moisture content variation or fouling level

In their study, Carpenter at al.[80], point out the usage of radar detectable geosynthetics during the construction of railways in order to promote the preciseness of depth of ballast measurements after the construction overcoming the often-encountered limitation i.e., loss of reflector at the base of ballast.

Olhoeft et al. [81] developed an automated system using GPR to assess various maintenance problems along the railway where automated processing, calibration, and modeling of data by means of straightforward indices are performed for annual surveys over 800.000 km in the United States. Hyslip et al. [12] also give an overview of an ongoing study to use substructure indices, which are considered to be based on layer contours, moisture content in the substructure layers and fouling material quantity in the ballast, for easier understanding and interpretation of GPR data. In their research, Sussmann et al. [70] indicated a good example of railway subgrade investigation with GPR, where condition indicators were used to make the data interpretation process simpler.

The importance of optimizing the central frequencies of the antennas used in railway surveys according to the type of inspection is emphasized [56]. Also, antenna configuration was optimized in the work of Al-Qadi et al.[82] in multiple-frequency GPR system (composed of two 2GHz and one 500MHz antenna) for railroad substructure assessment. In North America, prosperous tests have been achieved with 1GHz antenna [81], whereas in Finland [73,83] and U.K. [11,15] several satisfactory surveys were performed with 400 and 500MHz antennas, respectively. In the last decade, low-frequency antennas have been replaced by higher frequency

(1GHz÷2GHz) air-coupled systems, resulting in numerous benefits in terms of ballast condition evaluation [30,68]. Figure 4.2 demonstrates the different types and brands of GPR sets used in railway surveys.

Figure 4.2. Different GPR sets used in Railways [56]: a) Swedish Mala ground-coupled antenna (photo by Mala Geoscience), b) multichannel GSSI air-coupled system (from Olhoeft et al. [81]), c) GSSI 400MHz ground-coupled antenna and d) Radar Team Sweden 350MHz 1.2GHz Sub-Echo HBD antennas (photo Mika Silvast)

Fouling assessment of railway ballast using GPR has attracted many other researchers, who addressed this critical issue partially or wholly in their studies [11,15,20–23,25,28,68,77,82,84–90].

Clark et al. [11] present findings related to the electrical properties of ballast in laboratory conditions, particularly relative permittivity values in a comparative way between clean versus fouled ballast and wet versus dry ballast expressing that clean ballast has lower relative permittivity than fouled ballast and likewise, dry ballast has also lower relative permittivity than wet ballast.

The signal velocity of EM waves through ballast is crucial in converting time scale of GPR data to depth scale. Therefore numerous studies [8,11,27,77,91] have attempted to attain the EM wave velocity to be used for "time to depth GPR data conversion".

Hugenschmidt [8] found it reasonable to use an average signal velocity of 14 cm/ns for ballast medium after comparing the radar data with those from the trenches. In a similar way, Jack and Jackson [27] took an average signal velocity of 13 cm/ns for ballast in their research. Göbel et al. [91] offered the ranges of signal velocities from 12 to 21 cm/ns for clean ballast and from 0.8 to 1.2 cm/ns for spent ballast. Both of the values offered in [8] and [27] are close to the lower limit of the range of the signal velocity of clean ballast proposed by [91]. This can be explained by the water being present in the real conditions of track [27]. Maturana et al. [77] measured the signal velocity for clean ballast as 17 cm/ns whereas they found a value of 10 cm/ns for highly fouled ballast.

Published RDP values from various studies for clean and fouled (spent) conditions of granite and limestone ballast were presented in Table 4.1 [93].

Table 4.1. Published RDP values of ballast adapted from Lalagüe [93]

Published RDP values of ballast			
Ballast Material	Clark et al. [11]	Sussmann [94]	Leng & Al-Qadi [65]
Type	Granite	Granite	Granite & Limestone
Dry Clean	3.0	3.6	3.25 (granite) 3.96 (limestone)
Moist Clean (5%)	3.5	4.0	
Saturated Clean	26.9		
Dry spent	4.3*	3.7	3.77 ** (granite) 4.84 ** (limestone)
Moist Spent (5%)	7.8*	5.1	
Saturated Spent	38.5*		
*The spent ballast in these tests was at the end of its economic life, where the fines have reached 10% of the total mass of the ballast			
** 50 % level of fouling corresponding to the 50% of air voids volume filled with dry clay			

In a recent study, Benedetto et al. [20] characterized clean and fouled ballast by means of using GPR, through extensive laboratory experiments, signal processing, and numerical modeling.

Scattering amplitude envelope method based on scattering energy from voids has been used to distinguish between the clean and fouled ballast [68,84,85,88,89].

Clark et al. [95] present other nondestructive methods such as infrared thermography together with GPR in visualizing the railway track bed with emphasis on the speed of the surveys.

Khakiev et al. [96] made a research which quantitatively processed GPR data in order to attain the refractive index and conductivity of railway constructional layers along with the assessment of ballast fouling.

Moisture content evaluation in soil by means of GPR data is one of the most influential and favored topics in scientific research related to GPR [77,96]. Khakiev et al. [97] in another study, investigated the long-term moisture content variation in the subgrade of a railway track bed in Russia by proposing a variable "integral reflectivity" and correlating this variable with the moisture content. In their work, direct estimation of moisture content from amplitude analysis was carried out without the calculation of dielectric permittivity.

In a number of studies, the basic difficulties in data collection with GPR on railways are mentioned [5,8,56,81]. The common drawbacks to overcome during data acquisition with GPR over railways could be counted as:

- interference from rails and sleepers (especially concrete sleepers)
- electrical wires in case of unshielded air coupled antennas
- various subsurface and near-track railway assets which require ground and side clearances for the moving antennas
- wavelength-sized ballast (in case of using higher frequencies over large sized ballast medium)

Al-Qadi et al. [5] developed a time-frequency method, which removed to an extent the interference and noise inherent in the railway environment (noise from telecommunication and signaling systems of railways, rails, overhead cables etc.), in order to enhance the quality of the GPR data in assessing the ballast condition.

As indicated in [30], frequency-based analyses, which reveal useful information about the status of the ballast, has drawn the interest of researchers in a great deal. Short-time Fourier transform methodology has been exploited in order to monitor the character changes in ballast in both time and frequency domains simultaneously [5,65,82,98]. Besides, an automatic classification system for GPR traces has been developed relying on the magnitude spectrum analysis and support vector machines to classify ballast fouling [1].

Lately, a new research trend of generating synthetic GPR responses which enables to extend real and experimental conditions in railway ballast assessment studies by means of simulation has attracted great attention of scientists since it provides a significant reduction in cost and time [30]. Finite difference time domain technique is used to simulate GPR signal in the studies [21,99–102].

However, there seems to be an open and challenging issue for evaluation of GPR signal through railway ballast under concrete sleepers and rails as it is laid in the real case. Concrete sleepers with the reinforcement bars inside them have significant masking effects in the GPR signal. In order to have clearer images of ballast, these effects should be addressed by minimizing or removing them.

Researchers also sought for the optimum surveying procedures and antennas configurations to account for the influence of ties and rails [12,82,103,104].

In early stages, surveying between the cribs (the regions between the sleepers) was one of the solutions to produce the GPR profile by overcoming the effects of sleeper [79]. Nonetheless, the information beneath the sleepers is more valuable than the ones in the cribs [68,105]. Hugenschmidt [8] used a set of processing steps namely, migration, horizontal scaling, stacking and background removal in order to reduce the effects caused by sleepers, whereas a 40-trace running average was applied to the data in an attempt to remove the ringing effect of the sleepers in another study [71]. In a

recent study, sleeper noise suppression is achieved via an algorithm where GPR data was filtered by multiband-pass filter adjusted according to the spectrum features of the sleeper noise [106]. Researchers used the uniform spacing between sleepers and designed a wavenumber notch filter. The resulting image was free from the backscattering from the concrete sleepers which made reflections clearly visible [107]. Liao et al. [108] employed parabolic radon transform in order to eliminate the effects from railway sleepers. In a recent study in China, a time-space filter screen possessing the interference information was developed and used to suppress the multiple waves and diffraction occurred due to the sleepers, which in turn led to the improvement of the signal to noise ratio of the GPR records [109].

5   USED GPR EQUIPMENT, HARDWARE & SOFTWARE

In this chapter, GPR equipment used for the laboratory and field surveys will be elaborated. GPR hardware will be explained in detail. And software used for data acquisition and data post-processing will be introduced with their main features.

5.1   GPR Sets and Hardware Used

Three different GPR sets were used during the dissertation work.

- a GPR kit, which is owned by the Department of Transport Structures at the Faculty of Transport Engineering, University of Pardubice
- Within the scope of co-operation with SŽDC, part of their GPR set was used
- GPR set of Engineering Department of University of Roma Tre

5.1.1   GPR set owned by University of Pardubice

RIS Hi-Pave system provided by Ingegneria Dei Sistemi S.p.A. (IDS) was used. It consists of multichannel controllers DAD Fast Wave (described below), 12V 12Ah battery, pair of antennas (described below), the measuring wheel (odometer), an aluminum frame and glass fiber shoulder, mechanical fastening TR Dual F, coaxial, power and data cables as well as the Panasonic CF-53 Toughbook for recording and processing of data.

A wooden GPR antenna holder frame was constructed and used in the experiments realized under the Sections 6.2, and 6.3 which is explained in detail in Sub-Section 6.2.2. For undertaking the measurements on real tracks, a special GPR railway cart was designed and constructed in the laboratories of Educational and Research Centre in Transport, Faculty of Transport Engineering, University of Pardubice. The details of the GPR railway cart, which is used for the field track surveys is described in Sub-section 6.4.3.

5.1.1.1 DAD Fast Wave Dashboard from IDS

The DAD Fast Wave Control Unit, described in Figure 5.1, is the controller responsible for antennas management and digitization of acquired GPR data.
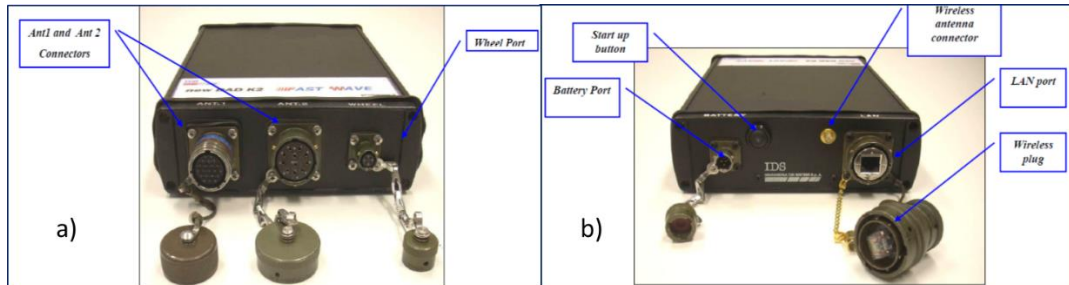
Figure 5.1. DAD Fast Wave: a) side with connections to position sensor and antenna b) side with Battery Port, Lan Port and wireless connector [110].

Technical specifications of control unit DAD Fast Wave:

- Pulse frequency: 400kHz;
- Scanning speed: up to 4760 scans per second (@ 128 samples per scan)
- Range: up to 9999ns;
- Number of A / D converters: 2;
- Data acquisition frequency (A / D clock): 400kHz;
- Sampling: 16bit;
- Resolution: More than 5 psec;
- Number of samples per scan: 128-8192 (1 channel); 128-4196 (2 channels); 128-2048 (4 channels);
- Ports: Antenna 1, Antenna 2, Odometer, LAN, Battery;
- Maximum number of antennas: 2 standard; up to 8 TR with expansion box; up to 4 TR DUAL F;
- Number of Channels 8;
- Dimensions: 22cm x 17cm x 5.5cm;
- Weight: 1.5 kg;
- Dust and water resistance (IP 64);
- Average consumption: <10 W

5.1.1.2 Used IDS antennas

Two sets of antennas are used both of which are shown in Figure 5.2, i) air-coupled shielded dipole antenna HN-2000 with central frequency of 2GHz, ii) ground-coupled TR Dual Frequency antenna with central frequency of 400/900MHz.

Figure 5.2 IDS antennas: left picture air-coupled 2GHz horn antenna, right picture ground-coupled TR dual frequency antenna (400/900MHz)

Technical specifications for the antennas:

Technical specifications for the antennas are demonstrated in Table 5.1.

Table 5.1. Technical specifications for the antennas

	Air-coupled antenna	**Ground-coupled antenna**
Antenna model	HN-2000 antenna	TR DUAL-F 400/900
Antenna type	shielded dipole horn	bow-tie
Number of channels	1	2
Central frequency	2000MHz	400/900MHz
Dimensions	60cm x 22cm x 40cm	43cm x 37cm x 20cm
Weight	7 kg	6 kg
Operating humidity	<90%	<90%
Water resistance	IP 65	IP 65
Operating temperature	-40 ° C to 50 ° C	-40 ° C to 50 ° C

5.1.2   GPR set of SŽDC

The GPR set and GSSI antennas of SŽDC were used during the field surveys described in Section 6.4. The available information about those antennas are the central frequencies (400MHz for the ground-coupled antenna, 1GHz for the air-coupled horn antenna). Antennas and GPR sets to hold them are depicted in Figure 6.23 in Sub-section 6.4.3.

5.1.3 GPR set Engineering Department of University of Roma Tre

The experimental tests were conducted using 4 air-coupled systems all of which were manufactured by IDS (Figure 6.38), with three different nominal frequencies of 1000MHz (RIS Hi-Pave HR1 1000), 1500MHz (RIS Hi-Pave VEE 1500), and 2000 MHz (RIS Hi-Pave HR1 2000 and 2000 NA). Regarding the 2000 MHz radar systems, one normal (i.e., 2000MHz EU) and one depowered (i.e., 2000MHz NA) version of the horn antenna for the European (EU) and the North-American (NA) markets, respectively, were used. The same type of DAD Fast Wave control unit as in the case of GPR set of the University of Pardubice was used. Antennas are illustrated in Figure 6.38 in Sub-section 6.5.2.

5.2 Software

In this Section, software used for calibration, recording, storing, processing and interpretation of the measured GPR data will be explained.

Special software, namely K2 Fast Wave, produced by IDS and designed to acquire data, was used in this work.

For post-processing and the interpretation of the data, ReflexW software was utilized. As for GSSI unit of SŽDC, Radan software produced by GSSI is used for both data acquisition and post-processing to the author's knowledge.

5.2.1 K2 Fast Wave

The K2 Fast Wave Data Collection Software is designed to work with IDS DAD Fast Wave control units. K2 Fast Wave is able to support up to 8 antennas connected in a string and allows you to display two radar screens simultaneously in real time. It provides tools for adjusting parameters for data collection, antenna setup and calibration of individual channels. Pre-determined EM wave velocity is entered. This system can be connected to GPS and other external devices such as a digital camera. [66,110].

5.2.2 ReflexW

The ReflexW software allows the user to process and interpret data in an environment that suits the specific needs of the user. It enables import and integration of all common data formats. The 2D data analysis module provides the processing of 2D data in particular, GPR, seismic, and ultrasonic methods Moreover, it offers many data processing capabilities (filtering, profiling, composite and multi-reflection removals, static corrections, migration, etc.). including the possibility of processing the Common Mid-point (CMP) method, Normal Moveout (NMO) analysis [66,111].

6 LABORATORY AND FIELD EXPERIMENTS

This Chapter is composed all the experimental work both in the laboratory and in the field. There exist five Sections where each of the experimental work is explained in detail. All the relevant experimental data will be given in Appendices in a CD-ROM.

6.1 GPR Performance Compliance Tests

All the laboratory experiments in this Section was realized in the laboratories of Educational and Research Centre in Transport, Faculty of Transport Engineering, University of Pardubice with the GPR set of the University of Pardubice.

6.1.1 Aims and Objectives

The aim of this Section is to evaluate the performance of available GPR equipment through GPR system performance compliance tests.

6.1.2 Background

GPR systems should be calibrated periodically and their reliability of performance should be ensured, in accordance with the manufacturer's recommendations and specifications [112].

Each antenna has unique parameters and performance. Performance of antennas may change over time. Prior to initiating the measurement with an untested GPR system, it is appropriate first to test its stability and performance in data collection. This could eliminate mistakes and interpretation of unexpected distortions in the data [66].

Since GPR is considered as a powerful tool providing considerably accurate and reliable data in a continuous and fast way, the necessity to assure that a GPR system is functioning properly and serving reliable and good quality results, has arisen. In order to address this necessity, the performance of the GPR set should be assessed at regular intervals.

The American Society for Testing and Materials (ASTM) has published several standard test methods [113–115] related to GPR, however, none of them was focused

on an elaborated analysis of the system performance, especially in view of exactness and partiality (bias) of the testing variable of concern [116].

Within the scope of COST TU1208, guidelines, which were oriented towards the performance of GPR antennas, were defined to test the performance of GPR equipment. Proposed guidelines define four tests; i) signal to noise ratio, ii) signal stability, iii) linearity in the time axis and iv) long-term stability [112]. Several members of COST TU1208 Action at different countries conducted these tests at different times and evaluation and discussion of the results of those tests yielded well-organized guidelines. Although the same threshold values stated in the ASTM Standard D 6087-08 [113] were used in the proposed guidelines, it should be noted there are still discussions on those threshold values whether they are over-restrictive or not. An alternative set of threshold values is proposed in [112].

6.1.3 Tests, Parameters, and Criteria [112]

COST TU1208 guidelines for the performance compliance of GPR systems propose procedures for four tests: Signal-to-Noise Ratio, Signal Stability, Linearity in the Time Axis and Long-term Stability test. The test procedure is similar for all tests, where antennas are placed at a certain height above the metallic reflector and then a certain number of traces are recorded. Common parameters for all tests are [112]:

- Warm-up time – should be at least 30 minutes or according to recommendations by the manufacturer.
- Size of the square metal reflector (L) – depends on the central frequency of the antenna, and is given by equation (5):

$$L = 2 \cdot \sqrt{5} \cdot \lambda_C \qquad\qquad (5)$$

where $\lambda_C = c/f_c$ is the wavelength at the central frequency (f_c), and c the speed of light.

6.1.3.1   Test 1: Signal-to-Noise Ratio

Two series of measurements are performed in these tests, Considering two different heights between the metal plate and the antenna.

In the first series of this test, parameters are as follows:

- The height of the antenna is $h_1 = 2\lambda_c$;
- The time window (TW): at least twice the two-way travel time from the antenna to the metal plate (TW>$8\lambda_c$/c).
- 100 traces are to be recorded.

The average amplitude "A_{mp}", i.e., the average peak-to-peak amplitude of the first echo coming from the metal plate is taken.

For the second series of measurements, GPR parameters are the same as in the first series. However, the height of the antenna from the metal plate and the measured amplitude is different.

- The height of the antenna is $h_1 = 2\lambda_c$
- The suggested relevant time window starts $2\lambda_c$/c [ns] after the absolute maximum amplitude of the signal and the suggested relevant time window is $2\lambda_c$/c [ns] long.
- The average amplitude "A_n", which is the average peak-to-peak amplitude of the noise, over a relevant time window is measured.
- 100 traces are to be recorded.

After calculating both "A_{mp}" and "A_n", from the first and second sets of measurements, respectively, an indicator value for the signal-to-noise ratio can be calculated, by using the following equation (6):

$$Indicator_{SNR} = \frac{A_{mp}}{A_n} \tag{6}$$

The GPR system is supposed to have an indicator value higher than 20 (+26.0 dB), to pass this test.

6.1.3.2   Test 2: Signal Stability

Signal Stability test uses the same test configuration as in the first series of measurements in Signal-to-Noise Ratio test is used, with h_1. The TW should be at least twice the two-way travel time (TW>$8\lambda_c$/c) and 100 traces at the maximum data acquisition rate of the GPR system have to be recorded. The signal stability should be evaluated using the following equation (7):

$$SS = \frac{A_{max} - A_{min}}{A_{avg}} \qquad (7)$$

where A_{max} is the maximum, A_{min} the minimum and A_{avg} the average peak-to-peak amplitude of the metal plate reflection, selected among all 100 recorded traces, and *SS* is the signal stability indicator ratio. This ratio should be less than 1 %.

6.1.3.3   Test 3: Linearity in the time axis

Three sets of measurements are carried out in test 3. The same test configurations as described in Signal-to-Noise Ratio test are used. For the third set of measurements, $h_3 = 2.5\lambda_c$ is used. The TW should be at least twice the two-way travel time, at the longest distance h_2 (TW>$12\lambda_c$/c). A single trace is recorded per configuration. For each configuration, i (i = 1, 2, 3), corresponding to h_i, the time delay Δt_i is determined. The time delay is defined as the difference between the absolute maximum amplitude of the direct wave and the absolute maximum amplitude of the signal coming from the metal plate.

The absolute differences are calculated as: T_{21}=|$\Delta t_2 - \Delta t_1$|; T_{31}=|$\Delta t_3 - \Delta t_1$|

Then, the corresponding speed factors C_{21} and C_{31} are then calculated from equations (8) & (9):

$$C_{21} = \frac{h_2 - h_1}{T_{21}} \qquad (8)$$

$$C_{31} = \frac{h_{3} - h_{1}}{T_{31}} \tag{9}$$

The relative variation in the measured speed can be evaluated by calculating the speed factor (sf) from equation (10):

$$sf = \frac{2 \cdot |C_{21} - C_{31}|}{C_{21} + C_{31}} \tag{10}$$

The speed factor (sf) should be less than 0.02 (2%).

6.1.3.4 Test 4: Long-term stability

The same test configuration as described in Test 1, with h_1, is used. TW should be at least twice the two-way travel time ($TW > 8\lambda_c/c$). Every minute, for 120 minutes, 10 traces should be acquired. Thus, 1200 traces will be recorded in total. For each trace w (w = 1, ... , 1200) the peak-to-peak amplitude A_w of the echo from the metal plate is going to be determined.

The sliding-average amplitudes M_q (q = 1, ..., 1200 − (N − 1)) will be calculated, by using equation (11). The suggested value for N is 10.

$$M_q = \frac{1}{N} \sum_{h=0}^{N-1} A_{q+h} \tag{11}$$

The long-term stability factor is the maximum between the following two quantities obtained by equations (12) & (13):

$$Q_1 = \frac{M_{max} - A_1}{A_1} \tag{12}$$

$$Q_2 = \frac{|M_{min} - A_1|}{A_1} \tag{13}$$

where M_{max} and M_{min} are the largest and smallest values, respectively, among the M_q values. For $N = 10$, the long-term stability factor should be less than 3 %. It is advised to plot Mq against time since such a graph assists to understand the behaviour of the GPR system over time.

6.1.4 GPR Performance Compliance Tests with the GPR set of the University Pardubice

All four tests have been performed with all antennas of GPR set of the University of Pardubice, i.e., for 400MHz, 900MHz and 2GHz central frequencies. The traces were collected at auto-stacking mode. Test parameters according to the frequency of antennas are presented in Table 6.1.

Table 6.1. Parameters for GPR performance compliance tests according to the frequencies of antennas.

Characteristics of Antennas and Survey Parameters for Tests			
Frequency and Type of Antenna	400MHz - Bowtie- Ground Coupled	900MHz - Bowtie- Ground Coupled	2000MHz - Horn -Air Coupled
Time Window (ns)	15	40	60
Samples per trace	512	512	512
Wavelength λ (m)	0.75	0.33	0.15
LxL metal plate Required (m)	3.35	1.49	0.67
h1=2*λ (m)	1.50	0.67	0.30
h2=3*λ (m)	2.25	1.00	0.45
h3=2.5*λ (m)	1.88	0.83	0.38
TW>8*λ/c (ns)	20.00	8.89	4.00
TW>12*λ/c (ns)	30.00	13.33	6.00
time range for obtaining A_n, 2*λ/c (ns)	5	2.2	1

Some of the photographs taken during the measurements for the tests can be seen in Figure 6.1, where also 3.5 m x 3.5 m aluminum sheet is visible which is used as the total reflector.

Figure 6.1.Pictures during surveys for GPR performance compliance tests: left side pictures: ground-coupled antenna (400/900MHz), right side pictures: air-coupled antenna (2GHz)

6.2 Laboratory Determination of Variations in the RDP Values Granite Railway Ballast under Various Fouling Levels

All the laboratory experiments in this Section was realized in the laboratories of Educational and Research Centre in Transport, Faculty of Transport Engineering, University of Pardubice with the GPR set of the University of Pardubice.

Present Section targets to improve the current GPR railway investigation practices, where laboratory-measured RDP values of dry railway ballast by GPR under different fouling levels can reveal beneficial information during the field railway surveys with GPR. In the present work, numerous experiments have been handled by using 2 types of railway ballast and 3 types of fouling agents in a testing container. A common ballast type used on the railway lines of the Czech Republic, namely coarse granite ballast and a finer sized granite ballast were utilized. Three types of fouling agents were inserted

into both ballast materials at different times; i) sand, ii) fine-sized gravel and iii) a volumetric mixture of these two materials. Those fouling materials were placed and compacted within each ballast type in the testing container, in increasing volumes adjusted according to the air voids volume of the ballast materials. Air-coupled horn antenna with the central frequency of 2GHz was operated to collect GPR data. A metal plate i.e. total reflector at the bottom of the testing container was used during the experiments to receive a distinct reflection.

6.2.1 Aims and Objectives

The main aim of this Section is to comprehend the EM response of clean and fouled ballast materials. In order to accomplish this aim, the following objectives are set:

- To calculate the RDP of ballast under dry clean and dry fouled conditions by means of various estimation methodologies (by gradually increasing the volume of fouling material incorporated into the ballast material)
- To form a basis for the estimation of the level and type of ballast fouling by correlating the calculated RDP values from GPR acquisitions with fouling percentages based on the ballast materials and fouling agents used in the laboratory experiments, hence improve the assessment and monitoring efficiency of railway site investigations on the condition that similar ballast types used in these experiments are fouled by similar fouling agents in real track conditions.

6.2.2 Experimental Framework

This Subsection focuses on the experimental design, the methodology and the procedure followed for the experiments, the laboratory setup, and auxiliary devices.

6.2.2.1 Experimental Design & Methodology & Used Devices

A laboratory setup which is designed to fulfill the above-mentioned aims and objectives was realized in the laboratories of Educational and Research Centre in Transport, Faculty of Transport Engineering, University of Pardubice. To that effect, two types of granite ballast materials (different in sizes, finer and coarser), three types

of fouling materials (sand, fine-sized gravel, and mixture of the first two pollutants), and a GPR set owned by the Transport Structures Department of the University of Pardubice were used during the experiments. Both ballast aggregates were placed to form a railway ballast layer within a testing container in the shape of a circular truncated cone and made of polypropylene with the inner lower diameter of 82 cm, the inner upper diameter of 94 cm a with a height of 80 cm (Figure 6.2). Experiments were carried out with the available air-coupled GPR set to find out the RDP values of clean ballast firstly. Then these two types of granite ballast materials were filled up with three different fouling materials (sand, fine-sized gravel, and a mixture of these two) at different times in an increasing percentage of the volume of pollutant materials proportional to the air voids volume [65] of each ballast type at increments of 10%.
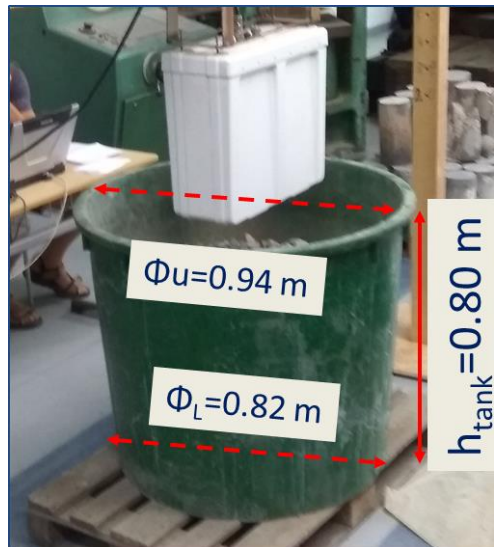
Figure 6.2. Basic dimensions of the container used during the experiments

A wooden GPR antenna holder frame was constructed and opposing holes were opened in the wooden columns to adjust the antenna to the desired height (Figure 6.3). The height of the antenna (i.e., the distance between the bottom of the antenna and the surface of the ballast) was 30 cm through all the experiments. The antenna was attached to a wooden beam.

Figure 6.3. Wooden GPR antenna holder frame

Moreover, all the necessary complementary tools (metal plate, compactors, sieves, vertical indicator sticks, etc.) were procured and prepared for the experiments. In order to acquire a distinctive signal from the bottom of the ballast, a circular metal plate (Figure 6.4a) with the diameter of 75 mm was cut out from a square metal plate in the workshop to fit the bottom of the container. And for measuring the height of the ballast, vertical indicator sticks were used with height marks on them (Figure 6.4a). The ballast height was arranged to 50 cm for the fine-sized ballast and 45 cm for the coarse-sized ballast material. For cross-checking of the thickness of the ballast, the heights of 45 cm and 50 cm were pointed inside the container with a board marker. In order to evenly distribute the contaminant materials (fouling materials), a metal grid (0.20 m x 0.20 m) was fabricated in the workshop. Equal amounts of fouling materials were placed through each opening of the metal grid at each increment of fouling process and then compacted with the compactor in order to homogenize the mixture of the ballast and fouling material for each type of ballast and fouling material. Both the metal grid and compactor are displayed in Figure 6.4b and Figure 6.4c. GPR data were collected at each fouling level for each fouling material to assess the effect of fouling phenomenon on the reflected EM signal of each type of ballast. Besides, RDP values were calculated for each fouling level from the GPR data.
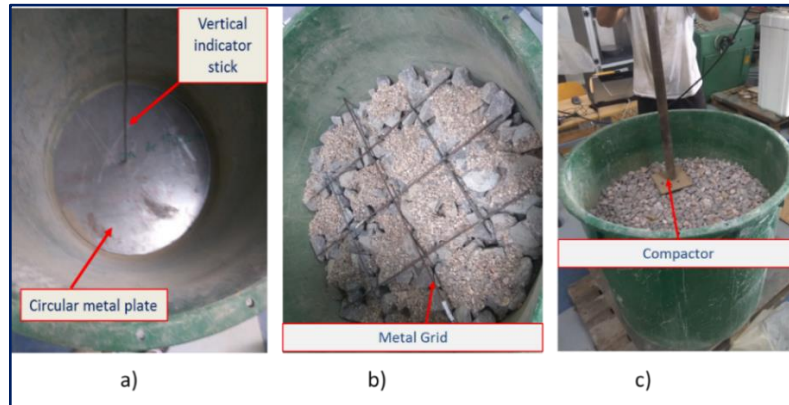
Figure 6.4. Tools used in the experiments a) metal plate and vertical stick, b) metal grid (0.20 m x 0.20 m), c) compactor

The steps below were followed in the sequence of experiments in summary:

i) Place the metal plate reflector at the bottom of the container

ii) Fill the container with ballast to the required thickness

iii) Add pollutant material proportional to the air void volume of the ballast progressively from the clean condition of ballast (0%) to the desired level of fouling. During the addition of pollutant material, use metal grid and compactor to prepare a mixture as homogenous as possible.

iv) Collect GPR data for each increment of pollutant material.

v) Empty the container and sieve out the mixture (ballast plus fouling material)

vi) Proceed from step i) to v) for the next fouling material

vii) Proceed from step i) to vi) for the second ballast material

Clean configuration and the fouled configurations with sand, fine-sized gravel and the mixture of these two fouling agents for finer granite ballast are illustrated in Figure 6.5.

Figure 6.5. Configurations of a) clean b) sand-fouled c) fine gravel-fouled d) mixture-fouled finer granite ballast

Clean configuration and the fouled configurations with sand, fine-sized gravel and the mixture of these two fouling agents for coarser granite ballast are depicted in Figure 6.6.
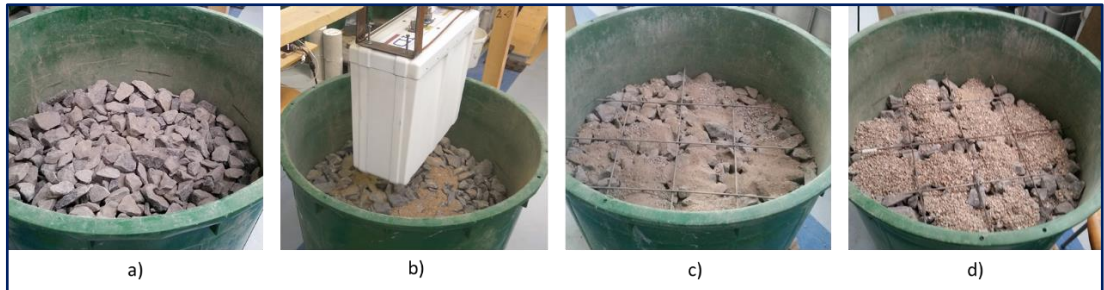
Figure 6.6. Configurations of a) clean b) sand fouled c) fine gravel fouled d) mixture fouled coarser granite ballast

6.2.2.2 *Materials and Equipment Used:*

The basic properties of the materials and equipment used during these sets of experiments are elaborated here.

Ballast:

Two types of granite aggregates were used during the experiments. One of the types was fine-sized crushed stones (with size fraction: 0-31.5 mm) produced in the Chvaletice quarry whereas the other type was coarse-sized crushed stones (with size fraction: 31.5 – 63 mm) which were procured from Žumberk quarry. The coarse-sized aggregate was amphibolite granite ballast type also used commonly in some of the railways in the Czech Republic. The ballast used during the experiments are exhibited in Figure 6.7.a whereas the same kind of ballast laid in the railway segment in Rozhovice, in the Czech Republic can be seen in Figure 6.7. And sample taken from the railway segment in Rozhovice is depicted in Figure 6.7c.
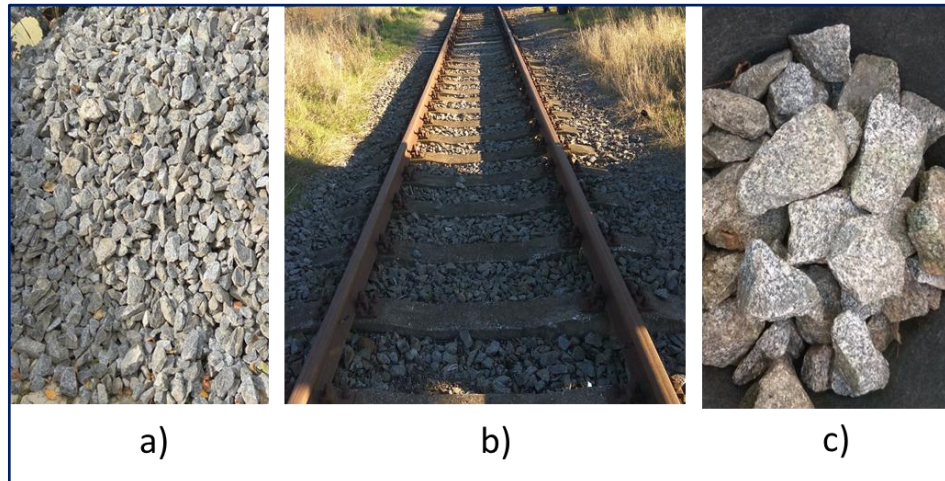
Figure 6.7. a) Coarse-size granite ballast used in the laboratory experiments, b) the same kind of granite ballast laid in the railway segment in Rozhovice, in the Czech Republic, c) sample taken from the railway segment in Rozhovice

The fine-sized granite ballast stones used during the experiments were demonstrated in Figure 6.8a, while Figure 6.8b demonstrates the same type of crushed stones which were employed during the construction of the ballasted test track with narrow track gauge (600 mm) in the Educational and Research Centre in Transport, Faculty of Transport Engineering, University of Pardubice. The technical information for both ballast materials based on the standard EN 13242:2002+A1:2007 "Aggregates for unbound and hydraulically bound materials for use in civil engineering work and road construction" [117] can be seen in detail in Appendix 1.

Figure 6.8. a) Fine-sized granite ballast stones used during the experiments, b) exactly the same type of granite aggregates used for the test track

Due to the unavailability of the sieve openings larger than 40 mm, sieve analysis for the coarse-sized ballast aggregate was not conducted. Sieve analysis for only the fine-sized granite ballast aggregate was performed as it can be seen in Figure 6.9. As revealed in the technical sheet in Appendix 1, the size fraction 0-31.5 mm and the tolerance in that fraction G_A80 (meaning minimum 80% of the materials pass the bigger size in that fraction which is 31.5 mm in this case) is also verified by the sieve analysis below in Figure 6.9, where 95% of the particles passed the sieve with the opening of 31.5 mm.
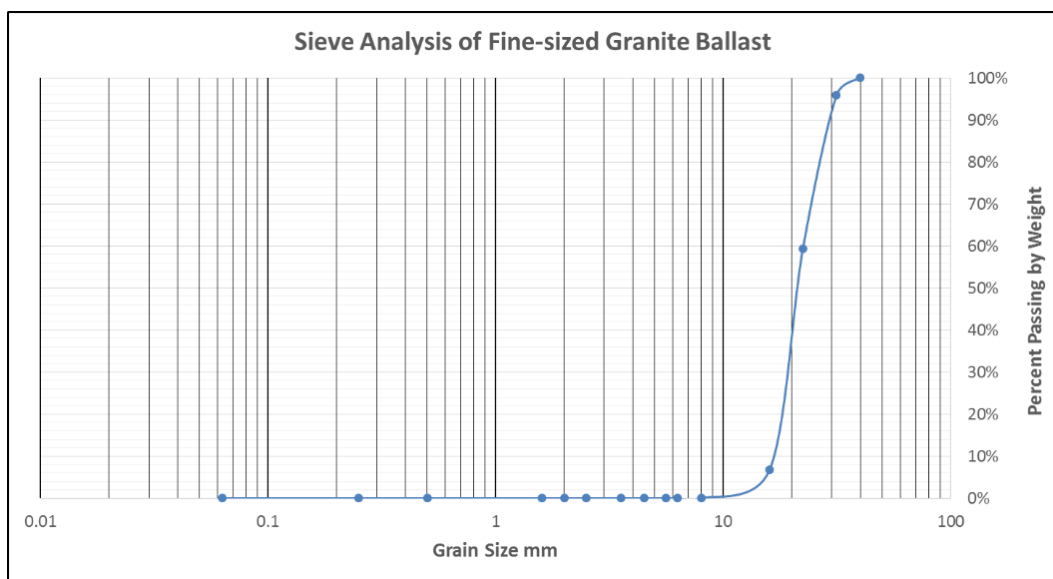
Figure 6.9. Sieve analysis of fine-sized granite ballast

According to technical sheet available in Appendix 1, the size fraction 31.5-63 mm and the tolerance in that fraction G_C85-15 (meaning minimum 85% of the materials are finer than the larger size in that fraction which is 63 mm in this case and maximum 15% of the materials are larger than the smaller size in that fraction which is 31.5 mm in this case). That means the majority of the particles i.e., 70% fall in between the size fraction values between 31.5 and 63 mm. Approximately, 450 kg of fine-sized ballast and 415 kg coarse sized ballast were utilized for the experiments. For air voids calculation within the ballast material, a laboratory container of known volume was employed as performed in a recent study by Benedetto et al. [20]. The container was filled with the ballast material until the top level and then known weights of water were added gradually into the container till the level of water reached the top of the container. Air

voids content of the ballast material was computed by dividing the total weight of water to the density of water at the temperature of this process (hence calculating the volume of water required to fill the container full of ballast), under the light of the assumption that the volume of water required to fill up the container to the top level is equivalent to the volume of air voids within the ballast (Figure 6.10). To increase the reliability of measurements, this procedure was repeated thrice for both ballast types. Average values for the air voids ratios of 38.8% and 40.1% were found out, respectively, for fine and coarse-sized, clean granite ballast types. Both values are in good agreement with the published values of clean granite ballast [65,118].

Figure 6.10. Calculation process of air voids content by volume for both ballast types a) coarse sized-granite ballast b) fine-sized granite ballast

The particle density values were 2.75 g/cm^3 and 2.63 g/cm^3 for the coarse-sized and fine-sized ballast particles, respectively, which are conformant with the expected values common (2.6-2.7 g/cm^3) in the literature for granite. Other technical data, such as the Los Angeles abrasion index, shape index, fine particles content, water absorption, sulfur content values, etc. related to both ballast types can be found in Appendix 1.

Fouling materials:

As mentioned in the Introduction Chapter, Selig and Waters [9] list the major sources of ballast fouling in the descending order of frequency of occurrence as follows: ballast breakdown (76%), underlying granular layer infiltration (13%), ballast surface infiltration (7%), subgrade infiltration (3%), sleeper wear (%1).

Fouling materials are selected with an aim to simulate the real track fouling scenarios considering the most encountered sources of ballast fouling. Fine-sized

granite ballast was mixed with three types of fouling materials (sand, fine-sized gravel, and a volumetric mixture of the first two materials). Particle infiltration from sub-ballast and/or underlying granular layer constitute a total of 16% of the sources of fouling. Besides, ballast surface infiltration has a role of 7% [9]. Together, they possess 23% of the total causes of ballast fouling, where the origin and size of the fouling material might be quite close to sand used herein. Likewise, 76% of ballast fouling originates from the breakdown of ballast itself due to mainly cyclic loading by trains [9]. Fine-sized gravel (4-8 mm) is used to replicate the ballast fouling caused by ballast breakdown with its similar size and relatively similar nature to the broken-down ballast. When the volumetric mixture of sand and fine-sized gravel is employed in addition to their individual usage as pollutants within the ballast, this combination of three fouling materials will likely to cover a substantial percentage of the sources of ballast fouling for each ballast type used in these experiments.

Sieve analyses of sand and fine-sized gravel are indicated in Figure 6.11 & Figure 6.12. According to Standard Proctor test results, sand has 1.75 g/cm^3 maximum dry unit weight with the optimum moisture content of 11.8%. Sieve tests were performed with the available 14 sieve sizes (40 mm, 31.5 mm, 22.4 mm, 16 mm, 8 mm, 6.3 mm, 5.6 mm, 4.5 mm, 3.55 mm, 2.5mm, 2 mm, 1.6 mm, 0.5 mm, 0.25 mm). The sieves were put into place on a sieve-shaker in a descending sieve opening (aperture) size from top to bottom. The samples were placed on top of the coarsest sieve and the cover was fixed and then the sieving process was started (Figure 6.13).

Required amounts of fouling materials were utilized which correspond to the desired fouling levels at increments of 10% of the air voids volume within both ballast materials at different times. As for the fouling materials of i) sand and ii) the mixture of sand and fine-sized gravel, fouling levels from 0% (clean ballast) to 100% (highly fouled) were gradually arranged at 10 % increments. However, when fine-sized gravel was used as fouling material, fouling levels from 0% (clean ballast) to 50% were uniformly distributed and compacted within the ballast. GPR data were not collected after 50% of fouling level was reached since compaction of the fine-sized gravel was not sufficiently effective and distribution of the fine-sized gravel into ballast material was not adequately uniform after this level of fouling.
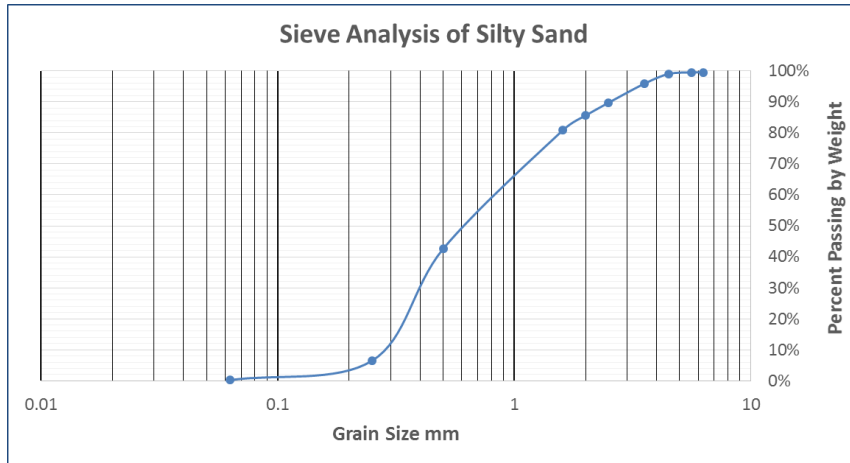
Figure 6.11. Sieve analysis of sand
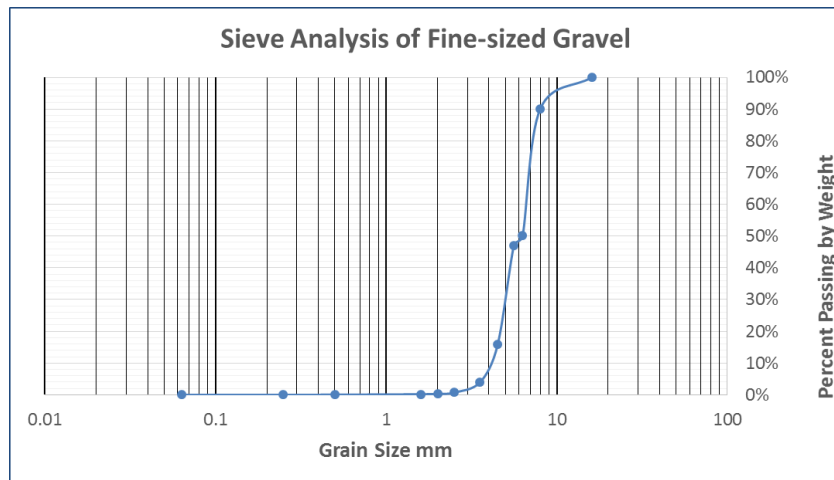
Figure 6.12. Sieve analysis of fine-sized gravel

Figure 6.13. Sieve-shaker

85

GPR Set:

The experiments were conducted using the 2GHz air-coupled horn antenna owned by the University of Pardubice, details of which were stated in Section 5.1. Data acquisitions were performed with a time windows of 15 ns and 512 samples per scan based on the recommendation of the manufacturer. The traces were recorded in auto-stacking (static) mode.

6.2.3 Relative Dielectric Permittivity (RDP) Estimation Methods:

RDP value (ε_r) of railway ballast gives a preliminary insight on the condition of ballast in terms of its fouling level (i.e. clean, fouled, and highly fouled) based on published literature values for that particular type of the ballast. Three methods were used to compute RDP values, namely, Surface Reflection Method (SRM), Known Height Method (KHM), and Complex Refractive Index Model (CRIM).

Before computing RDP values, Ionescu fouling index values were determined for finer ballast and the three types of fouling materials by means of the sieve analyses for those materials. However, 16 mm and 0.063 mm sieves, which were available in the laboratory and the closest to the ones used in the Ionescu formula (equation (2)), were used instead of 14 mm and 0.075 mm sieves, respectively. Therefore, obtained fouling index values are called modified Ionescu fouling indices. As a result, the following values were obtained which relate the percentage fouling levels to the modified Ionescu fouling index (Table 6.2), where also the fouling categorization values which were modified from [9] presented in Table 1.2 were used herein.

For coarser granite ballast, the index values presented in Table 6.2 can be accepted as valid, since the grading between the two types of ballast after 16 mm sieve can be assumed approximately the same. The abbreviations MF and F stand for "Moderately Fouled" and "Fouled", respectively in Table 6.2.

Table 6.2. Modified Ionescu fouling index values for finer granite ballast fouled by a) sand, b) fine-sized gravel, c) the mixture

Fine-Sized Granite Ballast + Sand									
Volume Percent of Fouling Material	10	20	30	40	50	60	70	80	90	100
Modified Ionescu Fouling Index	11.2%	15.2%	18.9%	22.2%	25.3%	28.1%	30.8%	33.2%	35.5%	37.7%
Fouling Category	MF	MF	MF	F						

Fine-Sized Granite Ballast + Fine-Sized Gravel									
Volume Percent of Fouling Material	10	20	30	40	50	60	70	80	90	100
Modified Ionescu Fouling Index	10.8%	14.4%	17.8%	20.9%	23.8%	N/A				
Fouling Category	MF	MF	MF	F	F	Should be fouled (F) since much more fouling material is added				

Fine-Sized Granite Ballast + Mixture of Sand and Fine-Sized Gravel									
Volume Percent of Fouling Material	10	20	30	40	50	60	70	80	90	100
Modified Ionescu Fouling Index	11.1%	15.0%	18.6%	21.8%	24.9%	N/A				
Fouling Category	MF	MF	MF	F	F	Should be fouled (F) since much more fouling material is added				

6.2.3.1   *Surface Reflection Method (SRM) [62]:*

This method is suitable for the GPR systems with only air-coupled antennas to prevent the near field zone effects. This phenomenon is caused by the strong EM field around the antenna within a radius of about 1.5 wavelengths of the central frequency generated by EM energy emitted from the antenna. In case of ground-coupled antennas near field zone is larger than the one in system with air-coupled antennas due to two reasons [62]: i) ground-coupled antennas are directly emplaced on the surface, causing the surface reflection remaining in the near field zone, whereas there is an air gap between the antenna and the surface in air-coupled systems, ii) generally ground-coupled antennas operate with lower frequencies compared to air-coupled antennas do. In this method, RDP value is calculated by comparison of the reflection amplitude from the surface of ballast with the same from the metal plate as indicated in equation (14) [56].

$$\varepsilon_a = \left(\frac{1 + \frac{A_s}{A_m}}{1 - \frac{A_s}{A_m}} \right)^2 \tag{14}$$

where ε_a is the RDP value of the ballast layer, A_s is the amplitude of the reflection from the ballast surface and A_m is the amplitude of the reflection from the metal plate (100% reflection case, i.e. total reflector).

6.2.3.2   Known Height Method (KHM):

Arguably, one of the most reliable and traditional methods to estimate the permittivity values is the so-called known height method where the height of ballast layer (either clean or fouled) is known. In this method, the temporal differences between the maximum reflection amplitudes of air/ballast interface and the ballast/metal plate interface are used as illustrated in Figure 6.14. This temporal difference is widely known as two-way travel time (twt) in GPR glossary. To obtain RDP (ε_r) of ballast, following formulas were used.

$$v_r = \frac{2 \cdot h}{twt} \tag{15}$$

$$\varepsilon_r = \left(\frac{c}{v_r} \right)^2 \tag{16}$$

where v_r is the EM wave velocity through the ballast medium, h is the known height of the ballast layer, twt is the two-way radar travel time that the EM wave is transmitted to and reflected back from the target or interface of interest (the ballast layer in this case), ε_r is RDP of railway ballast, c is the speed of light. The EM wave velocity through the ballast medium is computed from equation (15) since the height of the ballast layer is known and two-way travel time is obtained from GPR acquisitions as the time difference between the air/ballast surface interface and ballast/metal plate interface. These interfaces are identified according to the maximum amplitudes along the time samples of the averaged single trace. In ReflexW post-processing software [111], wavelet extract function was used to acquire a single averaged trace in order to

statistically filter the random noise out. Then using equation (16), RDP values were calculated.
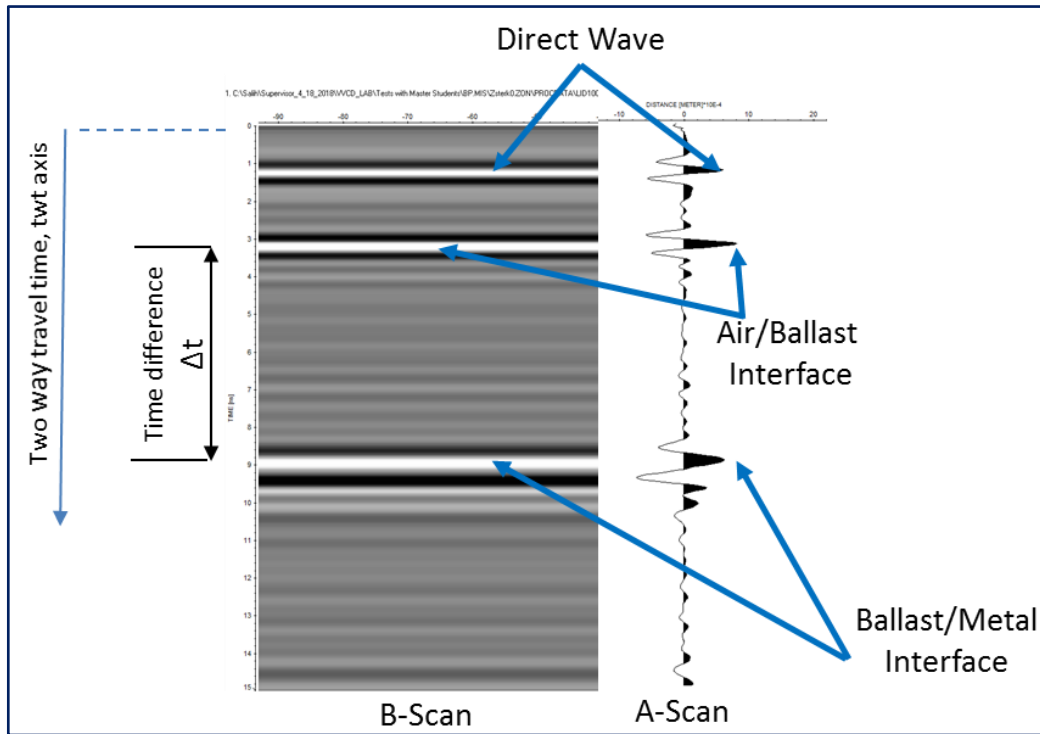
Figure 6.14. Representation of air/ballast interface and ballast/metal interface in A-scan and B-scan forms. A-scan and B-scan are both GPR acquisitions from the clean finer ballast.

6.2.3.3 Complex Refractive Index Model (CRIM) method:

Halabe et. al. [119] assessed various models for prediction of the RDP values of concrete based on parameters such as moisture and chloride content, which are likely to affect the performance of transport structures [120]. As a result of this research [119], a theoretical model, i.e., complex refractive index model (CRIM), which relates bulk dielectric features of a mixture to the same of its constituents to compute the RDP of the mixture (equation (17)), was reported to accurately estimate the RDP values of ballast for high frequencies [120].

$$\varepsilon_T{}^{\left(\frac{1}{2}\right)} = \sum_{i=1}^{n} \frac{A,i}{100} \cdot \varepsilon_{A,i}{}^{\left(\frac{1}{2}\right)} \tag{17}$$

where, $\mathcal{E}_T$ is RDP of the mixture, $\mathcal{E}_{A,i}$ is RDP of component i, and A_i=volumetric percentage of component i. Equation (17) is a specific form of the more general Lichtenecker-Rother equation developed in 1931 (equation (18)), where, a geometric factor α, which is based on the relationship between the direction of the effective layering of components and the direction of the applied electrical field, is taken as 0.5 [60]. Note that, this method does not account for micro-geometry of components and electrochemical interaction between components [60].

$$(\mathcal{E}_T)^\alpha = \sum_{i=1}^{n} \frac{A,i}{100} \cdot \left(\mathcal{E}_{A,i}\right)^\alpha \qquad (18)$$

CRIM method has been utilized for RDP estimation of clean and fouled ballast in various studies. In the research carried out by Su et.al. [87], EM wave velocities were measured by CMP method in order to calculate RDP values of ballast by means of equation (16) to be compared with the ones calculated by CRIM model. The difference between the results was reported to be within 5%, which proved the validity of the CRIM model [87]. Benedetto et al. [20], employed CRIM to verify the results of RDP values of clean and fouled limestone ballast with the ones calculated by KHM and SRM. CRIM model was also utilized to make baseline predictions for RDP values of granite ballast [120]. The values of the constituents of the mixture composed of ballast and sand and/or fine gravel used in these tests are presented in Table 6.3.

Table 6.3. RDP values of the components used in CRIM

Material	$\mathcal{E}_{A,i}$	Reference	Remark
Granite	5	Sussmann et al. [120]	The same value suggested was used.
Sand	4.5	Martinez and Byrnes [60]	Average value of lower and upper limits was used
Fine-sized Gravel	5.5	Saarenketo [56]	Average value of lower and upper limits was used

There is also a simpler version of equation (18), where the geometric factor α is taken as 1, as it can be seen in equation (19). This simple version of the mixing formula was used in [121] and was called as Effective Composite Dielectric Model.

$$\varepsilon_T = \sum_{i=1}^{n} \frac{A,i}{100} \cdot \varepsilon_{A,i} \qquad (19)$$

However, in the sets of experiments in this section, the difference of results between the RDP values (obtained by KHM and CRIM with respect to CRIM method) were within the range of 10% to 15% for finer ballast fouled by fine-sized gravel and within the range of 10% to 20% for coarser ballast fouled by gravel and mixture of sand and gravel, respectively, when this simpler formula (Effective Composite Dielectric Model) was used. Therefore, only the results from CRIM (using equation (17)) which matched well with the results from KHM are used.

6.3 Moisture Influence on the RDP Values of Granite Ballast under Clean and Fouled Conditions

All the laboratory experiments in this Section was realized in the laboratories of Educational and Research Centre in Transport, Faculty of Transport Engineering, the University of Pardubice with the GPR set of University of Pardubice

Moisture (water) can be trapped more frequently in the fouled ballast sections due to the replacement of air voids within the ballast by fouling agents hence reducing the drainage capability of the track infrastructure. The focus of this Section is on experimental assessment of the moisture influence in the clean and fouled coarse granite ballast on the GPR signal characteristics. Various tests have been figured out by using coarser granite ballast and 2 types of fouling agents in a testing container with a draining valve. Air-coupled horn antenna with the central frequency of 2GHz was utilized to acquire GPR data. Total reflector, i.e., a metal plate at the bottom of the testing container was placed during the tests to retrieve a strong reflection from the bottom of the ballast.

6.3.1   Aims and Objectives

The aim of this Section is to comprehend the influence of moisture (water) in the clean and fouled coarse granite ballast on the GPR signal characteristics. In order to achieve this aim, the following objectives are set:

- to calculate RDP of ballast under wet clean and wet fouled conditions by means of different estimation methodologies (by gradually increasing the volume of fouling material and water to be added into the ballast material)
- to construct a baseline for the prediction of the RDP values of wet clean and wet fouled ballast by comparing the RDP values with the added volumetric percentage of water for a specific fouling level.

6.3.2   Experimental Framework

This Sub-section focuses on the experimental design, the methodology and the procedure followed for the tests and the laboratory setup.

6.3.2.1   Experimental Design & Methodology& Used Devices

Coarse-sized granite ballast and 2 types of fouling materials (the previously used two fouling agents in Section 6.2, i.e., sand and fine-sized gravel) were used to establish the clean and fouled ballast configurations. For clean ballast and for specific levels of fouling (10%, 30%, and 50%) water was added gradually to introduce the moisture effect within the ballast structure in the same way as the fouling materials were added in Section 6.2 (i.e., according to the air voids volume of the ballast). GPR acquisitions were collected at each increment of water addition to evaluate the influence of variation of moisture itself and the combined effect of the changes in fouling and moisture on EM characteristics of the ballast under various conditions.

A different testing container than used in the only fouling experiments, which is equipped with a water discharging valve, was used for these set of tests. Therefore, a half-cut Intermediate Bulk Container (IBC) made of HDPE, with base sides of 1 m x 1.2 m and a height of 0.50 m, was used during this experiment (Figure 6.15).
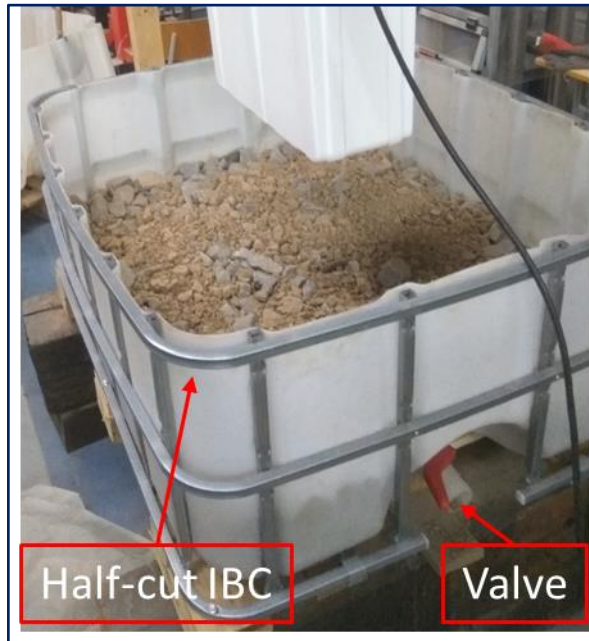
Figure 6.15. Half-cut IBC with the drain valve

The thickness of the coarse-sized ballast was 25 cm in these set of experiments. Vertical indicator sticks with height marks on them were used to measure the height of ballast as it was the case in fouling tests in Section 6.2. Also, the placement and compaction of fouling materials were performed in the same way as it was in fouling tests in Section 6.2. Approximately, 400 kg of coarse-sized ballast were used. Required amounts of fouling materials (i.e., sand, fine-sized gravel at different times), corresponding to the desired fouling levels were mixed and distributed evenly into the ballast material. Fouling levels from 0% (clean ballast) to 50% (fouled ballast) were gradually arranged for each of the fouling materials at different times. The gradual increase was realized at increments of 10% of the air voids volume within the coarse-sized ballast material. At the first half of the tests, the increments of water were 10% of the air voids, however, then 5% increments were used to better visualize the influence of the addition of the water on the overall system. As indicated in Figure 6.16, several GPR acquisitions were collected over the empty IBC and the metal plate with the base dimensions of 0.9 m x 0.9 m placed at the bottom i) without the steel grid bars surrounding the IBC, and ii) with the steel grid bars surrounding the IBC, in an attempt to evaluate the influence of these steel grid bars on the GPR signal. The reflected signals showed no differences in both cases. Therefore, the steel grid bars were not removed

during GPR measurements in order to resist the loads from the bulk materials inside the IBC (ballast, fouling material and water) which otherwise would have likely caused severe deformation of the IBC. The same wooden construction used in Section 6.2 was used to hold the GPR antenna. The height of the antenna (i.e., the distance between the bottom of the antenna and the surface of the ballast) was 30 cm through all the experiments.
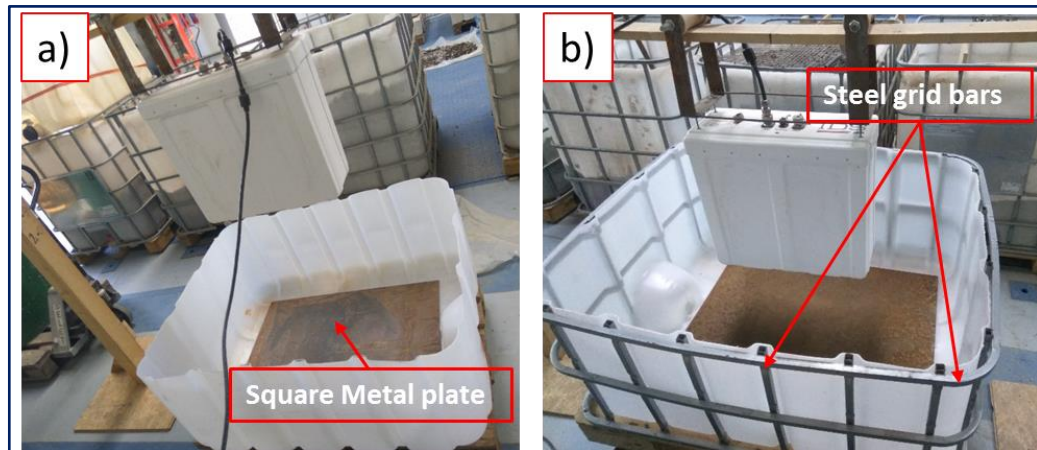
Figure 6.16. GPR trial measurements before the survey to test the effect of steel grid bars on GPR signal a) without steel grid bars surrounding the IBC b) with metal grid bars surrounding the IBC

After placing the metal plate at the bottom of the IBC and filling the tank with coarse-size granite aggregates, water was added into IBC at increments of 10%. At each increment of water addition, GPR data were collected. Then specific fouling levels of 10%, 30%, and 50% were arranged for the first two fouling materials at different times. After that for each specific level of fouling, water was added gradually and evenly into the fouled ballast until the air voids within the ballast are fully filled with fouling material and water.

The steps below were followed in the sequence of experiments:

i)   Place the metal plate reflector at the bottom of the IBC.

ii)   Fill the IBC with ballast to the required thickness.

iii)   Add water at 10% increments into the clean ballast and collect GPR data for each increment. Then remove water from IBC through discharging valve, dry the ballast

iv) Add fouling material proportional to the air void volume of the ballast from the clean condition of ballast (0%) to moderately fouled condition of 10%. At 10% of fouling level, add gradually water also proportional to the air voids of ballast into the IBC, from 0% to 90%, since 10% of fouling material and 90% of water together comprise the entire air voids in the ballast, theoretically. Acquire GPR data at each material increment. Then discharge water from IBC. Afterward, remove the mixture of wet ballast and fouling material from IBC. Sieve out the ballast and fouling material after drying them.

v) Add fouling material proportional to the air void volume of the ballast from the clean condition of ballast (0%) to moderately fouled condition of 30%. For 30% of fouling level, add gradually water also proportional to the air voids of ballast into the IBC, from 0% to 70%, since 30% of fouling material and 70% of water together comprise the entire air voids in the ballast, theoretically. Acquire GPR data at each material increment. Then discharge water from IBC. Afterward, remove the mixture of wet ballast and fouling material from IBC. Sieve out the ballast and fouling material after drying them.

vi) Add fouling material proportional to the air void volume of the ballast from the clean condition of ballast (0%) to fouled condition of 50%. At 50% of fouling level, add gradually water also proportional to the air voids of ballast into the IBC, from 0% to 50%, since 50% of fouling material and 50% of water together comprise the entire air voids in the ballast, theoretically. Acquire GPR data at each material increment. Then discharge water from IBC. Afterward, remove the mixture of wet ballast and fouling material from IBC. Sieve out the ballast and fouling material after drying them.

vii) Repeat steps iv), v) and vi) for the next fouling material.

Several test configurations such as clean dry, clean wet, fouled dry and fouled wet ballast, are illustrated in Figure 6.17.
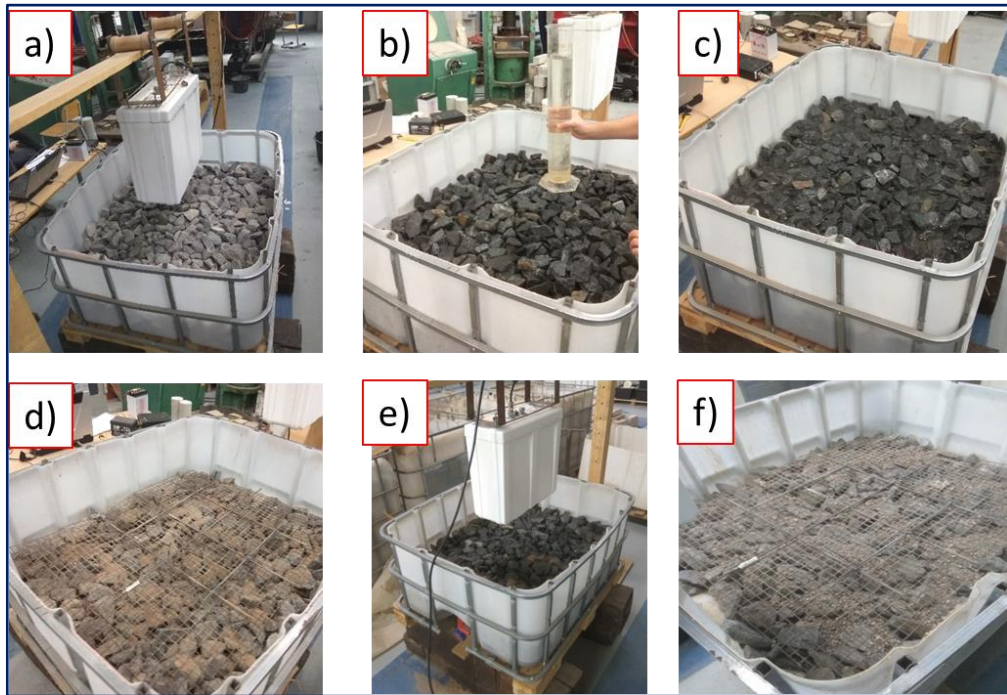
Figure 6.17. Test configurations for a) clean dry ballast, b) gradual addition of water to clean ballast via measuring cylinder, c) fully saturated ballast, d) dry ballast fouled with sand, e) wet ballast polluted with sand f) dry ballast fouled with fine gravel

6.3.2.2   Materials and Equipment Used:

The fundamental features of the materials and equipment used during these sets of experiments are described here.

Materials:

The properties of coarse-sized ballast and the first two fouling materials (sand and fine-sized gravel) used in these set of tests were already characterized in detail in Section 6.2.

GPR Set:

The experiments were conducted using the 2GHz air-coupled horn antenna owned by the University of Pardubice, details of which were stated in Section 5.1. Data acquisitions were performed with a time windows of 15 ns and 512 samples per scan based on the recommendation of the manufacturer. The traces were recorded in auto-stacking (static) mode.

6.4   Railway Field Surveys along Rozhovice Railway Station

This section presents the field surveys performed in a 138-m long railway segment nearby Rozhovice railway station passing through the road level crossing P4992. the GPR set of University of Pardubice and GPR set of SŽDC were used.

6.4.1   Aims and Objectives

The main aim of this Section is to analyze and comprehend the performance of GPR surveys on different types of sleepers with various nominal frequencies, types, and orientations of the antenna along a real railway track. In order to achieve this aim, the objective is to find out a agreement between the GPR data collected from a 138-m long railway segment nearby Rozhovice railway station and the ground truth data taken from 11 trenches (9 on the track axis, 2 on the shoulders) dug on the same railway segment including the road level crossing P4992.

The ballast material used in the railway segment is the same type of granite used in laboratories (coarse-sized granite), which provides us with the advantage of laboratory determined relative permittivity values of ballast which is one of the main unknowns when starting a GPR railway survey.

6.4.2   Location and Characteristics of the Survey Field in Rozhovice

GPR surveys were conducted in a small village called Rozhovice in Chrudim District, Pardubice Region of the Czech Republic on December 7th, 2017. The length of 138 m railway segment along the Rozhovice train station including the road level crossing P4992, was tested. The line has been closed since 2010 due to low demand for passenger transport which enabled a secure and safe survey and sufficient time for opening the 11 trenches. The ballasted railway line, which has three types of sleepers, namely, metal (in the shape of an inverted channel), wooden (made of oak tree) and concrete sleepers (SB 6 type), was constructed in 1899. However, there were no reconstruction information and no available as-built drawings of the track substructure. The weather was sunny with an average temperature of 3 C° on the measurement day of December 7th. No serious precipitation was registered recently before the

measurement day. Only a light precipitation was recorded on December 4th, 2017 [122]. The location of the performed field survey is illustrated in Figure 6.18. There was also a 10-m long road level crossing (P4992) (which is visible in both Figure 6.18 and Figure 6.19) starting at the 81.5 m of the 138-m long railway segment. Nearly half length of the tested railway segment had metal sleepers (67.5 m), whereas the portion with wooden sleepers compromises almost a quarter of the total length of the track under survey (36 m). Since the transition zones approaching the road level crossings are very critical [123] and they deform and require maintenance at faster rates than most of the railway substructure components [124], SB 6 type reinforced concrete sleepers (24.5 m. in total) took place on both sides of the road level crossing P4992 with the aim of better distribution of loading from trains uniformly onto the ballast and sub-grade and better preservation of the rail alignment.
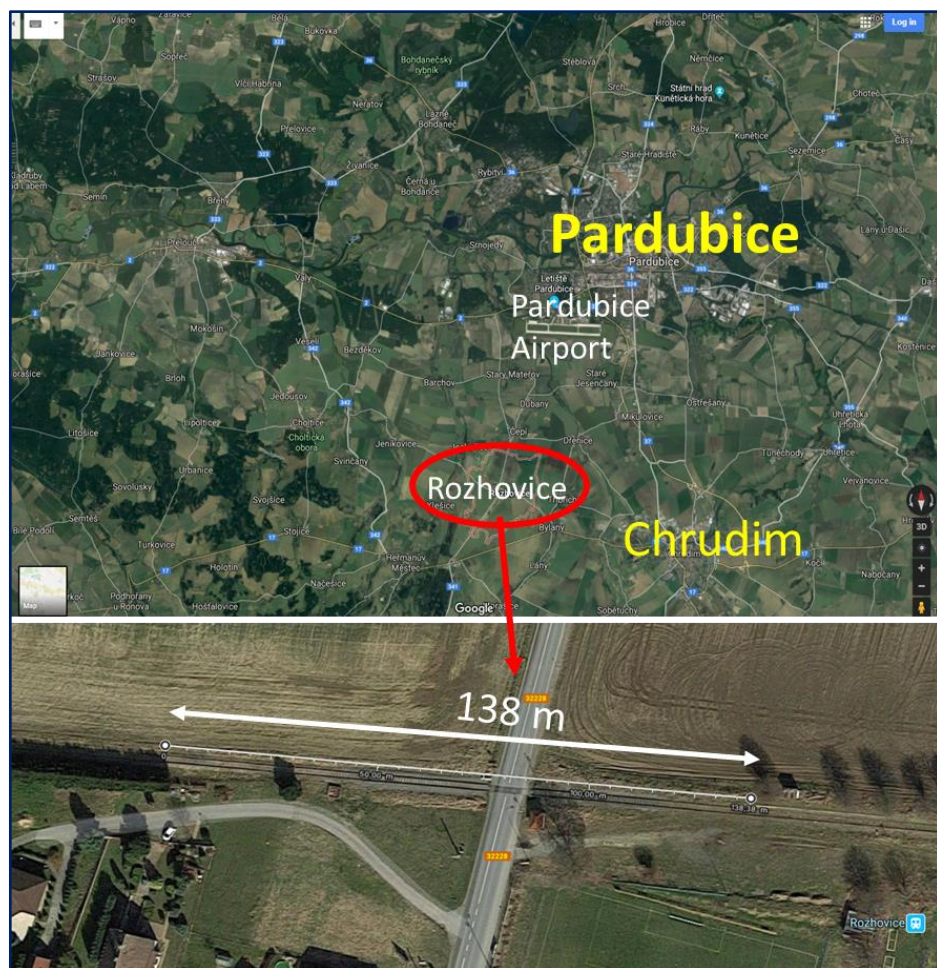
Figure 6.18. Location of Survey Field (Google Maps Overlay)

Total distribution of length of railway segment according to the type of sleepers with the mileages are depicted in Figure 6.19 which also shows the position of the ground truth trenches opened in the track axis. Two trenches, which are not situated along the track axis, but opened in the shoulders are not seen in Figure 6.19. However, they are in the same mileage as Trench 4 at 75 m. (T4 in Figure 6.19) and are positioned at offsets of 125 cm to the right and left (called briefly T4R and T4L, respectively) from the track axis.

ITINERARY OF THE SURVEYED RAILWAY SEGMENT IN ROZHOVICE (138 M LONG) WITH TYPE OF SLEEPERS ALONG AND LOCATION OF THE TRENCHES										
Additional Remarks					Level Crossing					
Mileage (m)	0	51	51	68	68	81.5	91.5	102.5	102.5	121.5	121.5	138
Type of Sleepers	Metal		Wooden (made of Oak Tree)	Concrete (SB 6 - Type)					Wooden (made of Oak Tree)		Metal
Location of Trenches (m)		T1 (54)	T2 (66)	T3 (70) T4 (75)		T5 (93) T6 (98)	T7 (106)	T8 (117)	T9 (124)		

Figure 6.19. Itinerary of the surveyed railway segment along Rozhovice station (138 m long) with the type of sleepers along and location of the trenches

6.4.3 Experimental Design & Methodology

The railway surveys were undertaken within the scope of the co-operation with Railway Infrastructure Administration in the Czech Republic (Správa železniční dopravní cesty – abbreviated as SŽDC). Therefore, this Sub-section will be divided into two parts i.e., the measurements with the GPR set of the University of Pardubice and the measurements with the GPR set of SŽDC.

6.4.3.1 Surveys with the GPR set of University of Pardubice

The railway segment was surveyed with the GPR set owned by the Transport Structures Department, Faculty of Transport Engineering, University of Pardubice. In terms of operating frequencies, both air-coupled antenna (2GHz) and ground-coupled antenna (400/900MHz), the properties of which were given in detail in Chapter 5, were utilized during the surveys. 2GHz antenna was used in three different orientations, namely, longitudinal (antenna long side axis parallel to the track axis as the way in Figure 6.20 a), oblique (angle between antenna long side axis and the track axis 45 ° as

the way in Figure 6.20b) and transverse (antenna long side axis perpendicular to the track axis as the way in Figure 6.20c) orientations. The ground-coupled antenna was used only in one orientation (longitudinal) generally recommended by the manufacturer.
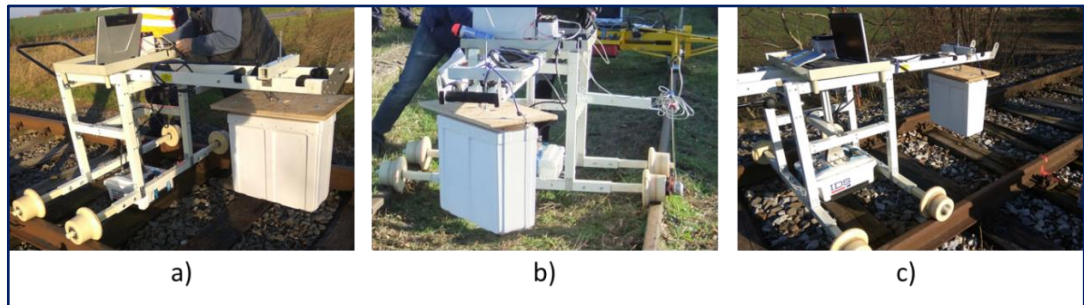
Figure 6.20. Orientations of the air-coupled antenna a) longitudinal b) oblique c) transverse

In order to smoothly perform the measurements on railways, a special GPR railway cart was designed and constructed in the laboratories of Educational and Research Centre in Transport, Faculty of Transport Engineering, University of Pardubice. All the main components of GPR set together with auxiliary parts and the constructed GPR railway cart can be seen in Figure 6.21. The detailed design drawings of this cart are available in Appendix 2. An optimum number of ironmongery (screws, nuts, angles, and washers) was used in order to both i) ensure the stability of the cart and ii) prevent the noise causing effects from the metal hardware. Railway wheels were made of polyamid and the cart was constructed with the glass-fiber reinforced plastic square profiles in an attempt to keep the signal to noise ratio as maximum as possible by minimizing the metal materials usage nearby antennas. Antenna orientations were changed by means of rotating the wooden plate (upper left corner in Figure 6.21) by 45° for oblique orientation and 90° for transverse orientation. The wooden plate is fixed to the plastic square profile over it with a screw. The orientation of the long axis of the wooden plate dictates the orientation of the antenna (the wooden plate is transversely oriented, so is the air-coupled antenna as shown in Figure 6.21).
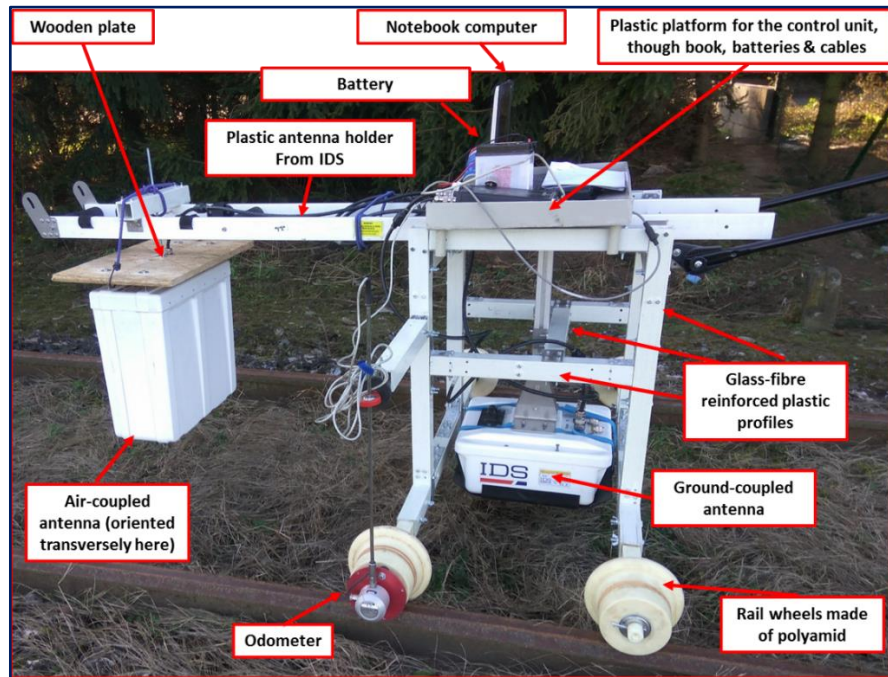
Figure 6.21. GPR cart designed for the railway surveys.

The air-coupled antenna was oriented longitudinally during the first survey. Then at the end of the first survey, the orientation of the air-coupled antenna was brought to oblique position and the second survey was overtaken way back to the starting point of the first survey. In the third survey, the antenna was oriented transversely and the advancing direction of the survey was the same as the one in the first survey. The orientation of the ground-coupled antenna was not changed between the surveys and it was always longitudinally oriented in all of the three surveys. Figure 6.22 depicts the advancing directions of the three surveys held with the GPR set of University of Pardubice.

Figure 6.22. Advancing directions of the GPR surveys held with GPR set of Univesity of Pardubice

Data acquisitions were figured out with time windows of 15 ns, and 60 ns for the air-coupled and ground-coupled antennas, respectively. And the number of samples per scan was 512 for all the antennas. A scan rate of 90 scans/m was used, resulting in over 12,000 scans for each run of the track segment under survey. Surveys were undertaken by hand-pushing the cart using the handler. The survey speed was the average walking speed i.e., 5 km/h. The air gap between the bottom of the air-coupled antenna and the surface of the ballast was 30 cm, while the gap between the ground-coupled antenna and the surface of ballast was 5 cm in average.

6.4.3.2   Surveys with the GPR set of SŽDC

400MHz ground coupled and 1GHz air-coupled GSSI antennas were used in the same railway line. Figure 6.23 below demonstrate the 400MHz antennas and 1GHz antenna attached to the cart. Surveys with longitudinal and transversal orientations with 1GHz air-coupled antenna and the survey with the 400MHz antenna located in the track axis were obtained with permission from SŽDC and used for comparison of results. GPR data collection was made with time windows of 40 ns, and 50 ns for the 1GHz air-coupled and 400MHz ground-coupled antenna, respectively. And the number of samples per scan was 1024 for all the antennas. A scan rate of 100 scans/m was used (13800 scans).
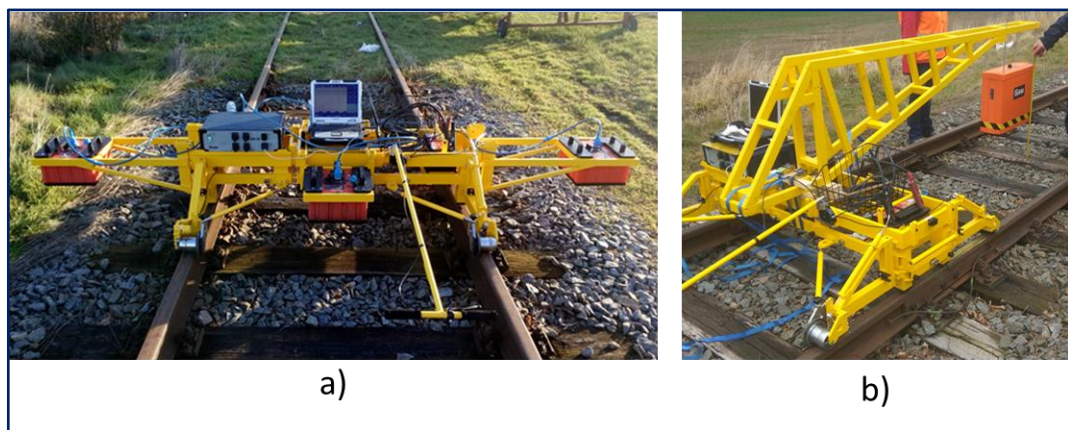
Figure 6.23. SŽDC Railway Cart with a) 400MHz ground-coupled antennas, b) 1GHz air coupled antenna in longitudinal orientation.

6.4.4 Ground Truth Data

In order to facilitate the interpretation of GPR data along the tested railway segment, 9 trenches were dug between the sleepers (cribs) on the track axis and 2 trenches were opened on the shoulder of the track. The relevant information about those trenches (mileage, type of sleepers, visual observation, layers identified, thickness etc.) are given in Table 6.4. Preliminary GPR results and coverage of all type of sleepers were taken into consideration in the selection process of the locations of the trenches.

Table 6.4. The relevant information about the trenches

Trench No	Mileage (m)	Type of Sleepers	Trench Position Track Axis (T.A.) Shoulder (S)	Visual Observation	Layers	Thickness	Total Thickness of ballast
T1	54.25	Wooden	T.A.	moderately clean ballast	#1	0-31	31
T2	65.67	Wooden	T.A.	moderately clean ballast	#1	0-28	28
T3	70.48	Concrete	T.A.	moderately clean ballast	#1	0-30	54
				moderately fouled ballast	#2	30-54	
T4	75.01	Concrete	T.A.	moderately clean ballast	#1	0-29	52
				moderately fouled ballast	#2	29-52	
T4R	75.01	Concrete	S	moderately clean ballast	#1	0-31	45
				moderately fouled ballast	#2	31-45	
T4L	75.01	Concrete	S	moderately clean ballast	#1	0-23	56
				moderately fouled ballast	#2	23-56	
T5	92.84	Concrete	T.A.	moderately clean ballast	#1	0-28	53
				fouled ballast	#2	28-53	
				underlayer-sub-balast	#3	53-72	
T6	98.40	Concrete	T.A.	moderately clean ballast	#1	0-27	53
				moderately fouled ballast	#1	27-53	
T7	106.20	Wooden	T.A.	moderately cleanballast	#1	0-30	30
T8	117.05	Wooden	T.A.	moderately clean ballast	#1	0-27	27
T9	124.20	Metal	T.A.	highly fouled and moist ballast	#1	0-39	39

The moisture (water) content w [%] of the samples were calculated by equation (19) below and presented in Table 6.5.

$$w = \frac{m_w - m_d}{m_d - m_c} \cdot 100 \qquad (20)$$

where m_w is the mass of wet the sample and the container, m_d is the mass of the oven-dried sample and the container, and m_c is the mass of the test container.

Table 6.5. Water contents of the samples from trenches

Water Contents of the samples taken from trenches								
T1	T2	T3	T4	T5	T6	T7	T8	T9
5.1%	1.2%	4.4%	3.0%	2.5%	3.5%	1.0%	5.8%	7.0%

The finer materials in the trenches were composed of a variety of materials. Mainly broken ballast and silty sand were observed. However, vegetal soil, especially under trench 9, was recorded.

Following series of pictures (Figure 6.24 to Figure 6.34) below represent the visual inspection of ballast before and/or during opening trenches, during taking samples and measuring the thicknesses of the relevant layers. The thicknesses of the relevant layers were measured in the opened trenches according to the interfaces or to the change of condition within the ballast layer based on visual observation.
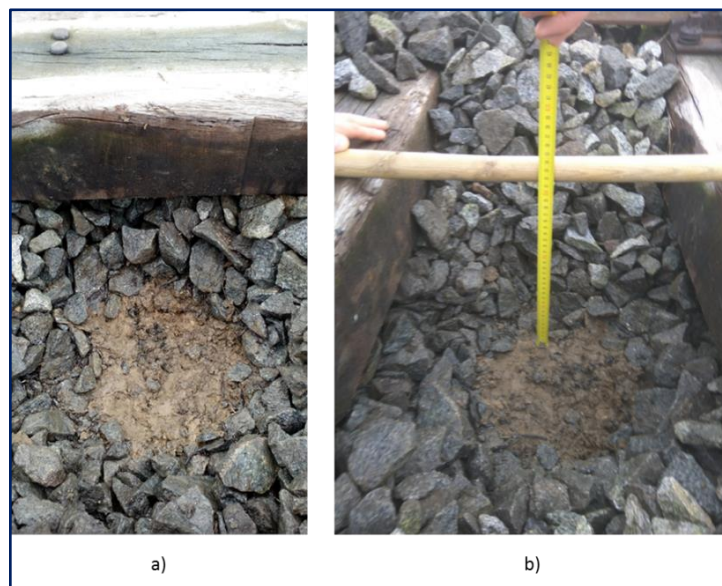
Figure 6.24. Trench 1: a) trench, b) moderately clean ballast layer thicknesses measurement
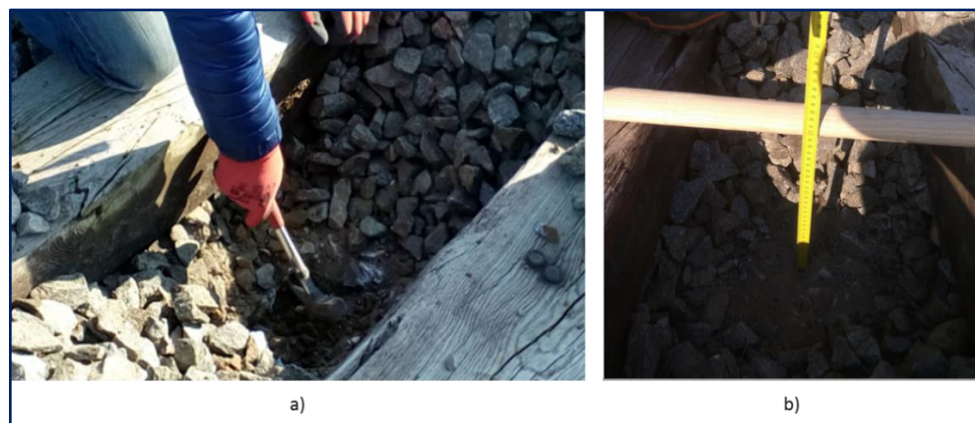
Figure 6.25. Trench 2: a) trench, b) moderately clean ballast layer thicknesses measurement

Figure 6.26. Trench 3: a) moderately clean ballast layer thicknesses measurement, b) moderately fouled ballast layer thicknesses measurement
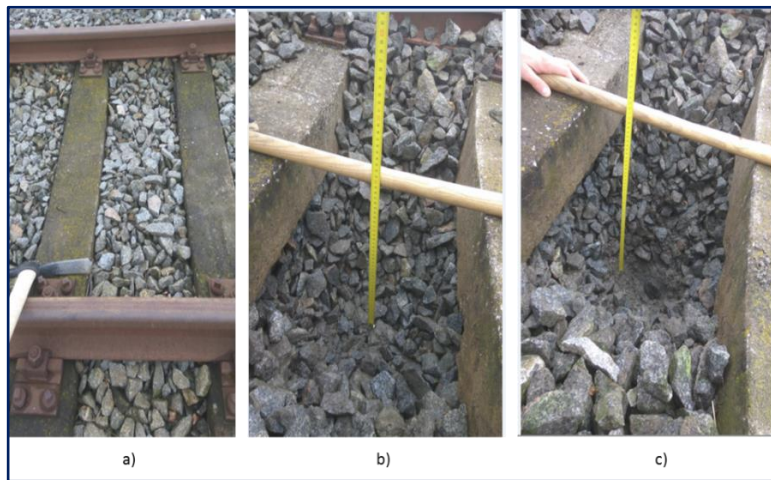
Figure 6.27. Trench 4: a) crib to be opened, b) moderately clean ballast layer thickness measurement, c) fouled ballast layer thickness measurement
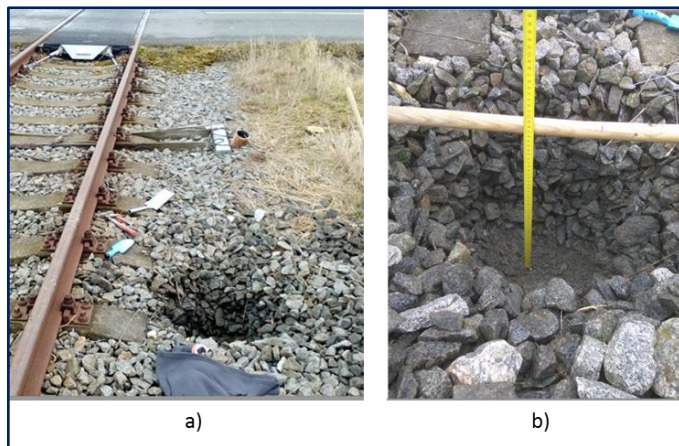
Figure 6.28. Trench 4R: a) trench itself, b) moderately clean and moderately fouled ballast layer thicknesses measurement
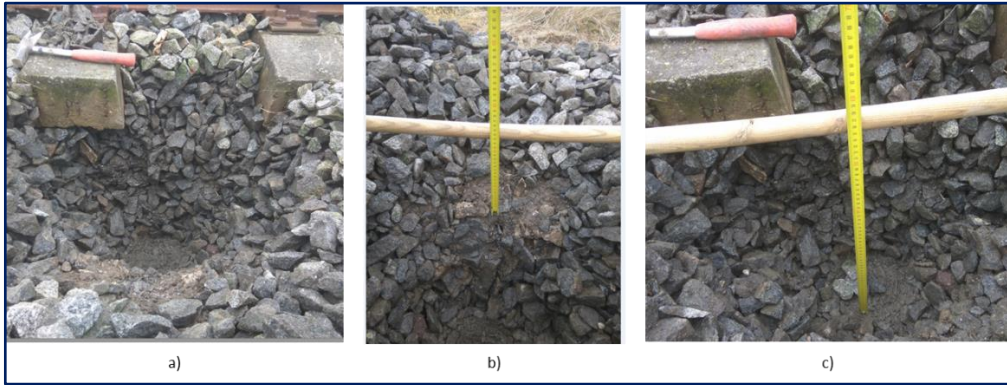
Figure 6.29. Trench 4L: a) trench itself, b) moderately clean ballast layer thicknesses measurement, c) moderately fouled ballast layer thicknesses measurement
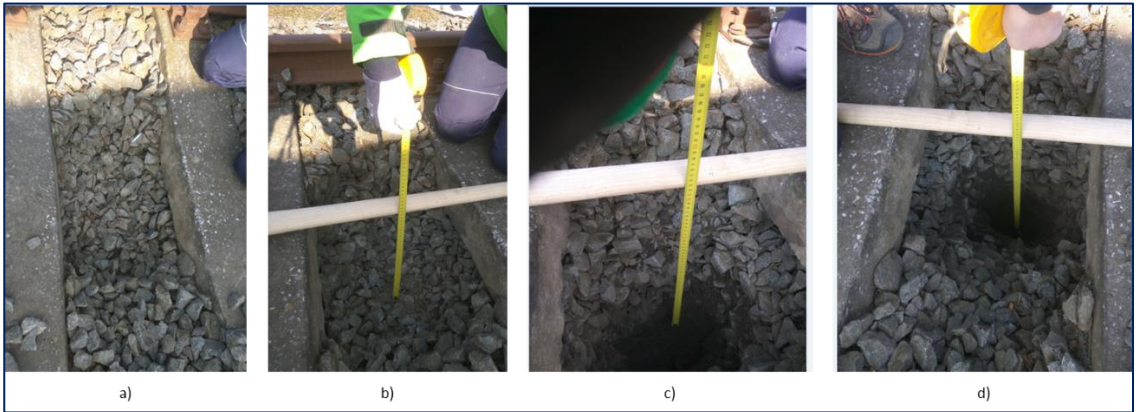
Figure 6.30. Trench 5: a) crib, b) clean ballast layer thickness measurement, c) fouled ballast layer thickness measurement, d) sub-ballast layer thickness measurement
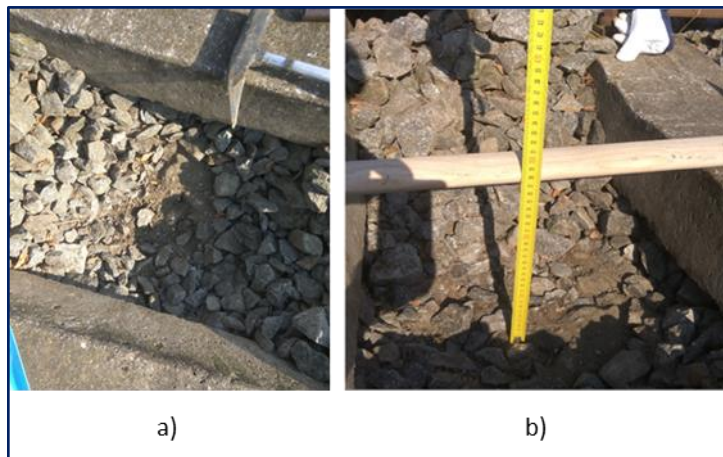
Figure 6.31. Trench 6: a) crib, b) ballast layer thickness measurement
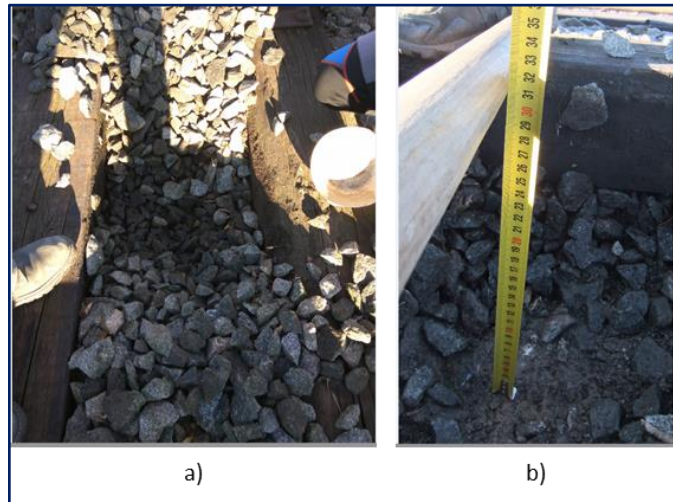
Figure 6.32. Trench 7: a) opening b) ballast layer thickness measurement
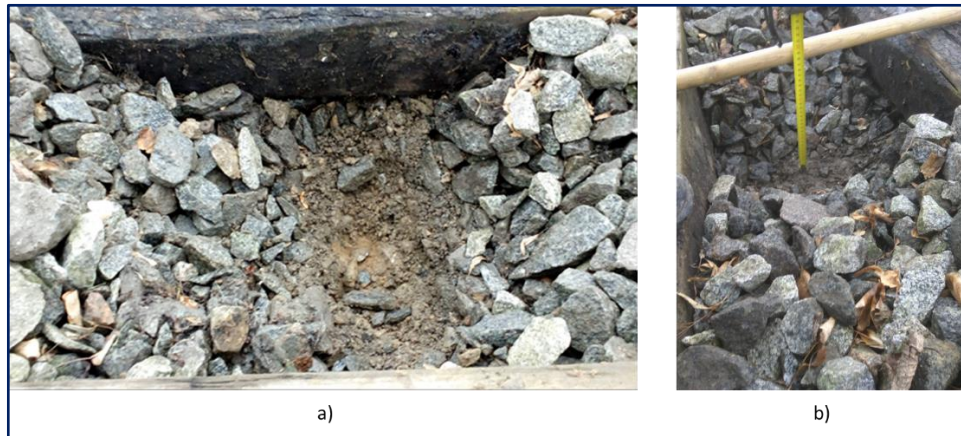
Figure 6.33. Trench 8: a) trench dug, b) moderately clean ballast layer thicknesses measurement
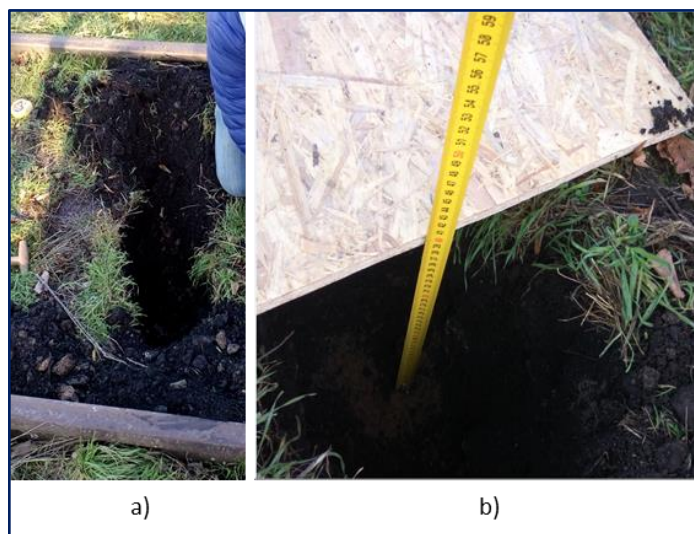
Figure 6.34.: Trench 9 a) crib b) ballast layer thickness measurement

6.5 Laboratory Assessment of Limestone Railway Ballast as a Function of Ballast Condition, Antenna Type and Frequency, Antenna Orientation, and Presence of Sleepers and Rails

All the experiments presented in this section were realized at the laboratory of Engineering department of University Roma Tre within the scope of Short Term Scientific Mission (STSM) under COST Action TU1208.

6.5.1 Aims and Objectives

The purpose of this section is to evaluate the EM response of limestone ballast material (coarsely crushed stones), under different configurations of laboratory experiments. Based on numerous different configurations, the main aim is to comprehend how and to what extent GPR signal is influenced by the clean and fouled configurations of ballast material with and without the reinforced concrete sleepers and rails by using 4 different air-coupled antennas in two different antenna orientations. A secondary goal is to determine the variation of RDP values of ballast material caused by fouling.

6.5.2 Experimental Framework and Methodology

6.5.2.1 *Preparation of the Laboratory Tests and Configurations*

As explained in very detailed in the research study of Benedetto et al. [20], ballast aggregate particles were gradually polluted with fine-grained silty soil (within the A4 group as per AASHTO) within a methacrylate tank representing a railway track bed structure. Almost 50 % of the ballast material fall in dimensions between 31.5 mm ÷ 50 mm categorically falls into Class A identified by the EN 13450:2002/AC:2004 standard [20], The ballast material in the flexi-glass was in highly fouled condition (24 %) [20] when the experiments described in this section started. Figure 6.35 given below depicts above-mentioned fouled condition.

Figure 6.35. The fouled condition of ballast in the tank at the beginning of the laboratory experiments

RFI 230 type sleeper was selected as per the code in Italy. Then, reinforced concrete sleepers were prepared accordingly. Reinforcement bars were tied. However, less number of stirrups was used in the sleepers in order just to hold the longitudinal bars and to evaluate only their effects to GPR response. Aggregates, sand, water, and cement were weighed according to the concrete mix design and sleepers were cast in concrete with required tools and appropriate workability condition of concrete provided. Preparation stage of sleepers and schematic representation of their cross-section can be seen in Figure 6.36 and Figure 6.37, respectively.

Figure 6.36. Preparation of Sleepers and placing them in the tank
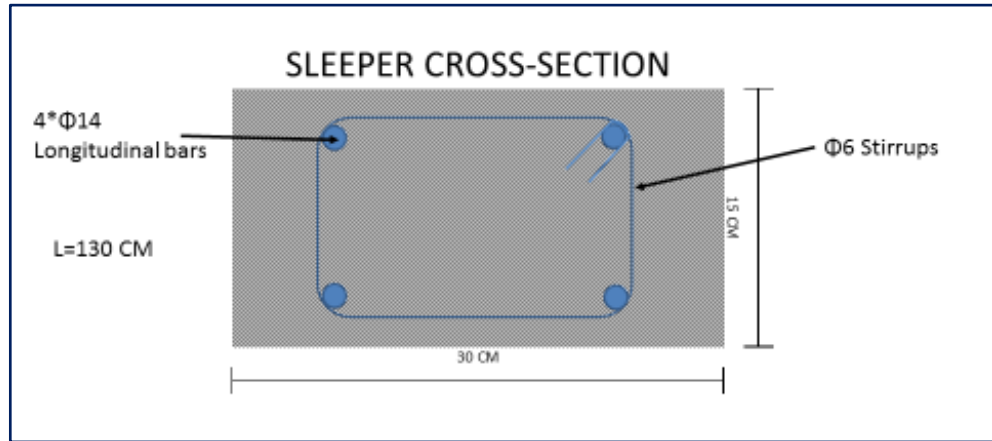
Figure 6.37. Sleeper Cross-Section

6.5.2.2   Instruments and Equipment Used for the Laboratory Experiments

The experimental tests were conducted using 4 air-coupled systems all of which were manufactured by IDS (Figure 6.38), with three different nominal frequencies of 1000MHz (RIS Hi-Pave HR1 1000), 1500MHz (RIS Hi-Pave VEE 1500), and 2000 MHz (RIS Hi-Pave HR1 2000 and 2000 NA). Regarding the 2000 MHz radar systems, one normal (i.e., 2000MHz EU) and one depowered (i.e., 2000MHz NA) version of the horn antenna for the European (EU) and the North-American (NA) markets, respectively, were used. Time windows of 25 ns for the 1000MHz and the 1500MHz systems were used and 15 ns were set for the 2000 MHz systems. 512 time samples were used for 1000MHz and 2000MHz antennas, whereas 1024 time samples were used for 1500MHz antenna.
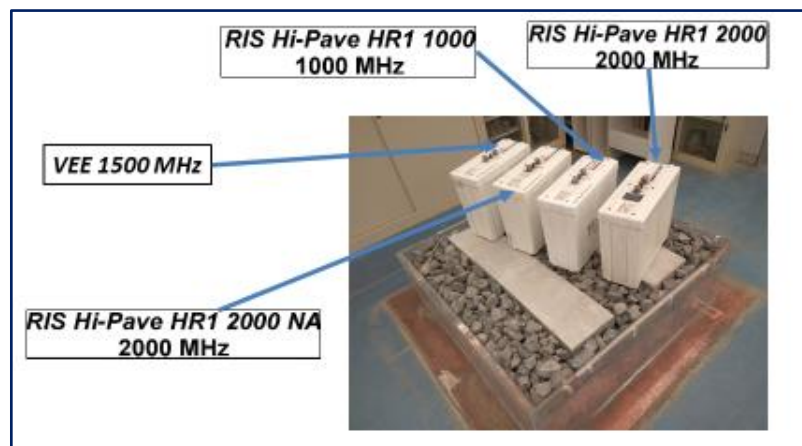
Figure 6.38. Instruments used for Laboratory Experiments

One side of the square-based total reflector metallic sheet at the bottom of the tank was 2 m by 2 m. And the square-based methacrylate tank with outer base sides and height of, respectively, 1.55 m and 0.55 m [20]. The air gap between the bottom of the antenna and the surface of ballast is 40 cm as recommended by the manufacturer of antennas (IDS). Two steel rods in a horizontal position are used to imitate the rails and they are placed such that standard rail gauge of 143.5 cm is ensured between them. The height of fouling material (silty soil) is 30 cm. All mentioned dimensions, equipment, and materials can be seen in Figure 6.39.

Figure 6.39. Basic Dimensions of the test set up

Characterization of railway ballast with respect to different configurations and scenarios in the laboratory is performed. 5 levels of parameters were tested. Figure 6.40 indicates the parameters tested in order of hierarchy during laboratory experiments.
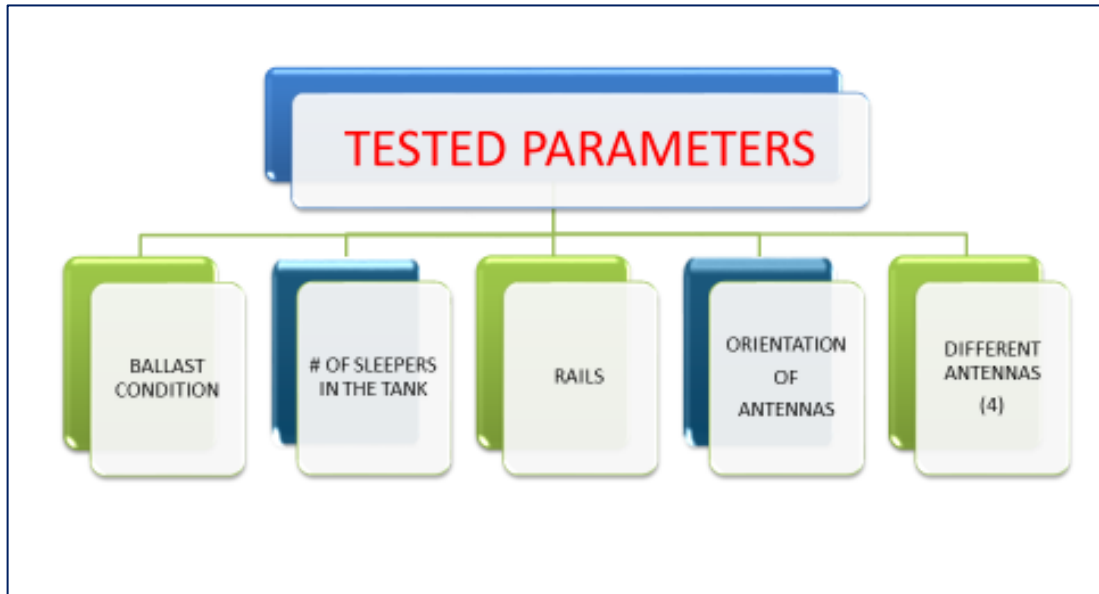
Figure 6.40. Parameters tested in order of hierarchy from left to right.

6.5.2.3   Tested Parameters

a) Ballast Condition

The major parameter tested was the fouling condition of ballast. There were two different scenarios. Fouled ballast condition (24 %) has been formed such that where the fouling material reached a height of 30 cm in the tank [20]. And the other scenario was clean ballast condition. As I expressed above, when I arrived at the laboratory of Universita' Degli Studi Roma Tre for STSM, the ballast material in the flexi-glass was already in fouled condition [20]. Then after the tests for fouled ballast have been completed, the silty soil was removed from the tank in order to perform the same tests for the clean ballast configuration. The fouled ballast configuration, removal phase of fouling material from the tank and the clean ballast configuration can be seen in Figure 6.41.
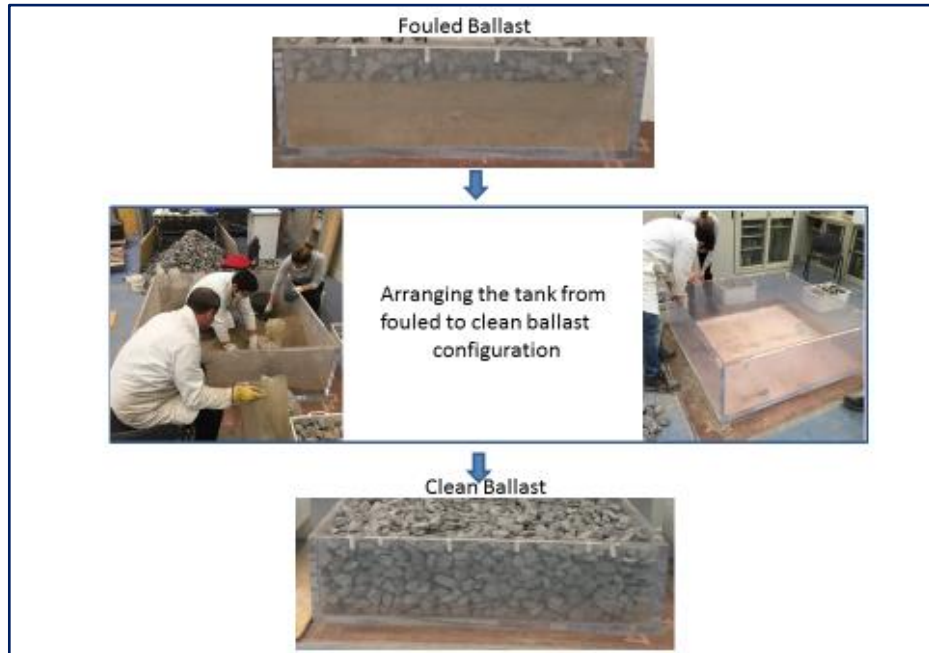
Figure 6.41. Fouled ballast configuration, the arrangement of the tank for clean ballast configuration and finally clean ballast configuration

b) Number of Sleepers in the tank

There have been three scenarios in this category; namely "no sleeper" case, "one sleeper" case and "two sleepers" case. These three different sleeper cases are tested under both fouled and clean ballast configurations as can be seen in Figure 6.42.
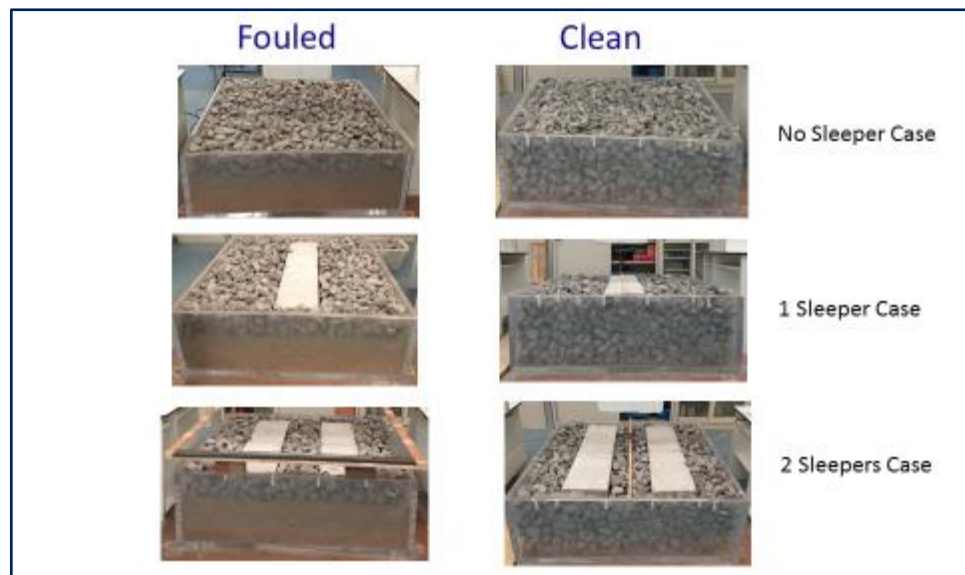
Figure 6.42. No sleeper, one sleeper, and two sleepers case in clean and fouled ballast

c) With or without rail imitating steel rods

Under "ballast condition" main category and "number of sleepers" sub-category, all the cases are tested with and without rails except for "no sleeper" case. Figure 6.43, the steel rods which are placed horizontally, are presented which are used to replicate the real rails together with "with rails" and "without rails" configurations. Also in fouled ballast condition with two sleepers case, we tried an additional steel rod which was placed vertically just under one of the horizontal steel rods to imitate the rail conditions better, however, as it will also be mentioned in the results part of this report, it turned out to have no significant effect compared to the same configuration without this vertical steel rod. Therefore, this vertical rod was not used for the other scenarios.
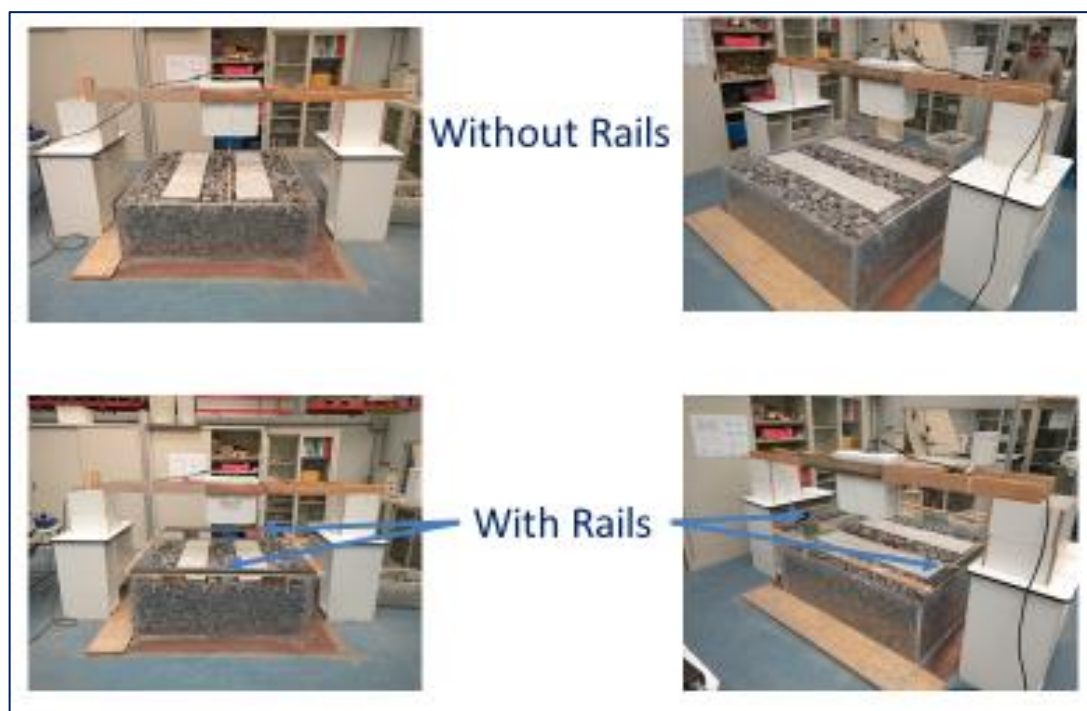
Figure 6.43. "Without rails", "With rails" cases and steel rods used to replicate the real rails

d) Antenna Orientation

This sub-category comprises two types of orientation, namely longitudinal and transverse orientations. In longitudinal orientation, the antenna is moved in such a way that the longer size of the antenna in its plan view is perpendicular to the sleepers. In other words, the antenna movement direction is the same direction as a train's traveling direction through a real track. On the other hand, in transverse orientation, the antenna

is moved in such a way that longer size of the antenna is parallel to the sleepers. Under "ballast condition" main category and "number of sleepers" sub-category and under "with rails" and "without rails" sub-category with all the cases are tested for longitudinal and transverse directions.

Figure 6.44 below, longitudinal orientations of antennas in one sleeper (upper part of Figure 6.44) and two sleeper cases (lower part of Figure 6.44) are present. The black arrows in Figure 6.44 indicate the movement of the antenna from one end to the other end. These ends are dictated by the edge influences of the tank on the GPR signal. Actually, the dimensions of the tank had been determined considering those edge effects after evaluation of the antenna's footprints as very well described in [20]. In the longitudinal orientation, the antenna is moved from -10 cm to +10 cm in 2 cm intervals at a total of 20 cm length to avoid edge effects. In figure 10, for both one and two sleeper cases, the leftmost part is the starting point of measurement with GPR antenna at -10 cm. The middle part is the central position of the route of the antenna where it is exactly located over the center of the tank, which is "zero" position. The rightmost part is the ending point of the measurement with GPR antenna at +10 cm. Figure 6.45 depicts the photographs taken exactly at the leftmost, middle and rightmost positions of the antenna during the longitudinal orientation measurements in the clean ballast configuration with two sleepers case.
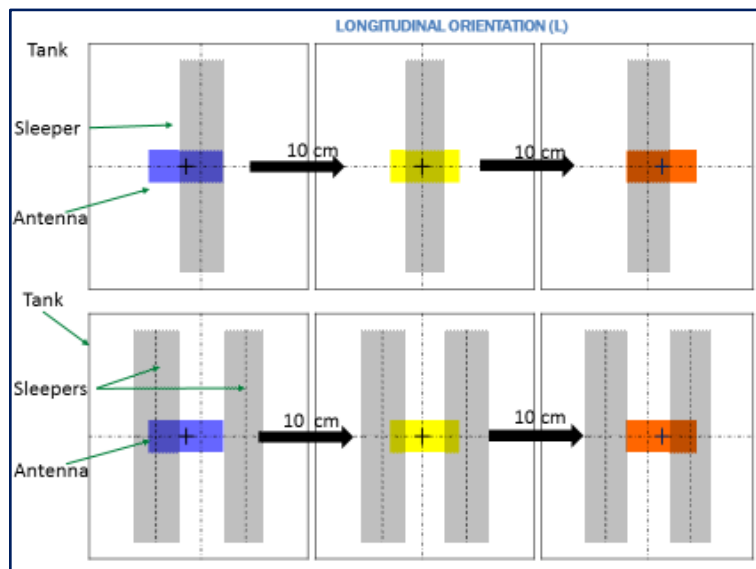
Figure 6.44. Longitudinal orientation of antenna with respect to sleepers-Upper part: One sleeper case – Lower part: Two sleepers case

From beginning point to the ending point of measurements, at each 2 cm station after moving the antenna forward, 11 acquisitions have been performed and at each data acquisition, at least 100 traces are collected in auto-stacking mode (static mode).
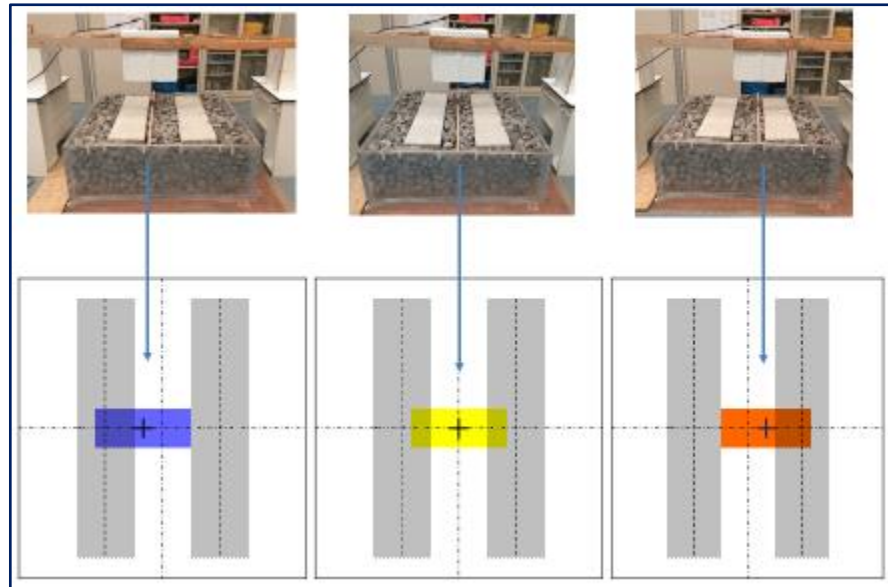
Figure 6.45. Photographs taken exactly at the leftmost, middle and rightmost positions of the antenna during the longitudinal orientation measurements in the clean ballast configuration with two sleepers case.

As for the transverse antenna orientation, measurements are performed again taking into consideration the edge effects. However, in this case, the orientation of antenna with respect to the tank allowed us to move the antenna a longer distance of 80 cm which resulted in a quite intense data collected at each 2 cm intervals from -40 cm to +40 cm in this case. In Figure 6.46 below, transverse orientations of antennas in one sleeper (left part of Figure 6.46) and two sleeper cases (right part of Figure 6.46) are shown. The black arrows in Figure 6.46 indicate the movement of the antenna from one end to the other end. These ends are dictated by the edge influences of the tank on the GPR signal. In the transverse orientation, the antenna is moved from -40 cm to +40 cm in 2 cm intervals at a total of 80 cm length to avoid edge effects. In Figure 6.46, for both one and two sleeper cases, the leftmost part where the yellow highlighted antenna can be seen, is the starting point of measurement at -40 cm. The middle placement of the antenna is the central position of the route of the antenna where it is exactly located over the center of the tank, which is "zero" position. The rightmost position is the

ending point of the measurement with GPR antenna at +40 cm. Figure 6.46 presents the photographs taken exactly at the leftmost, middle and rightmost positions of the antenna during the transverse orientation measurements in the clean ballast configuration with two sleepers case.
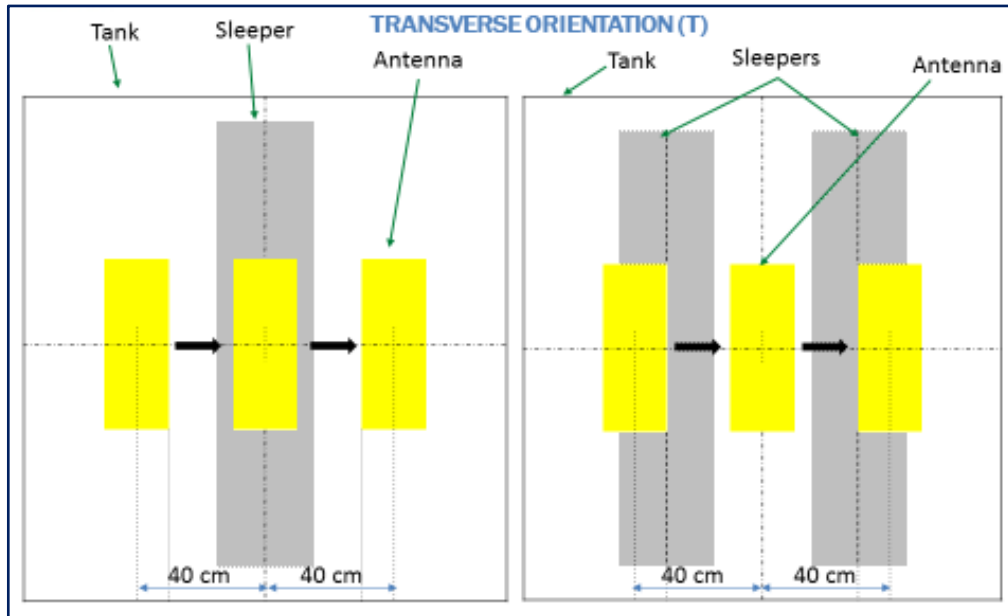
Figure 6.46. Transverse orientation of antenna with respect to sleepers;

Left part: One sleeper case – Right part: Two sleepers case

From beginning point to the ending point of measurements, at each 2 cm station after moving the antenna forward, 41 acquisitions have been performed and at each data acquisition, at least 100 traces are collected in the auto-stacking mode of (static mode).

e) Antennas used during the measurements

As already mentioned above, 4 air-coupled antennas (see figure 4 above) with 3 different central frequencies (1GHz, 1.5GHz, and 2GHz) are used for all the tests performed. For the antennas sub-category, under "ballast condition" main category and "number of sleepers" sub-category and under "with rails" and "without rails" sub-category, and under antenna orientation sub-category 4 antennas are tested with all the scenarios above them as can also be followed from Figure 6.40.

For data acquisition, K2 Fast Wave software was used, whereas ReflexW was used for data post-processing.
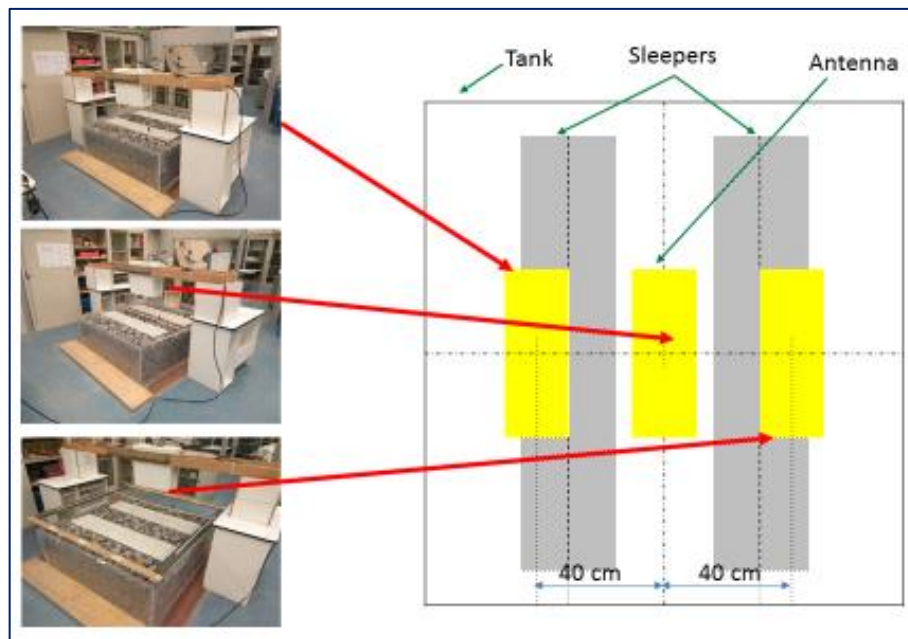
Figure 6.47. Photographs taken exactly at the leftmost, middle and rightmost positions of the antenna during the transverse orientation measurements in the clean ballast configuration with two sleepers case.

As a result of above-mentioned 5 parameters tested according to the Figure 6.40, following Table 6.6 and Table 6.7 present the main parameters (fouled and clean ballast conditions, respectively) and all the sub-categories under those main parameters together with the number of surveys performed.

Table 6.6– Tests performed under main category fouled ballast condition

Ballast Condition	Fouled Ballast														
# of Sleepers	No Sleeper				1 Sleeper				2 Sleepers						
With or Without Rails	~~With Rails only 2 hor. Metals~~		Without Rails		With Rails only 2 hor. metals		Without Rails		With Rails only 2 hor. metals		With Rails 2 hor.+ 1 ver.		Without Rails		
Antenna Orientation	~~L~~	~~T~~	L	T	L	T	L	T	L	T	L	T	L	T	
Antenna Type	2GHzE, 1 GHz, VEE, 2GHzN	2GHzE, 1 GHz, VEE, 2GHzN	2GHzE, 1 GHz, VEE, 2GHzN	2GHzE, 1 GHz, VEE, 2GHzN	2GHzE, 1 GHz, VEE, 2GHzN	2GHzE, 1 GHz, VEE, 2GHzN	2GHzE, 1 GHz, VEE, 2GHzN	2GHzE, 1 GHz, VEE, 2GHzN	2GHzE, 1 GHz, VEE, 2GHzN	2GHzE, 1 GHz, VEE, 2GHzN	2GHzE, 1 GHz, VEE, 2GHzN	2GHzE, 1 GHz, VEE, 2GHzN	2GHzE, 1 GHz, VEE, 2GHzN	2GHzE, 1 GHz, VEE, 2GHzN	42
# of Experiments	0 0 0 0	0 0 0 0	1 1 1 1	1 1 1 1	1 1 1 1	1 1 1 1	1 1 1 1	1 1 1 0	1 1 1 0	1 1 1 1	1 1 1 1	1 1 1 0	1 1 1 0	1 1 1 0	

Table 6.7– Tests performed under main category clean ballast condition

Ballast Condition	Clean Ballast																																																40
# of Sleepers	No Sleeper																1 Sleeper																2 Sleepers																
With or Without Rails	With Rails only 2 hor. Metals								Without Rails								With Rails only 2 hor. Metals								Without Rails								With Rails only 2 hor. Metals								Without Rails								
Antenna Orientation	L				T				L				T				L				T				L				T				L				T				L				T				
Antenna Type	2GHzE	1GHz	VEE	2GHzN	2GHzE	1GHz	VEE	2GHzN	2GHzE	1GHz	VEE	2GHzN	2GHzE	1GHz	VEE	2GHzN	2GHzE	1GHz	VEE	2GHzN	2GHzE	1GHz	VEE	2GHzN	2GHzE	1GHz	VEE	2GHzN	2GHzE	1GHz	VEE	2GHzN	2GHzE	1GHz	VEE	2GHzN	2GHzE	1GHz	VEE	2GHzN	2GHzE	1GHz	VEE	2GHzN	2GHzE	1GHz	VEE	2GHzN	
# of Experiments	0	0	0	0	0	0	0	0	1	1	1	1	1	1	1	1	1	1	1	1	1	1	1	1	1	1	1	1	1	1	1	1	1	1	1	1	1	1	1	1	1	1	1	1	1	1	1	1	

As seen in Table 6.6, for fouled ballast condition, 42 surveys have been conducted. And as seen in Table 6.7, for fouled ballast condition, 40 surveys have been conducted. The difference in the number of surveys performed between fouled and clean ballast conditions stem from the fact that we performed an additional pair of tests with an extra steel rod which was placed vertically just under one of the horizontal steel rods to imitate the rail conditions more realistically. However, no significant influence was observed compared to the same configuration without this vertical steel rod. Therefore, the vertical steel rod was not used for the other tests.

Some of the sub-categories in Table 6.6 and Table 6.7 are in strikethrough font, which means that those tests have not been conducted. For no sleeper case, horizontal steel rods which imitate rails were not used, since when we do not use sleepers, it does not make sense to have rails in the surveys. In specific surveys, we did not use the 2000MHz NA antenna.

If one asks about a summary of experiments performed during this set of experiments by numbers, the following will be the answer to this question:

- ➢ 1 week for preparation of sleepers (concrete casting and curing)
- ➢ 3 days for arranging the scenarios of clean and fouled ballast
- ➢ 5 levels of parameters tested
- ➢ 10 days for taking the scans from 4 antennas
- ➢ a total of 11 surveys and 82 acquisitions obtained

7 RESULTS & DISCUSSION OF RESULTS

This Chapter presents the results and discussion of results as per the experimental sections of Chapter 6.

7.1 Results of Section 6.1 "GPR Performance Compliance Tests" & Discussion

The results from the experiments described and carried out in detail in Section 6.1 will be presented in this Section together with the discussion of the findings.

All four tests have been performed with all antennas of GPR set of the University of Pardubice, i.e., for 400MHz, 900MHz and 2GHz central frequencies. The results are presented in Table 7.1.

Table 7.1. Results of GPR Performance Compliance Tests according to ASTM threshold values

Frequency in MHz	400	900	2000	Threshold Values
Signal to Noise Ratio Test- SNR	9.75	1.19	23.74	20
Signal Stability Test - SST	4.08%	15.89%	12.18%	1%
Linearity Test - LT	4.88%	3.39%	2.99%	2%
Long Term Stability Test - LST	0.14%	0.63%	1.22%	3%

According to the Table 7.1, 2GHz antenna passes the tests 1 and 4, whereas 400MHz and 900MHz antennas pass only test 4.

The threshold values, particularly for Signal Stability test are still under discussion, since the average of the results from 9 different antennas from 4 different research teams in 4 different countries (Belgium, Czech Republic, Portugal, Serbia) is 5.52% i.e., none of them passes this test [112] whereas the criterion dictates that the results should not be higher than 1%. The same is valid for also the linearity test, where the average from 5 different antennas is 6% [112] whereas the threshold value is 2% (meaning the values should be lower than 2%). It should be noted that all the GPR systems were produced by IDS and GSSI, both of which are among the most common used commercial GPR

systems. None of them were reported to show signs of malfunctioning. This situation might result in the modification of proposed threshold values, and set new values after having performed further tests to evaluate the performance of GPR systems and the results of those tests with more antennas. Further knowledge and experience in testing could yield the proposal of new threshold values together with modifications of test procedures [112]. For the time being, already new threshold values are proposed in [112] as follows:

- Test 1: Signal-to-Noise Ratio > 10

- Test 2: Signal Stability < 8%

- Test 3: Linearity in the Time Axis < 6.5%

- Test 4: Long-Term Signal Stability < 2.5%

The results are tabulated in Table 7.2 in comparison with the above-proposed threshold values, where the green highlighted cells indicate the tests passed by that GPR frequency according to the proposed threshold values. And red cells indicate the tests which did not meet the criteria according to the proposed threshold values. However, as noted above, threshold values and test procedures are still under discussion and needs further improvement.

Table 7.2. Results of GPR Performance Compliance Tests according to proposed threshold values

Frequency in MHz	400	900	2000	Proposed Threshold Values
Signal to Noise Ratio Test- SNR	9.75	1.19	23.74	10
Signal Stability Test - SST	4.08%	15.89%	12.18%	8%
Linearity Test - LT	4.88%	3.39%	2.99%	6.5%
Long Term Stability Test - LST	0.14%	0.63%	1.22%	2.5%

The amplitude values against time plots are given in Figure 7.1, respectively for 400MHz, 900MHz and 2GHz frequencies, which are the results of the performance tests that all three frequencies have passed.

Previous results of performance compliance tests with the GPR set of University of Pardubice, which were undertaken according to the previous version of the guidelines are present in the doctoral thesis of Borecky [66].
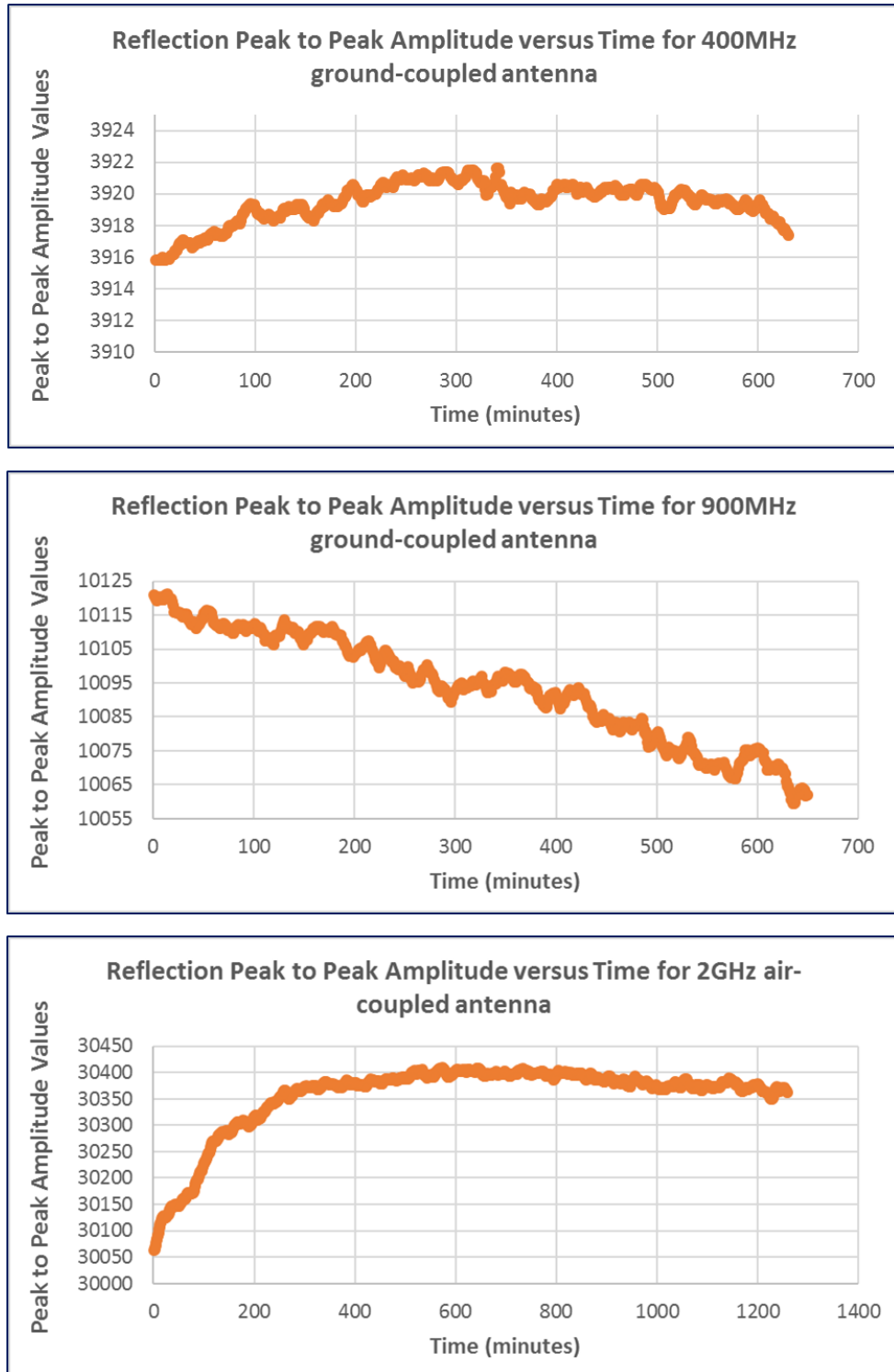
Figure 7.1. The amplitude values against time plots for 400MHz (upper chart), 900MHz (chart in the middle) and 2GHz (lower chart) frequencies for long-term stability test (Test 4)

7.2 Results of Section 6.2 "Laboratory Determination of Variations in the RDP Values Granite Railway Ballast under Various Fouling Levels" & Discussion

The results from the experiments described and carried out in detail in Section 6.2 will be presented in this Section together with the discussion of the findings.

7.2.1 Results for fine-sized ballast

7.2.1.1 SRM:

Surface Reflection method formula (14) was used to compute the RDP of the clean finer ballast. The result turned out to be 3.69 which is quite higher than the average value acquired by KHM. The average value of 5 different GPR measurements for RDP of clean finer ballast using KHM computations resulted in 3.257. The difference between two methods (SRM and KHM with respect to KHM) is 13.3%. SRM was also reported not to be suitable for ballast thickness measurements by GPR [56]. Moreover, RDP values obtained by SRM method tend to differ from the ones acquired by KHM and CRIM method [20]. Therefore, after having obtained such a difference for the RDP of clean, dry finer ballast between the methods, and based on similar results reported in the literature, surface reflection method was not further used for the fouled cases.

7.2.1.2 KHM:

The following charts (Figure 7.2a, b, and c) display the variation of the RDP values of fine-sized ballast with the three fouling materials, i.e. sand, fine-sized gravel, and a mixture of these two, in gradually increasing fouling levels. All the values were computed using KHM (equations (15) & (16)).

Figure 7.2. a) RDP values for fine-sized ballast fouled by sand, b) by fine-sized gravel, c) by the mixture of sand and fine-sized gravel – All values calculated by KHM

RDP values for fine-sized ballast fouled by sand range from 3.185 to 5.318, corresponding to 0% (clean) and 100% fouled conditions respectively. A strong linear trend with the coefficient of determination of 0.9958 was observed in Figure 7.2a. The RDP values for fine-sized ballast fouled by fine-sized gravel are found in between 3.122 to 3.787, corresponding to 0% (clean) and 50% fouled conditions, respectively. A strong linear trend with the coefficient of determination of 0.998 was observed in Figure 7.2b. The RDP values for fine-sized ballast fouled by the mixture of sand and fine-sized gravel fall into the range from 3.159 to 5.239, corresponding to 0% (clean) and 100% fouled conditions respectively. A strong linear trend with the coefficient of determination of 0.9823 was observed in Figure 7.2c.

The equations indicated in Figure 7.2a, b, and c, can be used to estimate RDP of fine-sized ballast polluted by sand, fine-gravel, and mixture of them, respectively for any fouling level. (Note that when sand and the mixture of sand and fine-sized gravel were used as a polluting material, fouling levels from 0% to 100% were achieved. However, when fine-sized gravel was used as the fouling material, fouling levels from 0% (clean ballast) to 50% were realized as already explained in the experimental design part of Section 6.2 previously.

RDP values from 0% to 50% for finer granite ballast for all three fouling materials are depicted in Figure 7.3.

Figure 7.3. RDP values from 0% to 50% for finer granite ballast fouled by sand, gravel and the mixture of them.

For each fouling level, RDP values of sand fouled ballast were found to be higher than the ones fouled by fine-sized gravel. The range of RDP values fouled by the mixed material fall into the values between sand fouled ballast and fine-sized gravel fouled ballast for each fouling level.

7.2.1.3 CRIM:

The values in Table 6.3 were used for RDP calculations using this method. Table 7.3 below, not only represents RDP values of finer granite ballast calculated both by CRIM and KHM (KHM values in Figure 7.2) fouled by sand, gravel and the mixture of two, but also compares the results from these two methods giving the relative error with respect to the theoretical one (CRIM).

Table 7.3. RDP values of finer granite ballast fouled by a) sand, b) gravel and c) the mixture of two - calculated both by the CRIM and KHM

a)

Volume Percentage of Components	$\varepsilon_{A,i}$	Volume of Fouled Material According to the Air Voids of Ballast (Percentage)										
		0	10	20	30	40	50	60	70	80	90	100
Finer Granite Ballast	5.000	61.3%	61.3%	61.3%	61.3%	61.3%	61.3%	61.3%	61.3%	61.3%	61.3%	61.3%
Sand	4.500	0.0%	3.9%	7.7%	11.6%	15.5%	19.4%	23.2%	27.1%	31.0%	34.9%	38.7%
Air	1	38.7%	34.9%	31.0%	27.1%	23.2%	19.4%	15.5%	11.6%	7.7%	3.9%	0.0%
Results (ε_T) obtained by CRIM		3.088	3.242	3.400	3.563	3.729	3.898	4.072	4.249	4.430	4.615	4.803
Results (ε_r) obtained by KHM		3.185	3.397	3.665	3.834	4.051	4.194	4.339	4.637	4.809	5.041	5.318
Relative Error between CRIM & KHM wrt CRIM		3.17%	4.78%	7.78%	7.61%	8.65%	7.58%	6.57%	9.13%	8.56%	9.23%	10.72%

b)

Volume Percentage of Components	$\varepsilon_{A,i}$	Volume of Fouled Material According to the Air Voids of Ballast (Percentage)										
		0	10	20	30	40	50	60	70	80	90	100
Finer Granite Ballast	5.000	61.3%	61.3%	61.3%	61.3%	61.3%	61.3%	61.3%	61.3%	61.3%	61.3%	61.3%
Fine-Sized Gravel	5.500	0.0%	3.9%	7.7%	11.6%	15.5%	19.4%	23.2%	27.1%	31.0%	34.9%	38.7%
Air	1	38.7%	34.9%	31.0%	27.1%	23.2%	19.4%	15.5%	11.6%	7.7%	3.9%	0.0%
Results (ε_T) obtained by CRIM		3.088	3.273	3.465	3.662	3.864	4.071	4.284	4.503	4.727	4.956	5.191
Results (ε_r) obtained by KHM		3.122	3.232	3.386	3.535	3.649	3.787					
Relative Error between CRIM & KHM wrt CRIM		1.10%	1.27%	2.26%	3.46%	5.55%	6.97%					

c)

Volume Percentage of Components	$\varepsilon_{A,i}$	Volume of Fouled Material According to the Air Voids of Ballast (Percentage)										
		0	10	20	30	40	50	60	70	80	90	100
Finer Granite Ballast	5.000	61.3%	61.3%	61.3%	61.3%	61.3%	61.3%	61.3%	61.3%	61.3%	61.3%	61.3%
Sand	4.500	0.0%	1.9%	3.9%	5.8%	7.7%	9.7%	11.6%	13.6%	15.5%	17.4%	19.4%
Fine-Sized Gravel	5.500	0.0%	1.9%	3.9%	5.8%	7.7%	9.7%	11.6%	13.6%	15.5%	17.4%	19.4%
Air	1	38.7%	34.9%	31.0%	27.1%	23.2%	19.4%	15.5%	11.6%	7.7%	3.9%	0.0%
Results (ε_T) obtained by CRIM		3.088	3.258	3.433	3.612	3.796	3.984	4.177	4.375	4.577	4.784	4.995
Results (ε_r) obtained by KHM		3.159	3.270	3.446	3.571	3.725	3.983	4.168	4.434	4.629	4.949	5.239
Relative Error between CRIM & KHM wrt CRIM		2.33%	0.39%	0.41%	1.12%	1.87%	0.02%	0.22%	1.35%	1.13%	3.46%	4.88%

RDP values calculated by CRIM were smaller than the ones computed with KHM for finer ballast fouled by sand (Table 7.3a). However, for fine-gravel fouled finer ballast, the values obtained by CRIM tend to be larger than the ones calculated by

KHM. The only exception was the 0% fouling (clean) case (Table 7.3b). For the finer ballast fouled by mixture, RDP values acquired by CRIM were smaller than the ones attained by KHM until the 20% fouling level. For the rest of fouling levels, the situation was vice-versa (Table 7.3c). Overall, the relative differences between two methods were rather small. All the relative errors were under 10% except for the sand fouled finer ballast fouled at 100% fouling level. In fact, all of the relative errors in the case of mixture fouled finer ballast were within 5%.

7.2.2   Results for coarse-sized ballast:

7.2.2.1   SRM:

Surface Reflection method formula (14) was utilized to calculate RDP of the clean coarser ballast. The result turned out to be 2.714 which is quite lower than the average value acquired by KHM. The average value of 12 different GPR measurements for RDP of clean coarser ballast using KHM computations was found to be 3.139. The difference between two methods (SRM and KHM with respect to KHM) is 13.5%. In the case of finer ballast, the result calculated by SRM was higher than the one obtained by KHM. Therefore, after having obtained such relative differences for RDP of clean, dry ballast between the methods, and based on the recommendations from literature [20,56], surface reflection method was not further employed for the fouled cases of coarser ballast as it was the case for finer ballast as well.

7.2.2.2   KHM:

The following graphs (Figure 7.4 a, b and c) display the variation of RDP of coarse-sized ballast with the three fouling materials, i.e. sand, fine-sized gravel, and a mixture of these two, in gradually increasing fouling levels. All the values were computed using KHM (equations (15) & (16)).
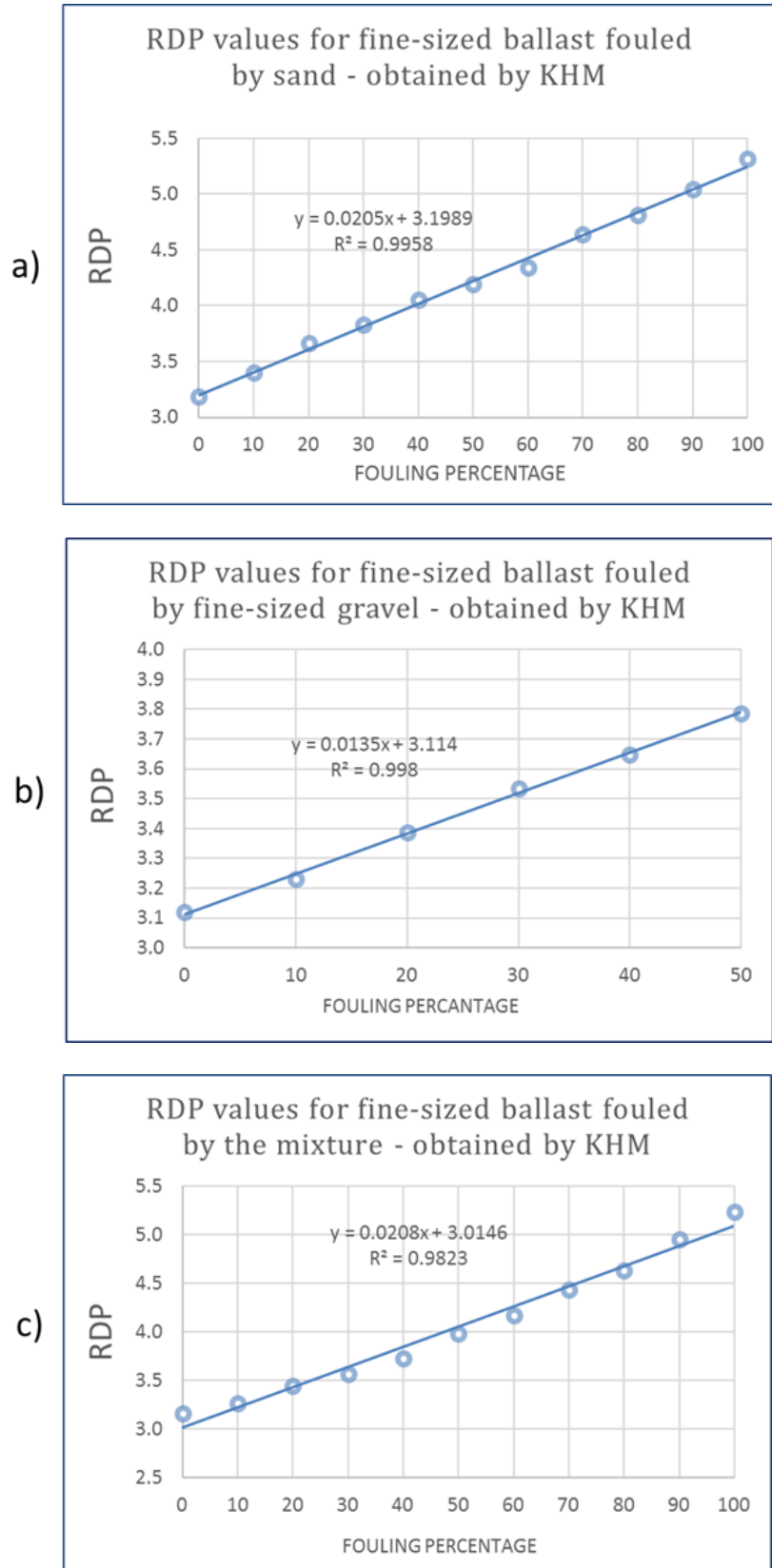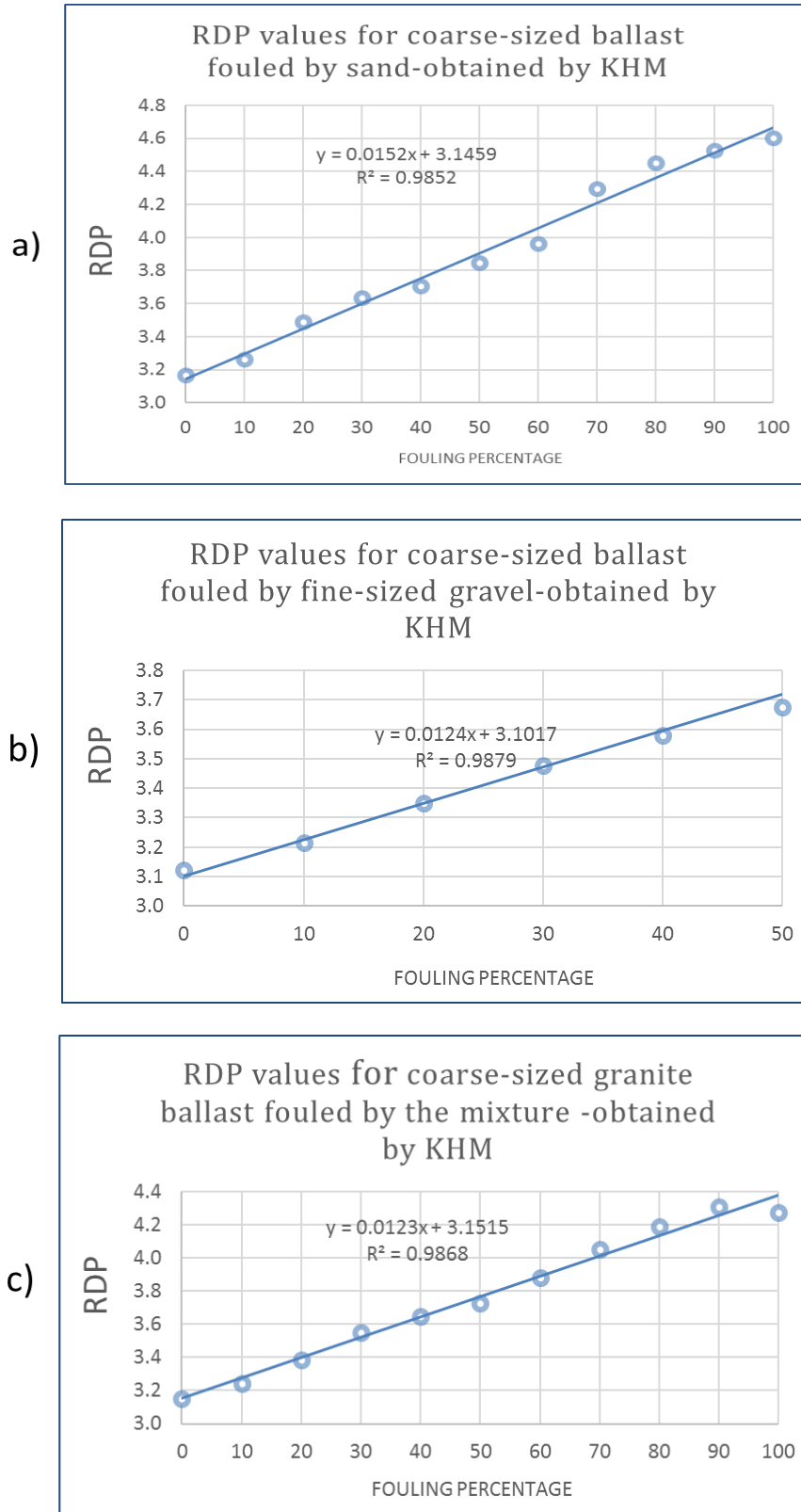
Figure 7.4. a) RDP values for coarse-sized ballast fouled by sand, b) by fine-sized gravel, c) by the mixture of sand and fine-sized gravel – All values calculated by KHM

RDP values for coarse-sized ballast fouled by sand range from 3.167 to 4.603, corresponding to 0% (clean) and 100% fouled conditions respectively. A strong linear trend with the coefficient of determination of 0.9852 was observed in Figure 7.4a. RDP values for coarse-sized ballast fouled by fine-sized gravel lie in between 3.121 to 3.675, corresponding to 0% (clean) and 50% fouled conditions, respectively. A strong linear trend with the coefficient of determination of 0.9879 was observed in Figure 7.4b. RDP values for coarse-sized ballast fouled by the mixture of sand and fine-sized gravel fall in the range from 3.154 to 4.307, corresponding to 0% (clean) and 100% fouled conditions respectively. A strong linear trend with the coefficient of determination of 0.9868 was observed in Figure 7.4c.

The equations indicated in Figure 7.4a, b, and c, can be exercised to predict RDP of coarse-sized ballast polluted by sand, fine-gravel, and mixture of them, respectively for any fouling level. (Note that when sand and the mixture of sand and fine-sized gravel were used as a polluting material, fouling levels from 0% to 100% were achieved. However, when fine-sized gravel was used as the fouling material, fouling levels from 0% to 50% were realized as already explained in the experimental design part of Section 6.2, previously.

RDP values from 0% to 50% for coarser granite ballast for all three fouling materials are presented in Figure 7.5.
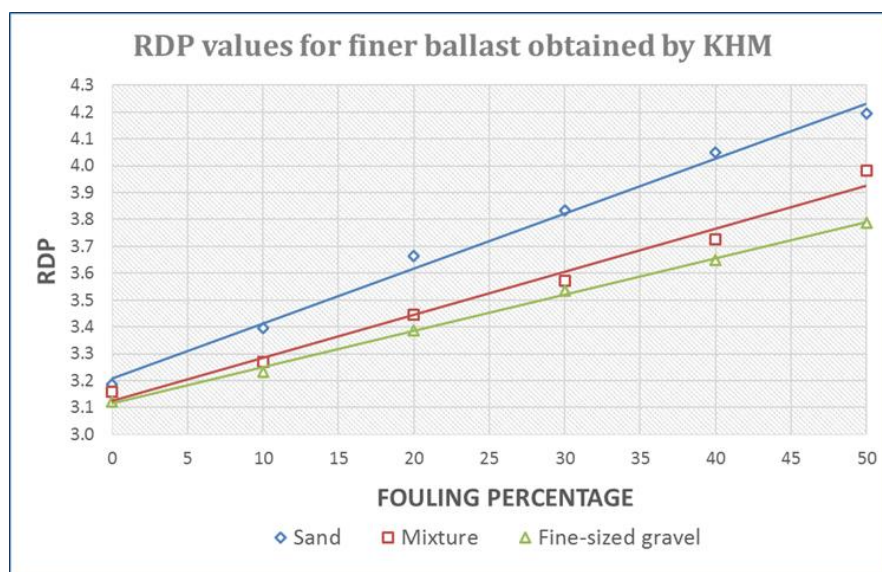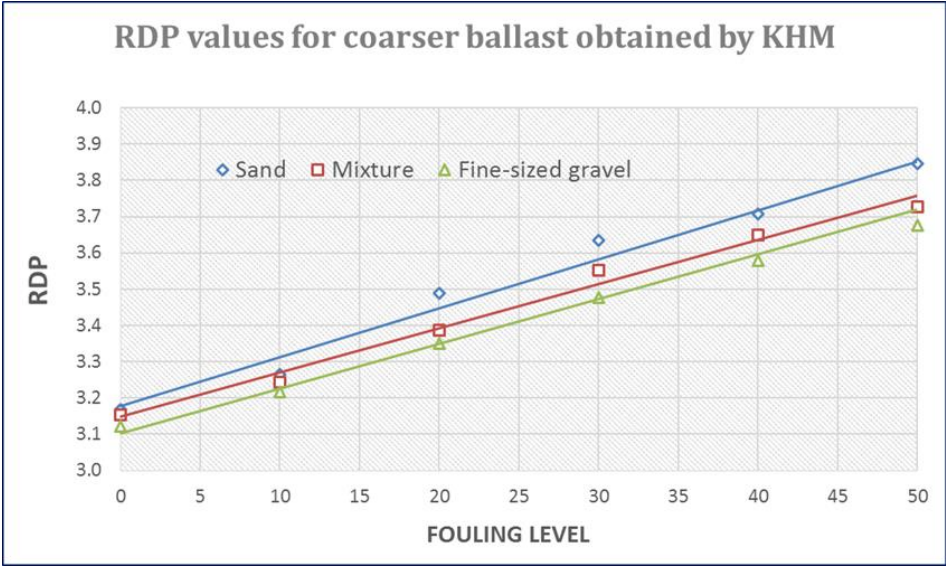

Figure 7.5. RDP values from 0% to 50% for coarser granite ballast fouled by sand, gravel and the mixture of them.

RDP values of coarse-sized ballast fouled by fine-sized gravel were smaller than the ones fouled by sand at each fouling level. RDP values of coarser ballast fouled by the mixed fouling agent take place between those of sand fouled ballast and fine-sized gravel fouled ballast at each fouling level.

7.2.2.3 CRIM:

Likewise, in the case of finer-ballast, the values in Table 6.3 were taken for RDP calculations of coarser ballast with this volumetric mixing method (equation (17)). Table 7.4 shows RDP values of coarser granite ballast acquired both by CRIM and KHM (KHM values in Figure 7.4) fouled by sand, gravel and the mixture of two. Moreover, comparison of results between these two methods with respect to the theoretical one (CRIM) was also given in Table 7.4.

Table 7.4. RDP values of coarser granite ballast fouled by a) sand, b) gravel and c) the mixture of two - calculated both by the CRIM and KHM

a)

Volume Percentage of Components	$\varepsilon_{A,i}$	Volume of Fouled Material According to the Air Voids of Ballast (Percentage)										
		0	10	20	30	40	50	60	70	80	90	100
Coarser Granite Ballast	5.000	59.9%	59.9%	59.9%	59.9%	59.9%	59.9%	59.9%	59.9%	59.9%	59.9%	59.9%
Sand	4.500	0.0%	4.0%	8.0%	12.0%	16.1%	20.1%	24.1%	28.1%	32.1%	36.1%	40.1%
Air	1	40.1%	36.1%	32.1%	28.1%	24.1%	20.1%	16.1%	12.0%	8.0%	4.0%	0.0%
Results (ε_T) obtained by CRIM		3.027	3.186	3.349	3.515	3.686	3.861	4.040	4.223	4.410	4.601	4.796
Results (ε_r) obtained by KHM		3.167	3.265	3.489	3.636	3.708	3.846	3.964	4.296	4.450	4.529	4.603
Relative Error between CRIM & KHM wrt CRIM		4.61%	2.47%	4.20%	3.42%	0.58%	0.38%	1.88%	1.74%	0.90%	1.57%	4.02%

b)

Volume Percentage of Components	$\varepsilon_{A,i}$	Volume of Fouled Material According to the Air Voids of Ballast (Percentage)										
		0	10	20	30	40	50	60	70	80	90	100
Coarser Granite Ballast	5.000	59.9%	59.9%	59.9%	59.9%	59.9%	59.9%	59.9%	59.9%	59.9%	59.9%	59.9%
Fine-Sized Gravel	5.500	0.0%	4.0%	8.0%	12.0%	16.1%	20.1%	24.1%	28.1%	32.1%	36.1%	40.1%
Air	1	40.1%	36.1%	32.1%	28.1%	24.1%	20.1%	16.1%	12.0%	8.0%	4.0%	0.0%
Results (ε_T) obtained by CRIM		3.027	3.186	3.415	3.617	3.826	4.040	4.260	4.485	4.717	4.955	5.198
Results (ε_r) obtained by KHM		3.121	3.215	3.350	3.476	3.579	3.675					
Relative Error between CRIM & KHM wrt CRIM		3.10%	0.92%	1.89%	3.91%	6.43%	9.03%					

c)

Volume Percentage of Components	$\varepsilon_{A,i}$	Volume of Fouled Material According to the Air Voids of Ballast (Percentage)										
		0	10	20	30	40	50	60	70	80	90	100
Coarser Granite Ballast	5.000	59.9%	59.9%	59.9%	59.9%	59.9%	59.9%	59.9%	59.9%	59.9%	59.9%	59.9%
Sand	4.500	0.0%	2.0%	4.0%	6.0%	8.0%	10.0%	12.0%	14.0%	16.1%	18.1%	20.1%
Fine-Sized Gravel	5.500	0.0%	2.0%	4.0%	6.0%	8.0%	10.0%	12.0%	14.0%	16.1%	18.1%	20.1%
Air	1	40.1%	36.1%	32.1%	28.1%	24.1%	20.1%	16.1%	12.0%	8.0%	4.0%	0.0%
Results (ε_T) obtained by CRIM		3.027	3.202	3.382	3.566	3.756	3.950	4.149	4.353	4.562	4.776	4.995
Results (ε_r) obtained by KHM		3.154	3.244	3.386	3.552	3.649	3.727	3.881	4.052	4.192	4.307	4.275
Relative Error between CRIM & KHM wrt CRIM		4.18%	1.30%	0.14%	0.40%	2.83%	5.64%	6.45%	6.91%	8.12%	9.81%	14.42%

RDP values calculated by CRIM were smaller than the ones computed with KHM for coarser ballast fouled by sand until fouling level of 40% was attained. For the rest of fouling levels (from 50% to 100%), the situation was vice-versa (Table 7.4a). As for fine-gravel fouled coarser ballast, the values acquired by CRIM were found to be also smaller than the ones calculated by KHM, but only until 20% fouling level. The situation was vice-versa for the rest of the fouling levels, i.e., from 30% to 50% (Table 7.4b). A similar situation was observed for the coarser ballast polluted by mixture fouling agent, where the values acquired by CRIM were found to be also smaller than the ones calculated by KHM, but only until 30% fouling level (Table 7.4c). It is noteworthy to express that the relative differences between two methods were in good agreement such that all the relative errors were under 10% except for the mixture fouled coarser ballast at 100% fouling level. Indeed, all the relative errors in the case of coarser ballast fouled by sand were found to be within 5%.

7.2.3   Discussion of Results:

RDP values for both dry clean ballast types calculated from SRM turned out to be much lower than those computed by other two methods (KHM and CRIM). Based on these results, and also similar findings from the literature [20,56], this method was not further utilized for fouled cases of ballast. The RDP values from other two methods, KHM and CRIM, were in good agreement with each other for both ballast types fouled by all three fouling agents at different times. In other words, experimentally obtained RDP values by means of KHM were verified by the theory-based results computed by CRIM. RDP values for clean and fouled granite ballast values are in good agreement with the published ones in Table 4.1, for both the clean and fouled granite ballast values published by [65]. As the replacement process of air voids by finer materials within the ballast increase, i.e., fouling level rises, RDP of the overall system tends to gradually increase with the increasing fouling percentages. This phenomenon is expected since the RDP of the pollutant materials is larger (RDP of sand is found to be 3.211 by KHM and fine-sized gravel is 3.157 by KHM) than that of the air (which has the value of 1).

The results show how the rise in the fouling levels in case of all three fouling agents leads to an increase in RDP values of both types of ballast and hence a decrease in the EM wave velocity (based on equation (16). The decrease in EM wave velocity is easily

observed through the scans taken from clean and fouled cases as the arrival time from the ballast/metal plate interface is delayed gradually as the fouling level increases. Figure 7.6 below well visualizes this phenomenon where the metal plate reflection from the bottom of the clean finer ballast (Figure 7.6a) is compared with finer ballast fouled by 50% of mixture fouling agent (Figure 7.6b) and also with finer ballast fouled by 100% of mixture fouling agent (Figure 7.6c). The arrival time from the reflection of the ballast/metal plate interface is approximately 9.05, 9.58 and 10.14 ns, respectively, for clean ballast, 50% fouled ballast and 100% fouled ballast indicating lower EM wave velocity values, thus higher RDP figures. The arrival time for air/ballast interface in all three cases is approximately 3 ns.

The range of RDP values for finer granite ballast when fouled by sand, fine gravel and the mixture of these two were found to be 3.185-5.318 (from 0% to 100% fouling level), 3.122-3.787 (from 0% to 50% fouling level), and 3.159-5.239 (from 0% to 100% fouling level), respectively by KHM. The range of RDP values for coarser granite ballast when fouled by sand, fine gravel and the mixture of these two were computed as 3.167-4.603 (from 0% to 100% fouling level), 3.121-3.675 (from 0% to 50% fouling level), and 3.154-4.307 (from 0% to 100% fouling level), respectively by KHM. Coarser granite ballast was observed to have slightly lower RDP values than finer granite ballast at the same fouling levels when fouled by the same fouling material for all three fouling materials.

As a result, for finer ballast, a range of RDP from 3.122 to 5.318 was observed including all three fouling material, while a range of 3.121 to 4.603 was registered for coarser ballast for all three pollutants.

For both ballast types, RDP values of sand fouled ballast were found to be higher than the ones fouled by fine gravel. RDP values for both types of ballast fouled by the mixed material fall into the values between sand fouled ballast and fine gravel fouled ballast. Strong linear trends (with coefficient of determination values greater than 0.9) exist (Figure 7.2 & Figure 7.4) between RDP values and fouling levels introduced with the three fouling agents for both ballast materials which enable to predict RDP of those types of ballast for any fouling level (also type of fouling) in real field surveys when

fouled by similar materials, hence improve the evaluation and monitoring efficiency of railway site investigations.
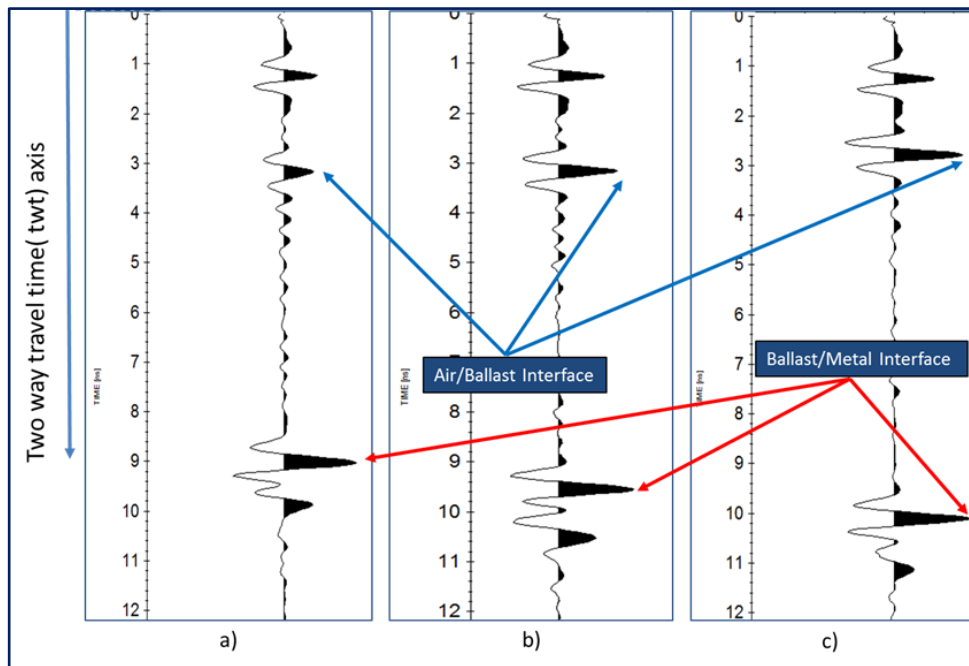
Figure 7.6. A-scans from a) clean finer ballast, b) finer ballast fouled with 50% mixture fouling agent, c) finer ballast fouled with 100% mixture fouling agent

7.3 Results of Section 6.3 "Moisture Influence on the RDP Values of Granite Ballast under Clean and Fouled Conditions" & Discussion

The results from the experiments described and carried out in detail in Section 6.3 will be given in this Section together with the discussion of the findings.

RDP values for each configuration of ballast were calculated by two methods, KHM and CRIM, which have also been used in Section 6.2. Surface Reflection Method (SRM) was not used based on the recommendation from the literature [20,56].

7.3.1 Results from KHM:

The results obtained from the clean ballast, and ballast fouled by sand and fouled by fine gravel are presented below.

The findings for RDP values of gradually water (at 10% increments) included coarser clean ballast are presented in Figure 7.7.
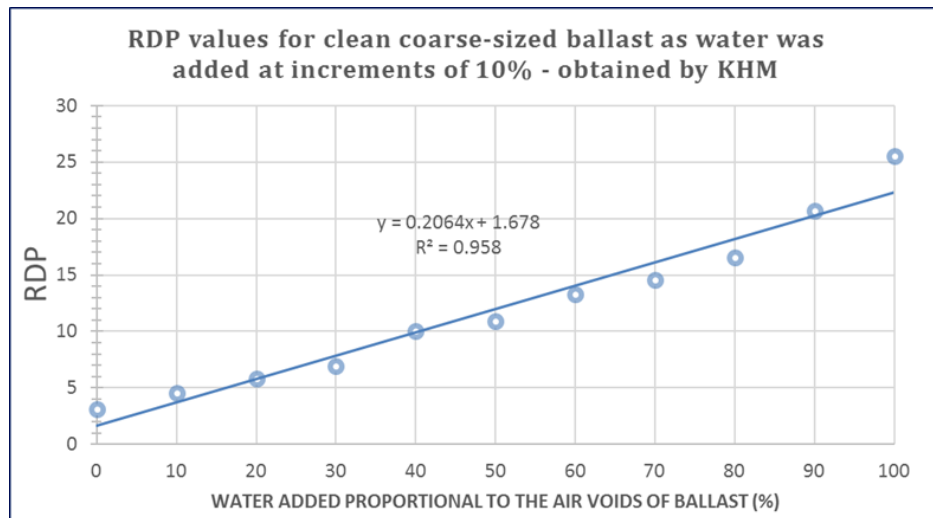
Figure 7.7. RDP values for clean coarse-sized ballast at various water contents

At water levels from 0% to 100%, calculated RDP values for clean coarse-sized ballast range from 3.090 (no water case) to 25.500 (saturated case). A strong linear trend with the coefficient of determination of 0.958 was observed Figure 7.7. The increase in RDP with increasing water content was also reported by other researchers [11,28,94]. After saturation level was reached, GPR data were collected and then water was discharged from the IBC. After 5 hours of removal of water, GPR data were collected on the same day. Then, GPR data were acquired in the first, third, sixth, seventh day after discharge of water. Finally, two more tests were carried out in the second and third weeks after removal of water. The corresponding RDP values versus days of GPR measurements are tabulated in Table 7.5 and demonstrated in Figure 7.8 below.

Table 7.5 RDP values vs dry, saturated and drained ballast

Day #	1	2	2	3	5	8	9	16	23
Condition	Dry Clean	Saturated Clean	Just after removal of water (same day)	After 1 day of Removal	After 3 days of Removal	After 6 days of Removal	After 7 days of Removal	After 2 weeks of removal	After 3 weeks of removal
RDP	3.090	25.500	3.876	3.203	3.146	3.146	3.125	3.139	3.150

RDP of saturated ballast upon the measurement just immediately after water addition was found to be 25.5, which is in line with the results from other studies [11,28,94]. GPR data revealed the RDP value of 3.876 just after removal of water. The average value of drained RDP values was 3.152, which is almost the same as the dry clean ballast.
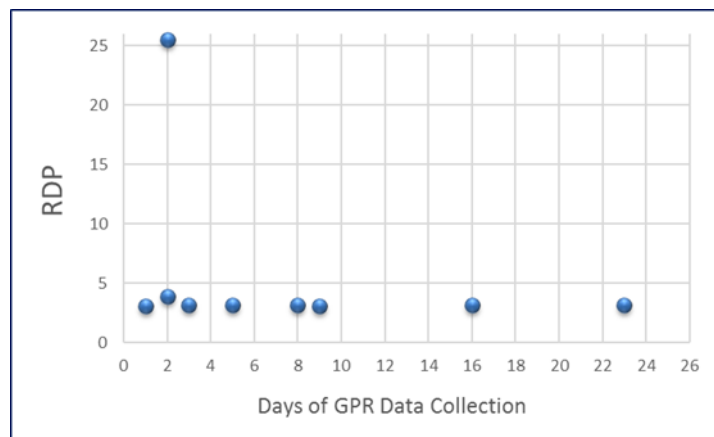
Figure 7.8. RDP values vs dry, saturated and drained ballast

7.3.1.2 *Coarse-sized Ballast Fouled by Sand:*

RDP values were computed for coarse-sized ballast at specific rates of sand fouling namely at 10%, 30%, and 50%. The results are demonstrated in Figure 7.9. RDP values for coarse-sized ballast fouled by 10% sand increased from 3.271 to 24.699, as water was added gradually from 0% to 90%, respectively. A strong linear trend with the coefficient of determination of 0.9343 was observed in Figure 7.9a. RDP values for coarse-sized ballast fouled by 30% sand are found between 3.538 to 19.774, as water was included progressively from 0% to 70%, respectively. A good linear trend with the coefficient of determination of 0.8939 was observed in Figure 7.9b. RDP values for coarse-sized ballast fouled by 50% sand fell into the range from 4.229 to 14.374 as water was added to the IBC step by step from 0% 50% respectively. A strong linear trend with the coefficient of determination of 0.9608 was noted in Figure 7.9c.

RDP values for 10% fouled coarse-sized ballast by sand as water was added at increments of 10% - by KHM

$y = 0.2087x + 1.9191$
$R^2 = 0.9343$

a)

WATER ADDED PROPORTIONAL TO THE AIR VOIDS OF BALLAST (%)

RDP values for 30% fouled coarse-sized ballast by sand as water was added at increments of 10% - by KHM

$y = 0.1994x + 2.4485$
$R^2 = 0.8939$

b)

WATER ADDED PROPORTIONAL TO THE AIR VOIDS OF BALLAST (%)

RDP values for 50% fouled coarse-sized ballast by sand as water was added at increments of 5% - by KHM

$y = 0.1857x + 3.7198$
$R^2 = 0.9608$

c)

WATER ADDED PROPORTIONAL TO THE AIR VOIDS OF BALLAST (%)

Figure 7.9. RDP values for fouled coarse sized granite ballast under gradual water addition at specific levels of sand fouling a) 10%, b) 30%, c) 50% sand fouled ballast

7.3.1.3   Coarse-sized Ballast Fouled by Gravel:

Coarse-sized ballast was polluted by gravel at specific percentages of fouling i.e., at 10%, 30%, and 50%. Calculated RDP values are given in Figure 7.10.

Figure 7.10. RDP values for fouled coarse sized granite ballast under gradual water addition at specific levels of fine gravel fouling a) 10%, b) 30%, c) 50% fine gravel fouled ballast

RDP values for coarse-sized ballast fouled by 10% fine gravel range from 3.260 to 16.159, as water was added gradually from 0% to 75%, respectively. It should be noted that after 75% of water addition, no clear reflection from the metal plate was received due to high attenuation. Therefore, the results after 75% water addition were not

reported. A strong linear trend with the coefficient of determination of 0.9846 was found in Figure 7.10a. RDP values for coarse-sized ballast fouled by 30% fine gravel are computed between 3.523 to 17.650, as water was included progressively from 0% to 70%, respectively. A strong linear relationship with the coefficient of determination of 0.9635 was noted in Figure 7.10b. RDP values for coarse-sized ballast fouled by 50% sand ranged from 4.135 to 13.021 as water was added to the IBC step by step from 0% to 50% respectively. A strong linear trend with the coefficient of determination of 0.9978 was noted in Figure 7.10c.

7.3.2 Results from CRIM:

The same values in Table 6.3 were used for RDP calculations with this volumetric mixing method (equation (17)) as it was the case in 6.2.

7.3.2.1 Clean Coarse-sized Ballast:

RDP values of clean coarser granite ballast calculated both by CRIM and KHM (results of KHM were presented in Figure 7.7) from water contents 0% (dry) to 100% (saturated) are given in Table 7.6 with also a comparison of the results computed from these two methods giving the relative error with respect to the theoretical one (CRIM).

Table 7.6 RDP values of clean coarse-sized granite ballast for water content range from 0% to 100% calculated both by the CRIM and KHM

Volume Percentage of Components	$\varepsilon_{A,i}$	Volume of Added Water at 10% Increments According to the Air Voids of Ballast (Percentage) for Clean Ballast										
		0	10	20	30	40	50	60	70	80	90	100
Coarser Granite Ballast	5.000	59.9%	59.9%	59.9%	59.9%	59.9%	59.9%	59.9%	59.9%	59.9%	59.9%	59.9%
Water	81.000	0.0%	4.0%	8.0%	12.0%	16.1%	20.1%	24.1%	28.1%	32.1%	36.1%	40.1%
Air	1	40.1%	36.1%	32.1%	28.1%	24.1%	20.1%	16.1%	12.0%	8.0%	4.0%	0.0%
Results (ε_T) obtained by CRIM		3.027	4.248	5.675	7.308	9.147	11.192	13.444	15.902	18.566	21.436	24.513
Results (ε_r) obtained by KHM		3.090	4.590	5.823	6.952	10.011	10.942	13.275	14.591	16.567	20.653	25.500
Relative Error between CRIM & KHM wrt CRIM		2.07%	8.06%	2.61%	4.86%	9.45%	2.24%	1.26%	8.24%	10.77%	3.65%	4.03%

The relative differences between the RDP values calculated by KHM and CRIM were overall in good agreement and within 10% error band. The only exception is at 80% of water content with the relative error of 10.77%.

7.3.2.2   Coarse-sized Ballast Fouled by Sand:

RDP values computed both by CRIM and KHM (results of KHM were plotted in Figure 7.9a) varying from 0% to 90% water percentages for sand fouled ballast at the fouling percentage of 10% were tabulated in Table 7.7. Besides, comparison of the results computed from these two methods giving the relative error with respect to the theoretical one (CRIM) was presented also in Table 7.7.

Table 7.7 RDP values of coarse-sized granite ballast fouled by sand at 10%, for water content range from 0% to 90 % calculated both by the CRIM and KHM

Volume Percentage of Components	$\varepsilon_{A,i}$	Volume of Added Water at 10 % Increments According to the Air Voids of Ballast for 10 % Fouled Ballast by Sand										
		0	10	20	30	40	50	60	70	80	90	100
Coarser Granite Ballast	5.000	59.9%	59.9%	59.9%	59.9%	59.9%	59.9%	59.9%	59.9%	59.9%	59.9%	
Sand	4.500	4.0%	4.0%	4.0%	4.0%	4.0%	4.0%	4.0%	4.0%	4.0%	4.0%	
Water	81.000	0.0%	4.0%	8.0%	12.0%	16.1%	20.1%	24.1%	28.1%	32.1%	36.1%	
Air	1	36.1%	32.1%	28.1%	24.1%	20.1%	16.1%	12.0%	8.0%	4.0%	0.0%	
Results (ε_T) obtained by CRIM		3.186	4.435	5.891	7.553	9.421	11.495	13.776	16.263	18.956	21.855	
Results (ε_r) obtained by KHM		3.271	4.621	5.970	7.414	10.073	11.629	13.442	14.955	17.050	24.699	
Relative Error between CRIM & KHM wrt CRIM		2.66%	4.18%	1.35%	1.84%	6.92%	1.16%	2.43%	8.04%	10.05%	13.01%	

RDP values calculated by KHM matched well with the ones computed by CRIM as can be seen in Table 7.7. The differences in results with respect to CRIM did not exceed 10% except for water contents of 80% and 90%.

RDP values by CRIM and KHM (results of KHM were plotted in Figure 7.9b) for the range of water contents from 0% to 70% for sand fouled ballast at the fouling level of 30% were displayed in Table 7.8. As the last row in Table 7.8 shows, the relative errors are lower than 10% until the water content level of 50% is reached, whereas the differences of results between the two methods are higher than 10% for water content levels of 60% and 70%.

141

Table 7.8 RDP values of coarse-sized granite ballast fouled by sand at 30%, for water content range from 0% to 70 % calculated both by the CRIM and KHM

Volume Percentage of Components	$\varepsilon_{A,i}$	Volume of Added Water at 10 % Increments According to the Air Voids of Ballast for 30 % Fouled Ballast by Sand										
		0	10	20	30	40	50	60	70	80	90	100
Coarser Granite Ballast	5.000	59.9%	59.9%	59.9%	59.9%	59.9%	59.9%	59.9%	59.9%			
Sand	4.500	12.0%	12.0%	12.0%	12.0%	12.0%	12.0%	12.0%	12.0%			
Water	81.000	0.0%	4.0%	8.0%	12.0%	16.1%	20.1%	24.1%	28.1%			
Air	1	28.1%	24.1%	20.1%	16.1%	12.0%	8.0%	4.0%	0.0%			
Results (ε_T) obtained by CRIM		3.515	4.823	6.336	8.056	9.982	12.114	14.452	16.997			
Results (ε_r) obtained by KHM		3.538	5.207	6.039	7.714	9.463	11.084	12.590	19.774			
Relative Error between CRIM & KHM wrt CRIM		0.63%	7.96%	4.70%	4.25%	5.20%	8.51%	12.89%	16.34%			

RDP values by CRIM and KHM (results of KHM were plotted in Figure 7.9c) versus water contents varying from 0% to 50% for sand fouled ballast at the fouling level of 50% are presented in Table 7.9. As observed in the last row of Table 7.9, percentage ratios of the differences between KHM and CRIM values are in good agreement, i.e., all of them are less than 10%. The only exception is at the 50% water content.

Table 7.9. RDP values of coarse-sized granite ballast fouled by sand at 50%, for water content range from 0% to 50 % calculated both by the CRIM and KHM

Volume Percentage of Components	$\varepsilon_{A,i}$	Volume of Added Water at 10 % Increments According to the Air Voids of Ballast for 50 % Fouled Ballast by Sand										
		0	5	10	15	20	25	30	35	40	45	50
Ballast	5.000	59.9%	59.9%	59.9%	59.9%	59.9%	59.9%	59.9%	59.9%	59.9%	59.9%	59.9%
Sand	4.500	20.1%	20.1%	20.1%	20.1%	20.1%	20.1%	20.1%	20.1%	20.1%	20.1%	20.1%
Water	81.000	0.0%	2.0%	4.0%	6.0%	8.0%	10.0%	12.0%	14.0%	16.1%	18.1%	20.1%
Air	1	20.1%	18.1%	16.1%	14.0%	12.0%	10.0%	8.0%	6.0%	4.0%	2.0%	0.0%
Results (ε_T) obtained by CRIM		3.861	4.518	5.226	5.986	6.797	7.660	8.575	9.541	10.559	11.628	12.749
Results (ε_r) obtained by KHM		4.229	4.828	5.733	6.428	7.336	7.936	8.937	9.117	11.315	11.746	14.374
Relative Error between CRIM & KHM wrt CRIM		9.52%	6.86%	9.71%	7.38%	7.93%	3.59%	4.22%	4.45%	7.16%	1.01%	12.75%

7.3.2.3 Coarse-sized Ballast Fouled by Gravel:

RDP values acquired both by CRIM and KHM (values obtained by KHM were plotted in Figure 7.10a) versus added water percentages ranging from 0% to 75% for fine gravel fouled ballast at the fouling level of 10% were indicated in Table 7.10, together with the comparison of the results from these two methods giving the relative error with respect to the theoretical one (CRIM).

Table 7.10. RDP values of coarse-sized granite ballast fouled by fine gravel at 10%, for water content range from 0% to 75 % calculated both by the CRIM and KHM

Volume Percentage of Components	$\varepsilon_{A,i}$	Volume of Added Water at 5% Increments According to the Air Voids of Ballast for 10 % Fouled Ballast by Fine-sized Gravel															
		0	5	10	15	20	25	30	35	40	45	50	55	60	65	70	75
Coarser Granite Ballast	5.000	59.9%	59.9%	59.9%	59.9%	59.9%	59.9%	59.9%	59.9%	59.9%	59.9%	59.9%	59.9%	59.9%	59.9%	59.9%	59.9%
Fine-Sized Gravel	5.500	4.0%	4.0%	4.0%	4.0%	4.0%	4.0%	4.0%	4.0%	4.0%	4.0%	4.0%	4.0%	4.0%	4.0%	4.0%	4.0%
Water	81.000	0.0%	2.0%	4.0%	6.0%	8.0%	10.0%	12.0%	14.0%	16.1%	18.1%	20.1%	22.1%	24.1%	26.1%	28.1%	30.1%
Air	1	36.1%	34.1%	32.1%	30.1%	28.1%	26.1%	24.1%	22.1%	20.1%	18.1%	16.1%	14.0%	12.0%	10.0%	8.0%	6.0%
Results (ε_T) obtained by CRIM		3.218	3.820	4.473	5.178	5.935	6.743	7.602	8.514	9.476	10.491	11.556	12.674	13.843	15.063	16.335	17.659
Results (ε_r) obtained by KHM		3.260	3.511	4.606	5.209	6.016	6.703	6.766	7.995	9.400	9.822	11.374	12.074	14.042	14.042	14.299	16.159
Relative Error between CRIM & KHM wrt CRIM		1.30%	8.10%	2.97%	0.60%	1.37%	0.59%	11.00%	6.10%	0.80%	6.37%	1.58%	4.73%	1.44%	6.78%	12.47%	8.50%

The last row of Table 7.10 presents the relative errors between two methods, where good agreement can be observed. All the differences are within 10% except for the 30% and the 70% water contents.

RDP values by CRIM and KHM (values obtained by KHM were plotted in Figure 7.10b) versus water contents varying from 0% to 70% for fine gravel fouled ballast at the fouling level of 30% are presented in Table 7.11.

Table 7.11. RDP values of coarse-sized granite ballast fouled by fine gravel at 30%, for water content range from 0% to 70 % calculated both by the CRIM and KHM

Volume Percentage of Components	$\varepsilon_{A,i}$	Volume of Added Water 5% Increments According to the Air Voids of Ballast for 30 % Fouled Ballast by Fine-sized Gravel														
		0	5	10	15	20	25	30	35	40	45	50	55	60	65	70
Coarser Granite Ballast	5.000	59.9%	59.9%	59.9%	59.9%	59.9%	59.9%	59.9%	59.9%	59.9%	59.9%	59.9%	59.9%	59.9%	59.9%	60%
Fine-Sized Gravel	5.500	12.0%	12.0%	12.0%	12.0%	12.0%	12.0%	12.0%	12.0%	12.0%	12.0%	12.0%	12.0%	12.0%	12.0%	12%
Water	81.000	0.0%	2.0%	4.0%	6.0%	8.0%	10.0%	12.0%	14.0%	16.1%	18.1%	20.1%	22.1%	24.1%	26.1%	28%
Air	1	28.1%	26.1%	24.1%	22.1%	20.1%	18.1%	16.1%	14.0%	12.0%	10.0%	8.0%	6.0%	4.0%	2.0%	0%
Results (ε_T) obtained by CRIM		3.617	4.254	4.942	5.681	6.473	7.315	8.210	9.155	10.153	11.202	12.302	13.454	14.658	15.913	17.220
Results (ε_r) obtained by KHM		3.523	4.468	5.117	5.991	6.548	7.129	7.944	8.802	10.172	10.223	11.895	12.940	13.006	13.548	17.650
Relative Error between CRIM & KHM wrt CRIM		2.60%	5.04%	3.55%	5.44%	1.16%	2.54%	3.24%	3.86%	0.18%	8.74%	3.31%	3.82%	11.27%	14.87%	2.50%

The average of relative errors between two methods was 4.81% indicating a good verification for the results of KHM is ensured by the theoretical CRIM. All the relative errors were lower than 10% but the ones at water contents of 60% and 65% (Table 7.11).

RDP values by CRIM and KHM (values calculated by KHM were depicted in Figure 7.10c) versus water contents varying from 0% to 50% for fine gravel fouled ballast at the fouling level of 50% are presented in Table 7.12.

Table 7.12. RDP values of coarse-sized granite ballast fouled by fine gravel at 50%, for water content range from 0% to 50 % calculated both by the CRIM and KHM

Volume Percentage of Components	$\varepsilon_{A,i}$	Volume of Added Water 5% Increments According to the Air Voids of Ballast for 50 % Fouled Ballast by Fine-sized Gravel										
		0	5	10	15	20	25	30	35	40	45	50
Ballast	5.000	59.9%	59.9%	59.9%	59.9%	59.9%	59.9%	59.9%	59.9%	59.9%	59.9%	59.9%
Fine-Sized Gravel	5.500	20.1%	20.1%	20.1%	20.1%	20.1%	20.1%	20.1%	20.1%	20.1%	20.1%	20.1%
Water	81.000	0.0%	2.0%	4.0%	6.0%	8.0%	10.0%	12.0%	14.0%	16.1%	18.1%	20.1%
Air	1	20.1%	18.1%	16.1%	14.0%	12.0%	10.0%	8.0%	6.0%	4.0%	2.0%	0.0%
Results (ε_T) obtained by CRIM		4.040	4.711	5.434	6.208	7.034	7.911	8.840	9.821	10.853	11.936	13.072
Results (ε_r) obtained by KHM		4.135	5.139	6.016	6.703	7.427	8.583	9.420	10.296	11.520	12.259	13.021
Relative Error between CRIM & KHM wrt CRIM		2.37%	9.10%	10.72%	7.98%	5.59%	8.49%	6.56%	4.84%	6.15%	2.71%	0.38%

The relative errors between two methods range from 0.38% to 10.72% (only 10.72% relative error value at 10% water content level exceeds the 10% envelope) revealing a reasonable confirmation for the results of KHM by the theoretical CRIM (Table 7.12).

7.3.3 Discussion of Results:

Introducing water into clean and fouled ballast increases RDP value meeting the theoretical expectations since the RDP of water is 81, which is remarkably higher than the ballast and fouling materials. RDP of saturated clean coarse granite ballast was found to be 25.5, whereas the average value of drained ballast (3.152) was observed to have similar values with the dry one (3.090) as indicated Table 7.5 & Figure 7.8.

Overall, RDP values obtained from KHM and CRIM matched each other quite well. The relative errors were within 10% in most of the cases. Exceptions for this situation occurred generally after 50% of water content. Therefore, RDP values obtained by KHM were validated by the theoretical mixing model i.e., CRIM.

For clean ballast and for fouled ballast at each fouling level, increase in the water addition led to a rise in RDP value of the mixture of ballast and fouling material. RDP values can be estimated for various water contents by the linear relationships whose equations are given in Figure 7.7, Figure 7.9 and Figure 7.10, respectively for clean ballast, sand fouled ballast, and fine gravel fouled ballast.

7.4 Results of Section 6.4 "Railway Field Surveys along Rozhovice Railway Station" & Discussion

The results from the field surveys described and realized in detail in Section 6.4 will be presented in this Section together with the discussion of the results.

7.4.1 Data Processing and Results

Aiming at the enhancement of signal to noise ratio, raw data collected during the field surveys were processed using ReflexW software, through a processing flow. For surveys which have the backward advancing direction (as Survey 2 in Figure 6.22), XflipProfile function in ReflexW was used to flip the backward advancing profiles to forward advancing ones. Once all the surveys are adjusted as forward advancing profiles, dewow filter was used to remove possible low-frequency part considering the central frequency of the antenna used. Then the traces are stacked eight times. Subsequently, the time-zero correction was applied to move the surface reflection atop in the radargram. Afterward, in order to draw the focus on trenches opened in the railway line, the part of the railway line from 50 m to 125 m were extracted. Also, the multiple reflections from metal sleepers do not allow for any interpretation in these removed sections of the railway segment (from 0 to 50 m, and from 125 to 138 m). Bandpass filtering (Butterworth filter) was applied such that the interval between the low pass filter and the high pass filter equals 1.5 times the central frequency of the antenna collecting the GPR data. Lastly, running average filter was implemented to suppress the trace dependent noise and to highlight horizontally coherent energy [111]. Raw data collected with 2GHz data in the longitudinal orientation and the processing steps applied to it can be seen from Figure 7.11 to Figure 7.17.
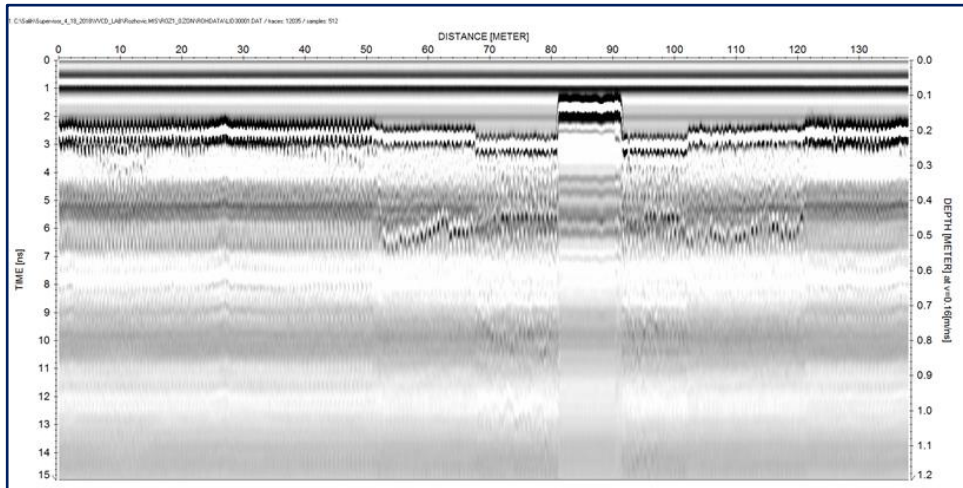
Figure 7.11. Raw 2000MHz GPR data
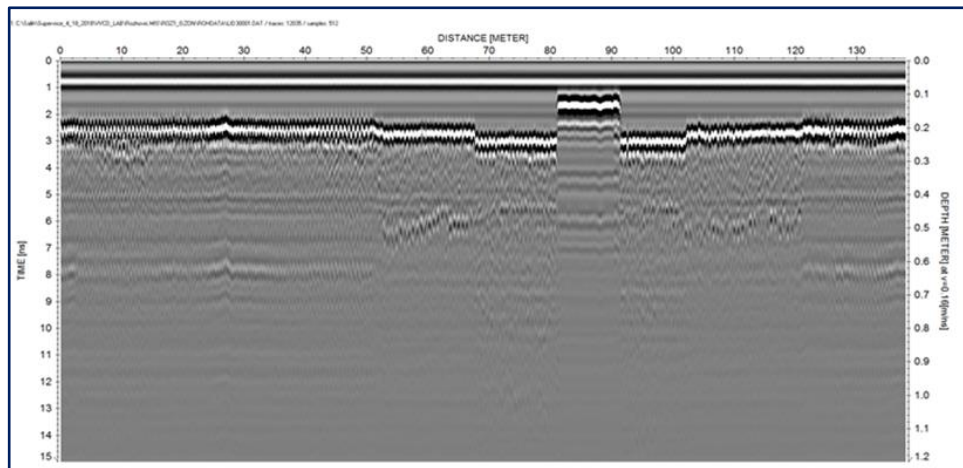
Figure 7.12. Dewow filter applied.
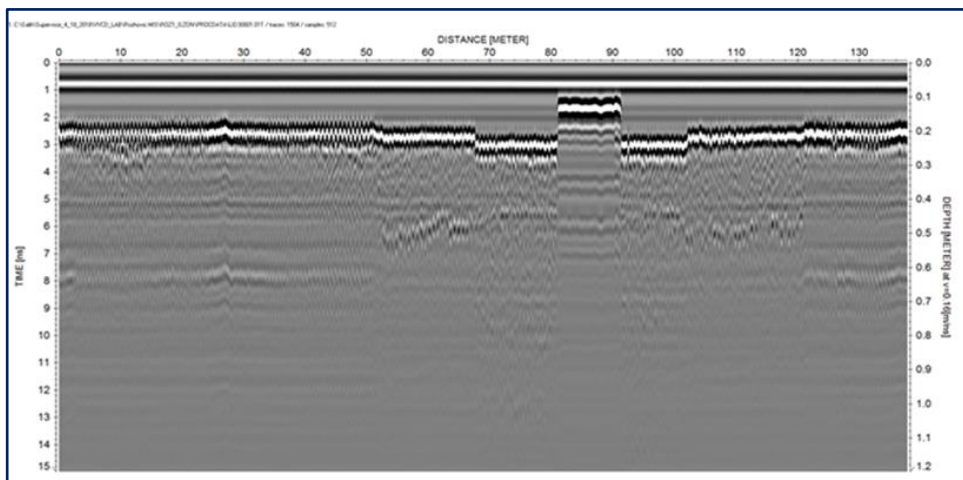
Figure 7.13. Stacking traces applied

146
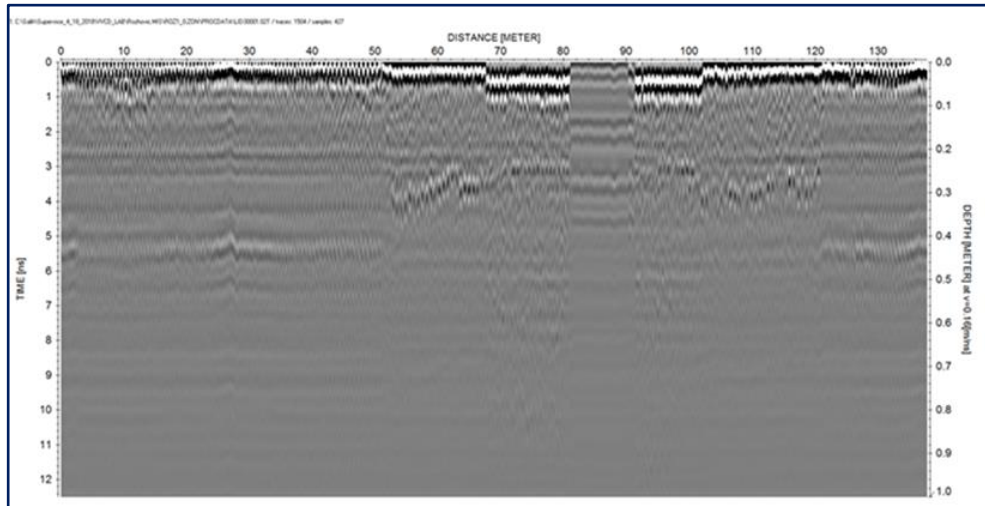
Figure 7.14. Time-zero correction applied.
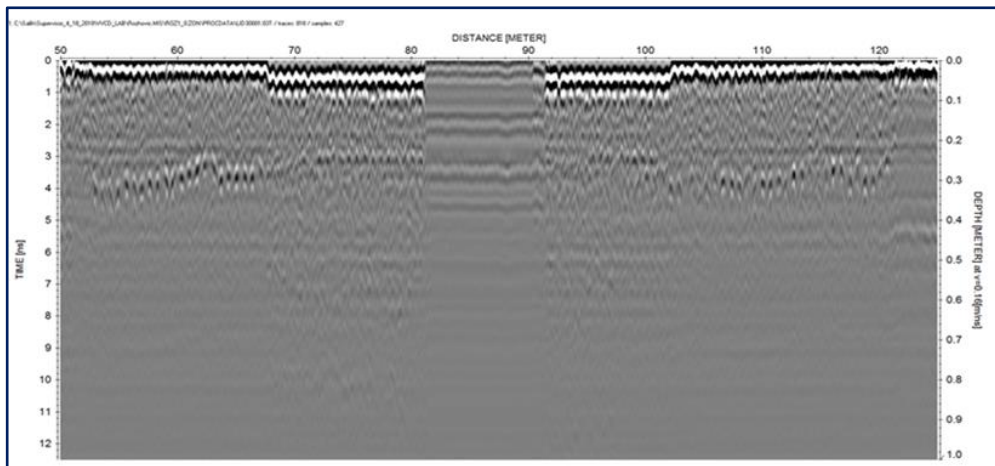
Figure 7.15. Extract traces applied.
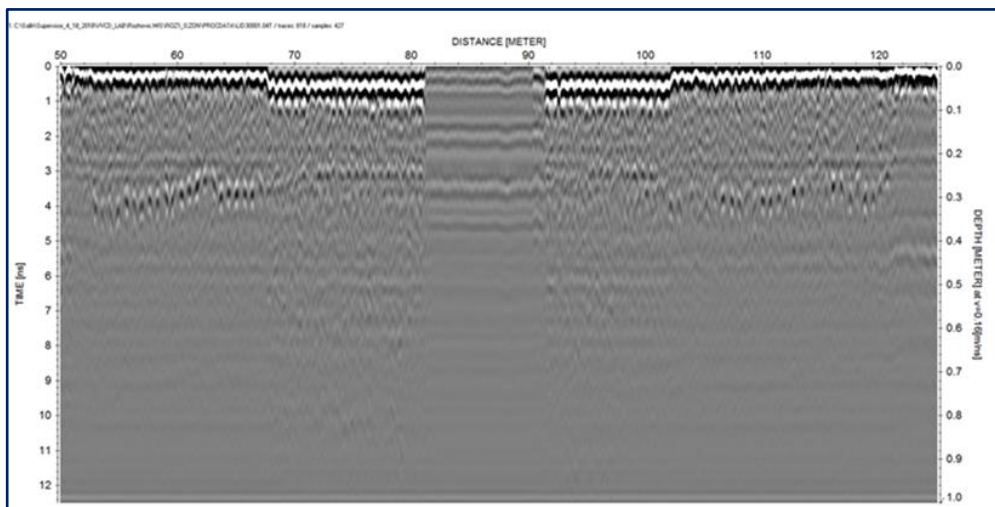
Figure 7.16. Bandpass filter (bandpass Butterworth applied)

147
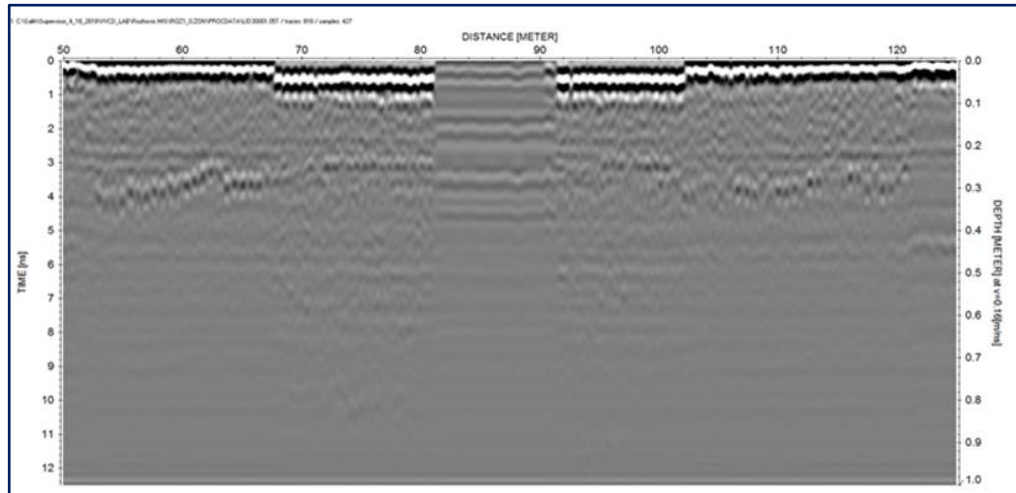
Figure 7.17. Running average applied.

Core data file was created in the form as it is described in the ReflexW software manual [111] and copied in the ASCII folder. In this core data file, the distance dimension of the trench, layer number of the trench, thickness of the trench, a quality factor, mean EM velocity and layer EM velocities were entered as inputs. An example of core data file is provided in Appendix 3.

Based on the entered EM velocities, a velocity file is created. According to this velocity file, a layer show (as in Figure 7.18) is formed where the depth of layers within the trench are shown together with the core data. The depths of layers are calculated according to the EM velocity values entered in the core data file. In order to find the best possible match between picked layers in the radargram and the core data, the layer EM velocity values in the core data file were modified manually. For the beginning EM velocity values to input in the core data file, the laboratory measured RDP values were used for coarse granite ballast obtained in Section 6.2. Then in an iterative way, EM velocity values in the core data file are changed until the best match between the picked layers and core data is found. When the core depths correspond to layer depths in the layer show (as in Figure 7.18), RDP values of the ballast in place were calculated easily from the velocity values entered in the core data file.

Figure 7.18 depicts the layer show for the GPR data from the 2GHz antenna in longitudinal orientation together with the nine trenches opened.

148
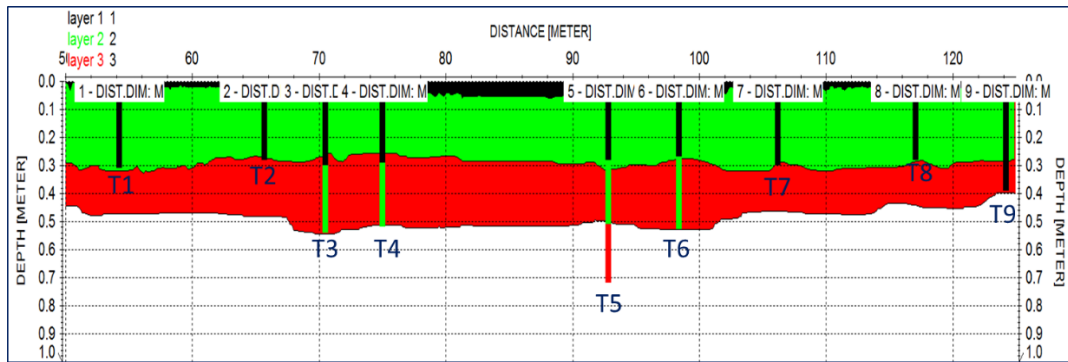
Figure 7.18. Layer show for 2GHz antenna in longitudinal orientation together with core data.

The 1st layer (green layer) is the moderately clean ballast and the 2nd layer (red) layer is the moderately fouled ballast by visual observation during the opening phase of trenches. The EM velocity values used in the core data file to obtain the best match between the picked layers in the radargram and the core data were found to be 0.1675 m/ns for the 1st layer and 0.160 m/ns for the second layer. From these velocity values, RDP values are computed by back-calculation from equation (16) as 3.208 and 3.516, respectively.

Approaching the fouling material as the mixture of sand and gravel (by visual observation) and with the knowledge that the ballast used in this railway line is the same type as the one used in Section 6.2 as the coarse sized granite ballast, referring to Figure 7.4c in Section 6.2 would be required. The equation in Figure 7.4c was used to obtain the fouling percentage of 4.6% corresponding to RDP value of 3.208 and the fouling percentage of 29.6 % corresponding to the RDP value of 3.516. In order to compute the modified Ionescu fouling index values, sieving tests had been performed for the ballast fouled by mixture of sand and gravel. Table 7.13 and Figure 7.19 below were used both of which represent the relationship between volume percentage of fouling material and modified Ionescu fouling index. Fouling categorization was already presented in Table 1.2 in Chapter 1. For trench 9 (T9) under the metal sleepers, it was observed that ballast was highly fouled when the trench was excavated. The EM velocity value used in core data file to match the thickness of fouled ballast in trench 9 was 0.145 m/ns, corresponding to RDP value of 4.281. Similar use of the equation in Figure 7.4c yielded a 91.8 % fouling percentage.

Table 7.13. Modified Ionescu fouling index vs volume percentages of fouling material

Coarse-Sized Granite Ballast + Mixture of Sand and Fine-Sized Gravel						
Volume Percentages	0	10	20	30	40	50
Modified Ionescu Fouling Index	6.8%	11.1%	15.0%	18.6%	21.8%	24.9%
Fouling Category	MC	MF	MF	MF	F	F

According to the equation in Figure 7.19, modified Ionescu fouling index values of 9% and 18% are calculated corresponding to 4.6% and 29.6% fouling percentages. From Table 1.2 in Chapter 1, 9% corresponds to moderately clean ballast (1st layer in Figure 7.18) and 18% corresponds to moderately fouled ballast (2nd layer in Figure 7.18) both of which were in line with preliminary visual observations. As for the trench 9 under metal sleepers, modified Ionescu fouling index value of 40.4% was calculated using the equation in Figure 7.19, corresponding to highly fouled ballast according to Table 1.2 in Chapter 1.

Modified Ionescu Fouling Index vs Fouling Percentage of Mixture on coarse sized granite ballast

$y = 0.0036x + 0.0735$
$R^2 = 0.9959$

(Y axis: MODIFIED IONESCU FOULING INDEX; X axis: FOULING PERCENTAGE ACCORDING TO THE AIR VOIDS)
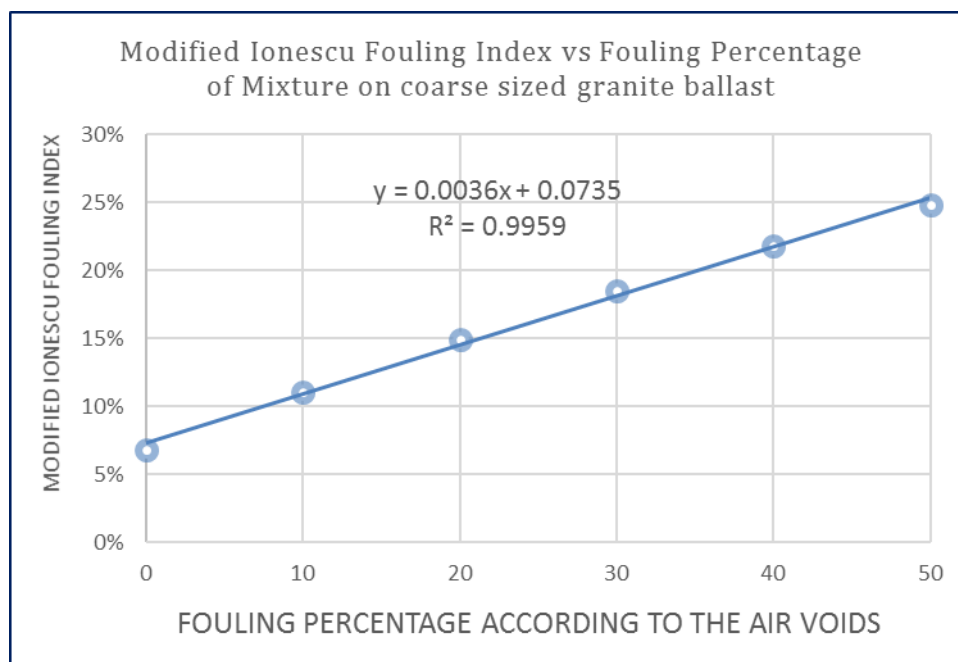
Figure 7.19. The relationship between modified Ionescu Fouling Index and fouling percentage of mixture of sand and fine-sized gravel

7.4.1.1 Types of Sleepers

In this part, the variation of GPR data according to the type of sleepers is briefly discussed. Nearly half length of the tested railway segment had metal sleepers (67.5 m). However, the sensitivity of GPR signals to total reflectors i.e., metal sleepers did not allow to interpret the data beneath the metal sleepers due to many multiple reflections caused as seen in Figure 7.20. Although the wooden sleepers may cause problems due to highly organic compounds that can develop inside with years, in this case, wooden sleepers made of oak tree did not cause any significant problem to image beneath the sleepers, whereas sections with concrete sleepers required antenna orientation change and dedicated processing steps to image under the sleepers and to identify layers and fouling.
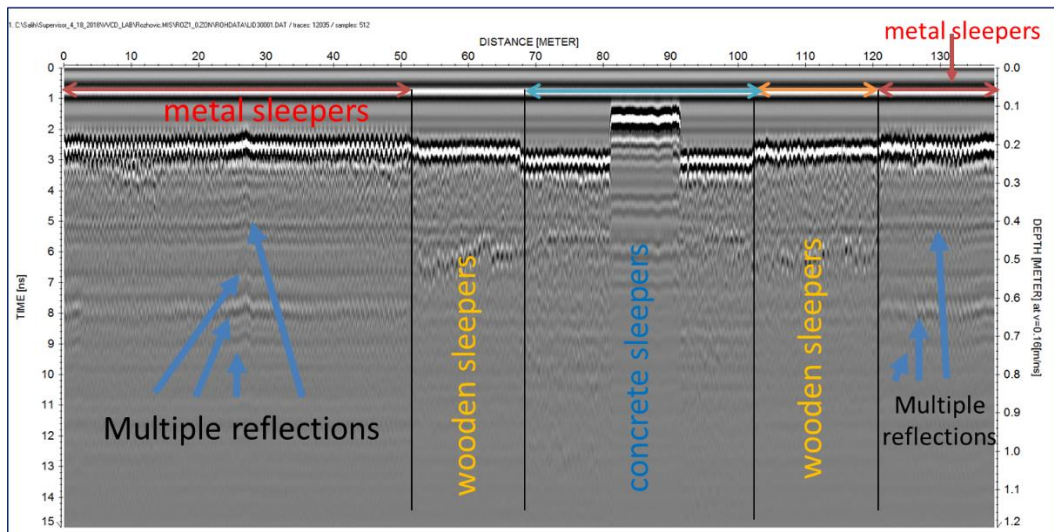
Figure 7.20. Raw 2GHz data of the surveyed railway segment along Rozhovice station (138 m long) with the type of sleepers

7.4.1.2 Type and frequency of antennas

Here, the results from the GPR data collected along Rozhovice train station are analyzed in terms of the frequency of antennas ranging from 400MHz to 2GHz.

400MHz (IDS & GSSI):

Figure 7.21 present the processed radargrams of 400MHz ground-coupled antennas of IDS and GSSI through the same processing steps applied to raw data through Figure 7.12 to Figure 7.17.
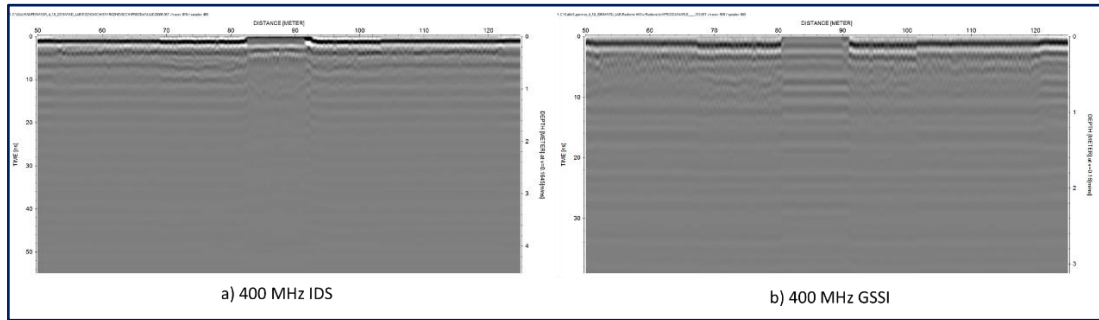
Figure 7.21. Processed radargrams a) 400MHz IDS, B) 400MHz GSSI

Although there are slight differences (reflections under the level crossing) in the processed profiles by 400MHz IDS and GSSI ground-coupled antennas, the reflections are very similar. They both cover a deeper region beyond the thickness of the ballast, which can be used for sub-ballast and formation inspections but with the cost of low resolution as it is the nature of low-frequency antennas.

The slight differences between two different brands but same frequency antennas (400MHz) may stem from the contrasting frequency sum spectrums of them depicted in Figure 7.22, where the peak frequency is 340MHz for IDS antenna and 440MHz for GSSI antenna.
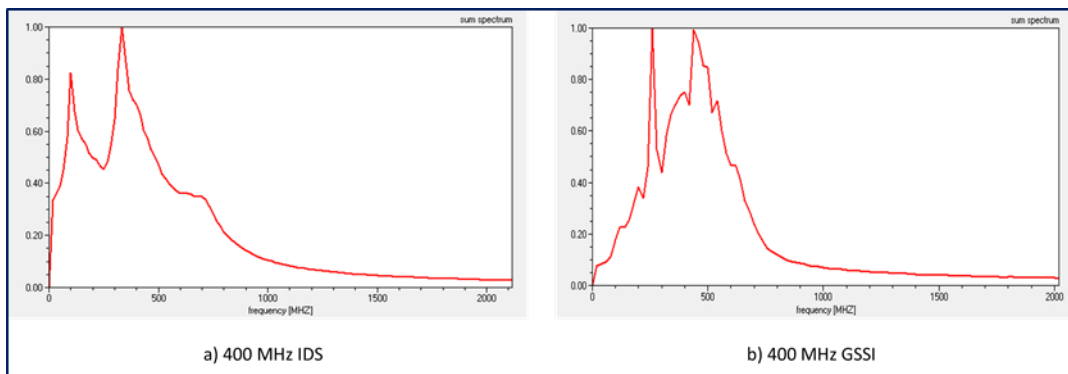
Figure 7.22. Frequency Sum Spectrum a) 400 MHz IDS, b) 400 MHz GSSI

900MHz (IDS):

Below, the processed (same processing steps mentioned above) data collected with IDS 900MHz ground-coupled antenna is presented in Figure 7.23. The first and the second layers could be barely detected after the processing. And as it was the case in 400MHz antennas, 900MHz ground-coupled antenna could be also used for inspections of substructure elements beneath the ballast.

152
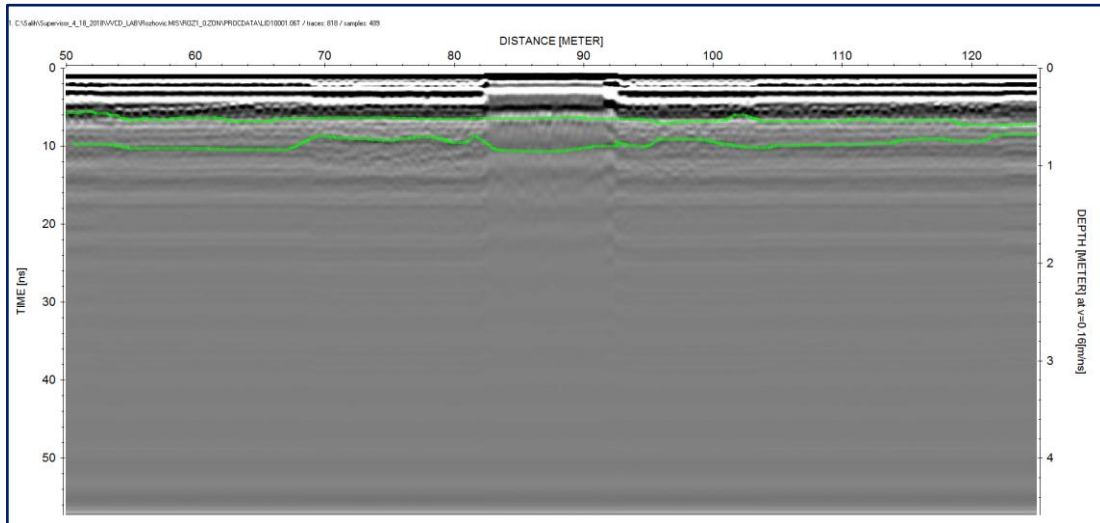
Figure 7.23. Processed data for 900MHz IDS antenna.

1000MHz (GSSI):

For 1000MHz air-coupled antenna from GSSI used by SŽDC, the ballast layer identification worked well as in the case of 2GHz antenna. This is mainly due to the high resolution provided by the frequency of the antenna. In Figure 7.24, processed data for transversely collected data by 1GHz GSSI antenna is presented, whereas Figure 7.25 illustrates the layer show for moderately clean ballast and moderately fouled ballast.
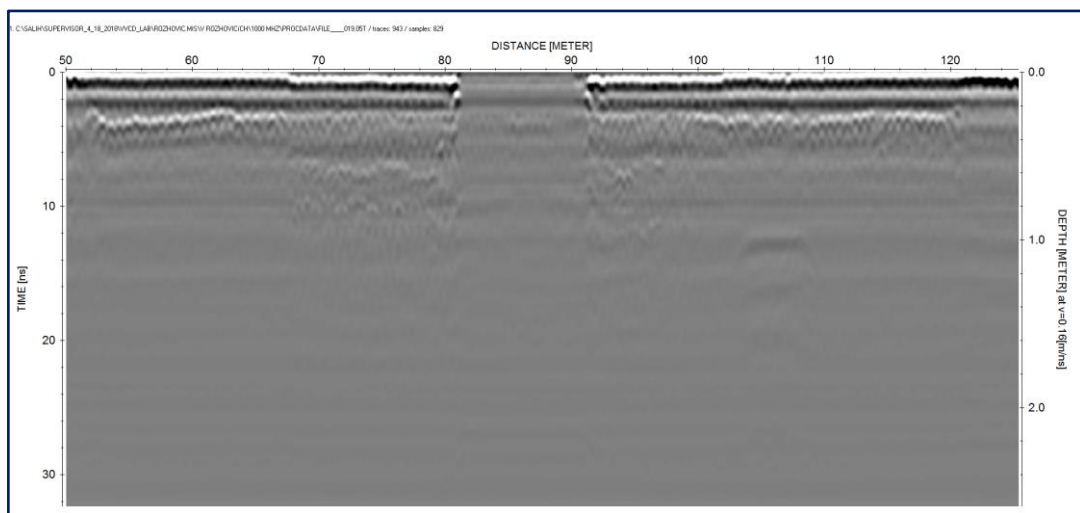
Figure 7.24. Processed data for 1GHz antenna (transverse orientation)
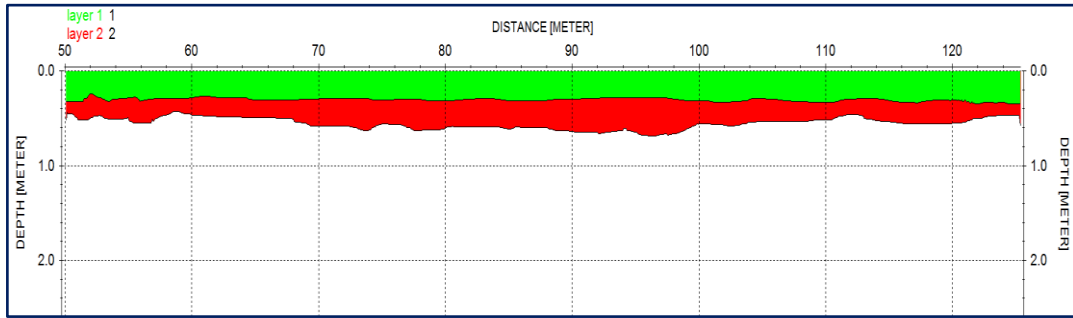
Figure 7.25. Layer show Processed data for 1GHz antenna (red layer: moderately clean ballast, green layer: moderately fouled ballast)

2000MHz (IDS):

As presented in Data Processing Part above, 2GHz antenna provides high-resolution data sufficient for identification of ballast layers (clean and fouled) and enables detection of ballast fouling. However, it is noteworthy that there exists the depth penetration limitation for 2000MHz antenna for inspection of the layers under ballast.

7.4.1.3   The orientation of Air-Coupled Antennas

This section focuses on the influence of orientation of antenna on the GPR data collected from the railway segment in Rozhovice.

1GHz GSSI antenna was oriented in two different configurations, i.e., longitudinally and transversely with respect to track axis, whereas three orientations were used for 2GHz IDS air-coupled antenna for data collection (longitudinal, oblique and transverse). Figure 7.26 shows the longitudinally (a) and transversally (b) collected data by 1GHz GSSI antenna. Both radargrams were processed through the same steps applied through Figure 7.12 to Figure 7.17 as it was step by step processed for 2GHz IDS antenna.

The moderately clean (green layer-first layer in Figure 7.18) and moderately fouled ballast layers (red layer-second layer in Figure 7.18) are both visible in both radargrams in Figure 7.26 (while they are slightly more recognizable in longitudinal compared to transversal orientation).

154
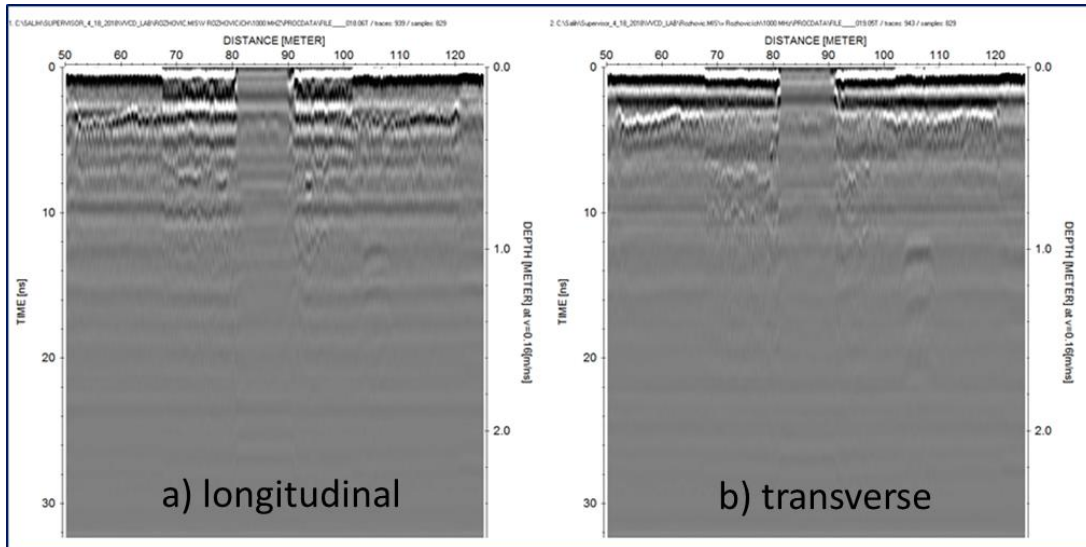
Figure 7.26. Processed 1GHz radargrams data collected in a) longitudinal, b) transversal orientations

However, the sub-ballast layer validated by trench 5 at 10 ns (at approximately 75 cm depth) is much more significantly discernible in longitudinal profile compared to transversal profile. Nevertheless, the transverse orientation provided less noisy reflections just under the sleepers compared to the longitudinal orientation.

Figure 7.27, Figure 7.28, and Figure 7.29 demonstrate the GPR data collected by 2GHz IDS antenna in longitudinal, transversal and oblique orientations, respectively. Longitudinal orientation gives slightly more noticeable layer interfaces compared to transverse orientation, however, both radargrams provide sufficiently distinguishable interface identifications. However, clearly the most noise-free GPR profile, particularly just under the sleepers, is acquired by the transverse orientation. And when oblique orientation is of concern, the noise level is in between the longitudinal and the transverse orientations, so as the identification of layers. Oblique orientation with lower antenna frequency could be used in the track axis to augment the signal noise ratio especially under sleepers and to enhance identification of the ballast layers and underlying layers and high-frequency antennas in the shoulders as in [82].
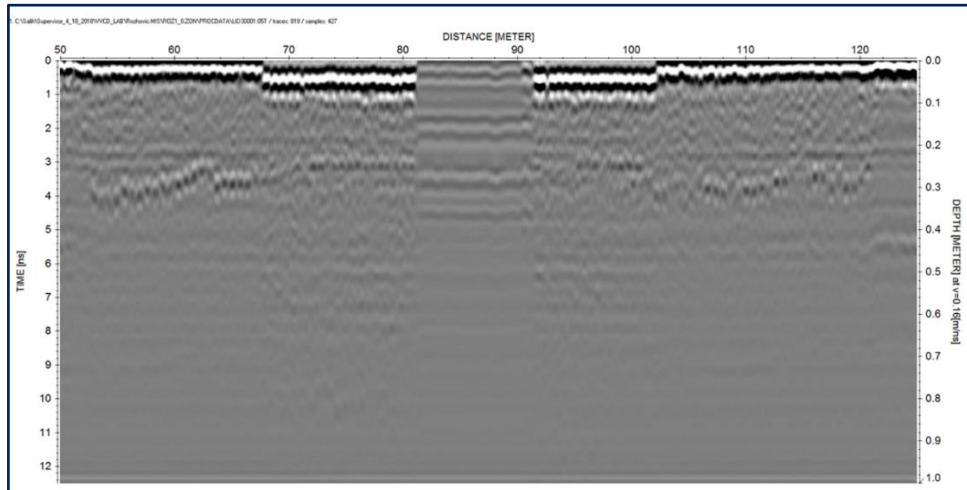
Figure 7.27. Processed 2000MHz GPR data in longitudinal orientation
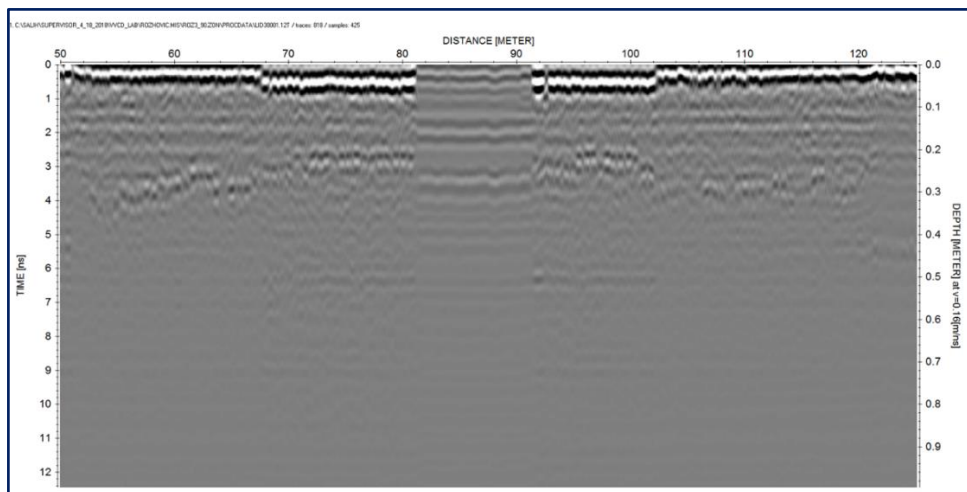
Figure 7.28. Processed 2000MHz GPR data in transversal orientation
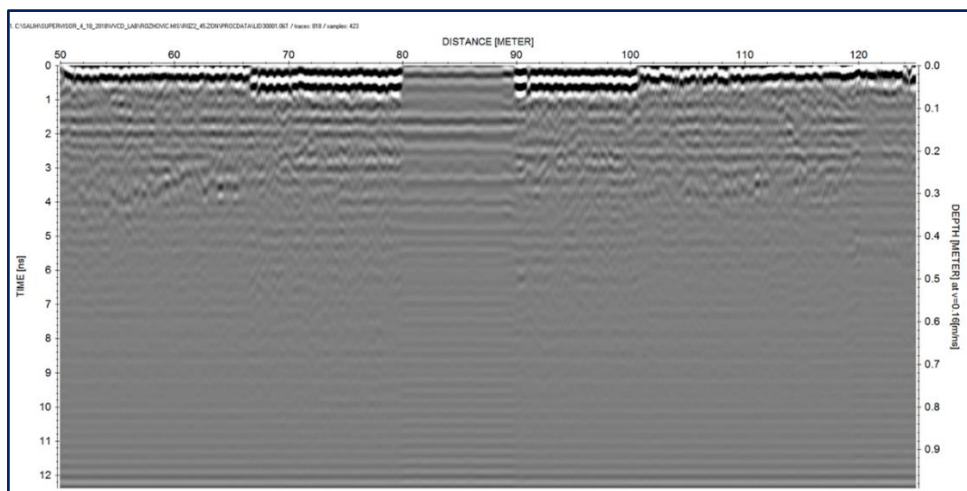
Figure 7.29. Processed 2000MHz GPR data in oblique orientation

156

7.4.2 Discussion of Results and Conclusion

In this section, GPR surveys on different types of sleepers with various nominal frequencies, types, and orientations of the antenna along a real railway track along Rozhovice train station were performed and the results were analyzed. Ground truth data from 9 different locations were collected to facilitate interpretation of the data.

Laboratory measured RDP values were used for the preliminary analysis of the railway track survey where same type granite ballast was used. The data from GPR surveys and ground truth data matched well which verifies the reliability and the eligibility of using various GPR antenna to image track substructure, identify layers and predict fouling conditions.

7.4.2.1 On the type of sleepers

Metal sleepers did not allow to image underneath the sleepers due to multiple reflections caused by them. Wooden sleepers did not influence the GPR signal in the test field which enabled imaging the layers under them. Data collected from sections with concrete sleepers were processed and antenna orientation modifications were required to identify layers and fouling.

7.4.2.2 On the type and frequency of antennas

Ground-coupled antennas:

400MHz and 900MHz IDS and 400MHz GSSI ground-coupled antennas were utilized during GPR surveys. 400MHz ground-coupled antennas image a deeper region beyond the thickness of the ballast, which can be used for sub-ballast and subgrade investigations at the cost of low resolution. 900MHz ground-coupled antenna could also be employed for inspections of substructure elements underlying the ballast layer with better resolution compared to 400MHz. However, ground-coupled antennas are not very suitable for railway inspections due to the facts that i) the clearance (5 to 10 cm at most in ground-coupled antennas) between the antenna bottom and the surface of ballast is not sufficient in most of the cases since there may be railway assets over the railway segments under survey, ii) generally they have low frequency which provides

a deeper penetration of EM signals at the cost of resolution resulting in low-quality imaging of track substructure.

Air-coupled antennas:

1000MHz GSSI and 2000MHz IDS antennas were used during the surveys. Both central frequencies functioned well for ballast layer identification clean and fouled due to their high resolutions. Air-coupled antennas are favorable for railway track surveys since i) they provide a clearance (air gap of 30-45 cm changing according to the brand and type of air-coupled antenna) resulting in a continuous non-destructive survey at normal traffic speeds free from the obstacles and railway assets, ii) high resolution for identification of clean and fouled ballast layers, and sub-ballast/formation layer in case of 1000MHz antenna since for 2000MHz the depth of penetration is not sufficient for detecting sub-ballast/formation layer.

7.4.2.3   On the orientation of the antennas

Profiles acquired by both 1000MHz and 2000MHz antennas in longitudinal orientations, irrespective of the central frequency, slightly provide more discernible layer identification of clean and fouled ballast layers compared to transverse orientations. Data collected with longitudinal orientation of 1000MHz antenna had a distinct reflection from sub-ballast/formation level whereas the transverse orientation of 1000MHz provided an ambiguous reflection at the same two-way time travel axis.

On the other hand, both air- coupled antennas when oriented transversally are less influenced by the concrete reinforced sleepers.

As for oblique orientation of 2000MHz antenna, it is noteworthy to state that the noise level under the sleepers is in between the longitudinal and the transverse orientations. In case of limited time and resources, which is the case most of the time, oblique orientation (45 ° with respect to track axis) could be evaluated as an alternative using lower frequency air-coupled antenna (e.g. 1GHz) to optimize the signal noise ratio under reinforced concrete sleepers hence identification of the ballast/sub-ballast layering and fouling.

7.5 Results of Section 6.5 "Laboratory Assessment of Limestone Railway Ballast as a Function of Ballast Condition, Antenna Type and Frequency, Antenna Orientation, and Presence of Sleepers and Rails" & Discussion

The results from the experiments described and carried out in detail in Section 6.5 will be given in this Section together with the discussion of the findings.

7.5.1 RDP Calculations

The RDP of railway ballast reveals the condition of ballast in terms of its fouling level (i.e. clean, fouled, and highly fouled). Therefore, the RDP values were computed with the KHM where the height of the tank full of ballast (either clean or fouled) is known.

In Table 7.14 below, the RDP values obtained for clean ballast can be seen as a function of the nominal frequency of antennas, (for 2GHz according to its being EU type or NA type), data processing and orientation of antenna (longitudinal or transverse).

Processing steps used in the radargrams from which the results of RDP values are as follows:

- Dewow (subtract-mean) function in 1D filter submenu to remove low-frequency content.
- Envelope function in complex trace analysis submenu to confirm identification and exact position of surface reflection.
- Move start time in static correction/muting submenu was used to adjust surface reflection to time zero level
- Extract wavelet function in 1D filter submenu to average traces in order to minimize random noises
- Insert profile function in edit traces/trace ranges submenu to combine all the statically acquired scans into a B-scan
- Bandpass Butterworth function in 1D filter submenu to remove very low and very high frequencies from the data

These post-processing steps were accomplished in ReflexW Software [111].

Table 7.14. RDP values obtained for clean ballast as a function of the frequency of antennas, antennas being EU type or NA type, data processing and orientation of antenna (long. or trans.)

	1GHz	1.5GHz (VEE)	2GHz (EU)	2GHz (NA)	Average ε_r
Raw-Long.	3.853	3.969	3.911	3.911	3.911
Raw-Trans	3.853	3.969	3.807	3.911	3.885
Proc.-Long	3.911	4.027	3.911	3.911	3.940
Proc.-Trans.	3.911	4.057	3.807	3.945	3.930
Average Long. ε_r	3.882	3.998	3.911	3.911	3.925
Average Trans. ε_r	3.882	4.013	3.807	3.928	3.907
Average Raw. ε_r	3.853	3.969	3.859	3.911	3.898
Average Proc. ε_r	3.911	4.042	3.859	3.928	3.935
Average ε_r	3.882	4.005	3.859	3.919	**3.916**

A representative value, which is the average of all 16 surveys, can be observed as 3.916 for limestone aggregates used. This result is quite in line with the values in Table 4.1, especially with the one published by Leng & Al-Qadi [65]. In the previous work of Tosti et. al., in the same laboratory in the University of Rome Tre with the same ballast materials an average relative permittivity for dry clean ballast was found as 3.757 [126]. Slightly higher representative value for clean ballast obtained during this sets of experiments compared to the previous work [126] may result from the fact that, the tank was filled with fouled ballast at first before arranging the tank for clean configuration. However, although enough attention is paid to remove the fouling material from the ballast stones during arrangement of clean ballast configuration, trace amounts of this fouling material (silty sand) could have remained within the perimeters of the stones. Since fouling material has a higher RDP (5.03 as stated in [20]) those trace amounts could have made that slight increase in the RDP value.

One of the first seen observations as can be seen from Table 7.14, is the RDP values obtained from 1.5GHz (VEE type) antenna are slightly higher than those values obtained with other antennas. This can be caused by the different nature of this antenna

(as notified by IDS) compared to other three horn antennas. No significant change is observed in the values dependent on the orientation of antenna whether it is longitudinal or transverse. Values acquired from processed data tend to have slightly higher values than the ones obtained from raw materials.

The following graphs in Figure 7.30 and Figure 7.31 are presented with the aim of better monitoring of the variations of RDP values which are already presented in Table 7.14. From Figure 7.30, it can be clearly seen that 2GHz NA antenna has better consistency in terms of the permittivity values under different scenarios compared to the other antennas.
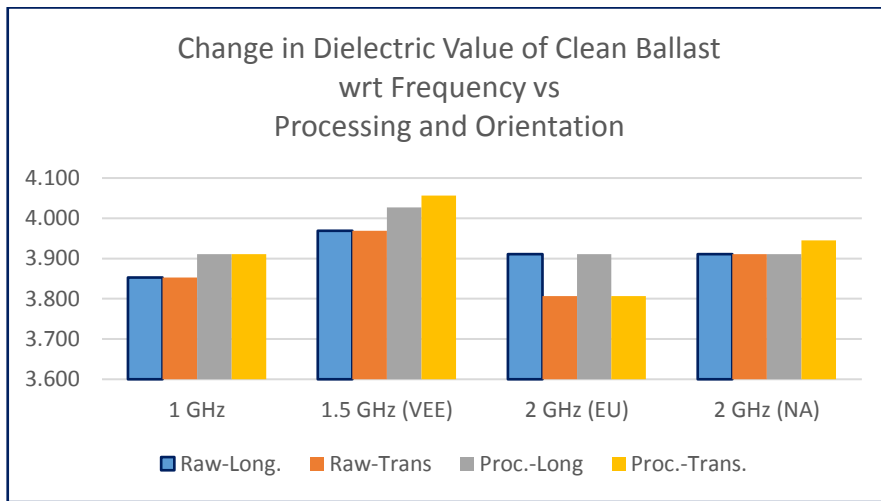

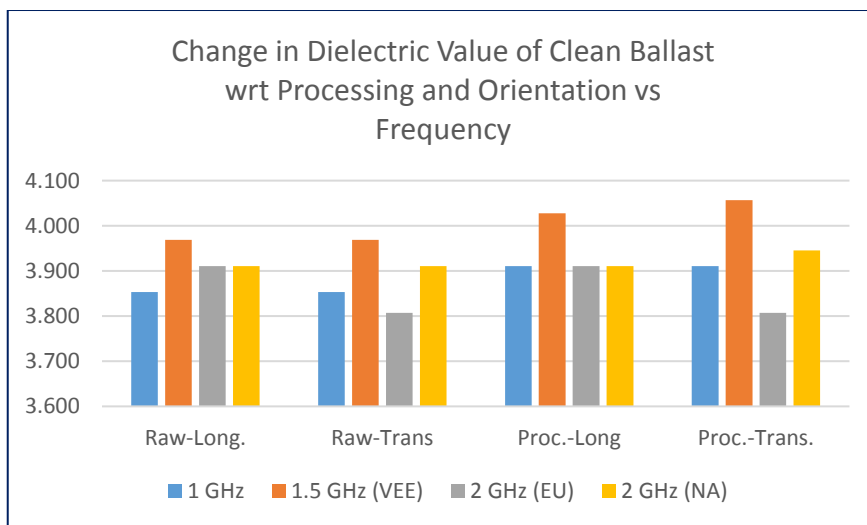**Figure 7.30. Change in RDP values of clean ballast with respect to frequency vs processing and orientation**

Figure 7.31. Change in Dielectric Value of Clean Ballast with respect to Processing and Orientation vs Frequency

161

And as for fouled ballast condition, similar calculations are performed. In Table 7.15 below, the results can be viewed.

Table 7.15. RDP values obtained for fouled ballast as a function of the frequency of antennas, antennas being EU type or NA type, data processing and orientation of antenna (long. or trans.)

	1GHz	1.5GHz (VEE)	2GHz (EU)	2GHz (NA)	Average ε_r
Raw-Long.	5.425	4.990	5.466	5.343	**5.306**
Raw-Trans	5.357	4.893	5.343	5.343	**5.234**
Proc.-Long	5.425	5.023	5.466	5.262	**5.294**
Proc.-Trans.	5.289	5.189	5.303	5.343	**5.281**
Average Long. ε_r	**5.425**	**5.007**	**5.466**	**5.303**	**5.300**
Average Trans. ε_r	**5.323**	**5.041**	**5.323**	**5.343**	**5.257**
Average Raw. ε_r	**5.391**	**4.941**	**5.404**	**5.343**	**5.270**
Average Proc. ε_r	**5.357**	**5.106**	**5.384**	**5.303**	**5.287**
Average ε_r	**5.374**	**5.024**	**5.394**	**5.323**	***5.279***

A representative value, which is the average of all 16 surveys, can be observed as 5.279 for limestone stones used in the STSM. This result is quite in line with the value of 4.84 in Table 4.1, which was the value for 50% fouled limestone ballast by Leng &Al-Qadi [65], and also very close to the RDP value of moist spent ballast which has the value of 5.1 published by Sussmann [94]. Similar to the clean ballast case, the RDP values obtained from 1.5GHz (VEE type) antenna are slightly different than those values obtained with other antennas. Contrary to the clean ballast case, this time those values are lower than the ones obtained by other frequency antennas. As in the clean ballast case, this slight difference is attributed to the different structure of the mentioned antenna. The following graphs in Figure 7.32 and Figure 7.33 can be seen below for a better visualization of the variations of relative permittivity values which took place in Table 7.15. It can be observed in Figure 7.32 that slightly higher relative permittivity values were acquired from raw data compared to ones acquired from processed data. From Figure 7.33 below, similar to the clean ballast case, it was observed that 2GHz NA antenna has better consistency in terms of the permittivity values.
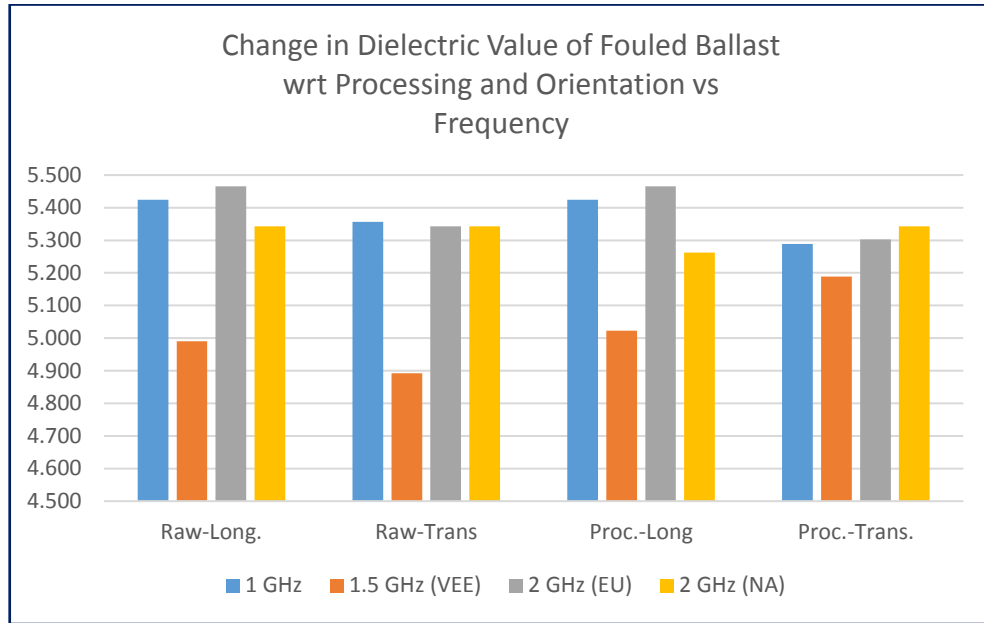
Figure 7.32. Change in dielectric value of fouled ballast with respect to frequency vs processing and orientation
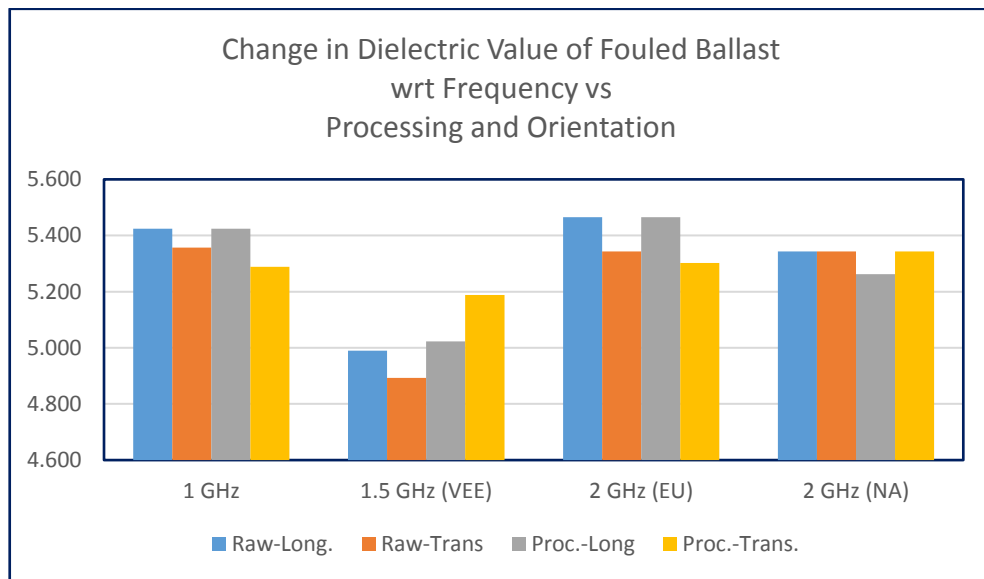
Figure 7.33. Change in Dielectric Value of Fouled Ballast with respect to Frequency vs Processing and Orientation

There exists also an alternative method in estimation of RDP values, SRM, however it had been observed in [20] this method yielded rather lower values which could be caused by the scattering of the limestone aggregates in the surface. Therefore, this method was not exploited.

163

7.5.2   Comparison & Interpretation of Radargrams from different scenarios

In this section, by means of comparing the radargrams under different scenarios, interpretations are figured out in order to evaluate the influence of tested parameters. For example, below in Figure 7.34, a radargram is presented from fouled ballast condition, in 1 sleeper case, with rails. 2GHz Europe antenna was used in transverse orientation. In this figure, from top to bottom, firstly antenna direct wave is seen. Then the surface reflection is visible. The effect of the sleeper is visible just under the surface reflection. The interface between fouled and clean ballast is seen and at the bottom total metal, reflector can be observed. One of the most obvious outcomes in this radargram is that the total metal reflector is masked when the antenna is over the sleeper which is expected due to longitudinal rebars existing in the sleepers.
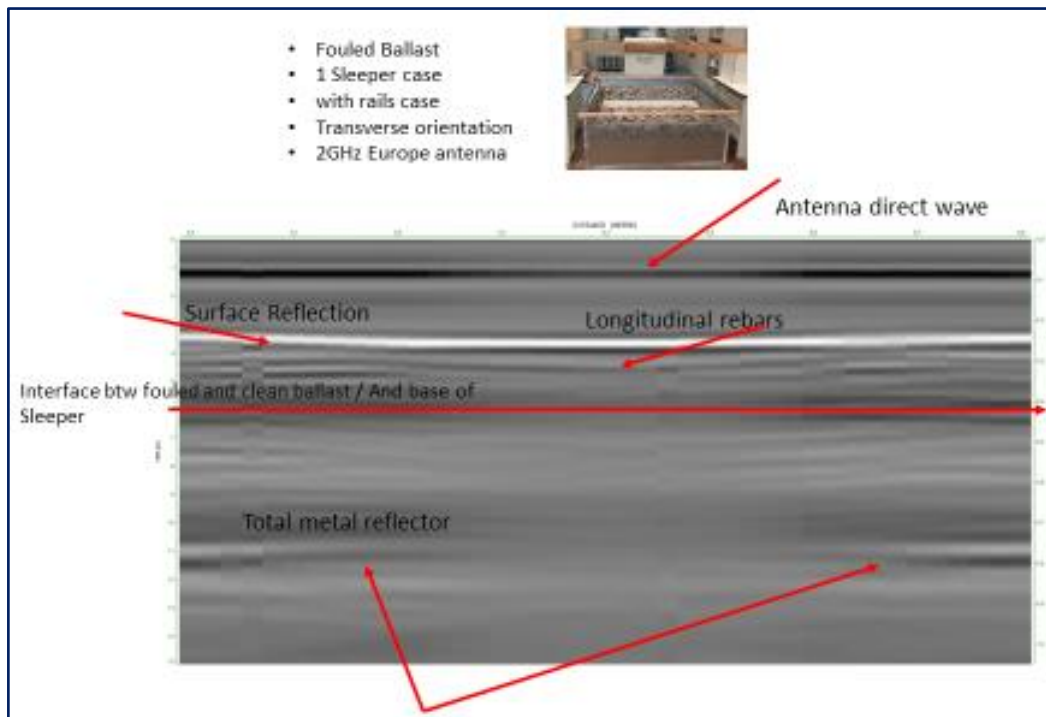
Figure 7.34. Radargram interpretation from the fouled ballast, 1 sleeper case, with rails, 2GHz EU antenna in transverse orientation

Masking of the metal plate is more obvious in Figure 7.35, where radargrams from 1GHz antenna in longitudinal direction were compared in terms of no sleeper and 1 sleeper cases in clean ballast. In the left part of Figure 7.35, which is the no sleeper

case, the metal plate reflection is quite high and visible while in the right part with 1 sleeper case, metal plate reflection is quite masked and barely visible.
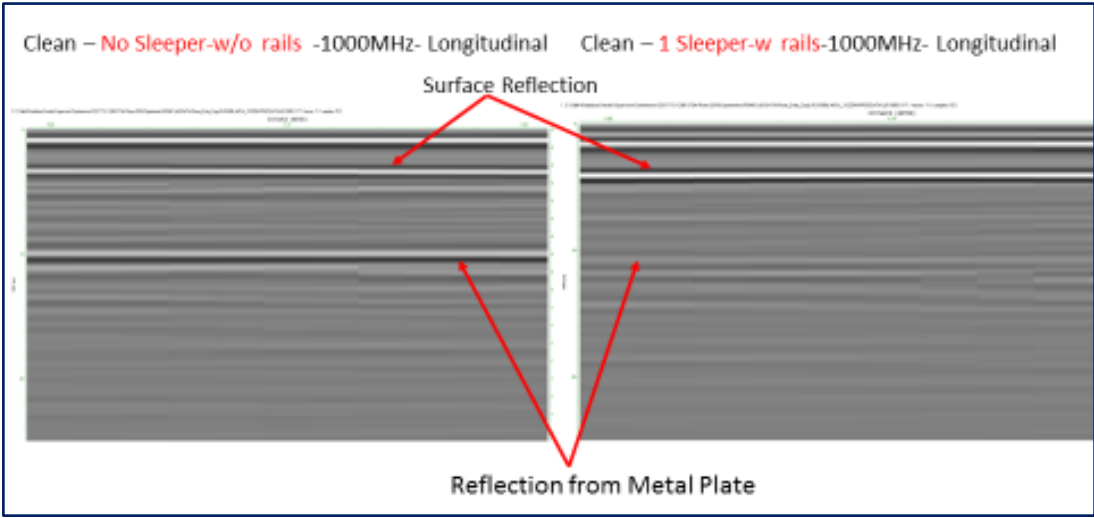
Figure 7.35. Comparison of radargrams from measurements with 1GHz antenna in longitudinal direction in terms of no sleeper and 1 sleeper cases in clean ballast

In Figure 7.36 below, two antennas (1GHz and 2GHz EU in transverse orientation) are compared with each other to see the influence of fouling. In case of fouled material where the RDP value is higher than that of clean ballast, EM wave velocity decreases which in turn results in a higher two-way travel time. In this case, metal plate reflection appears in a deeper location.
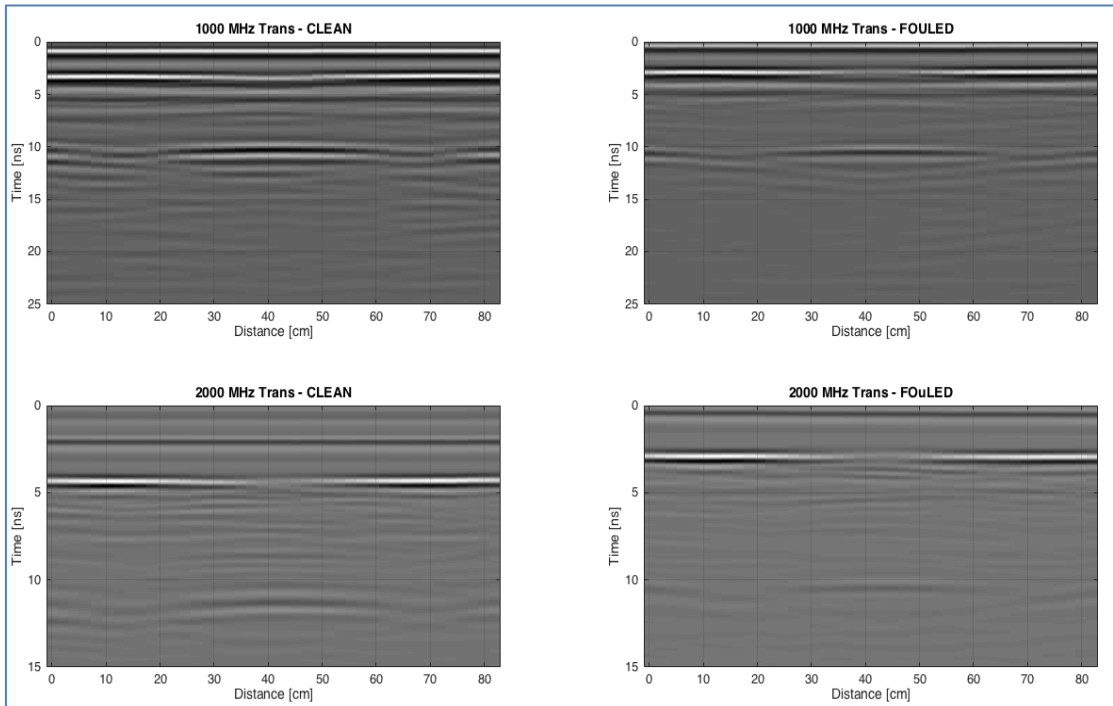
Figure 7.36. Comparison of radargrams from measurements with 1GHz and 2GHz antenna in the transverse direction in terms of clean and fouled ballast conditions.

In Figure 7.37 below, 2GHz NA antenna is used in fouled ballast condition with 1 sleeper case with rails. The comparison is made between the orientations of antennas. The upper part of the Figure 7.37 represents the longitudinal orientation whereas the lower part exhibits the transverse orientation. The sleeper masking effect is obvious in both of the radargrams since the metal plate reflection is almost invisible. The lower part of the Figure 7.37 (transverse orientation) gives a better imaging, better tracking of the surface reflection variation due to the fact that the antenna is moved along a longer distance (80 cm) compared to the case in longitudinal orientation (20 cm) as explained in detail above in the antenna orientation sub-section.

166
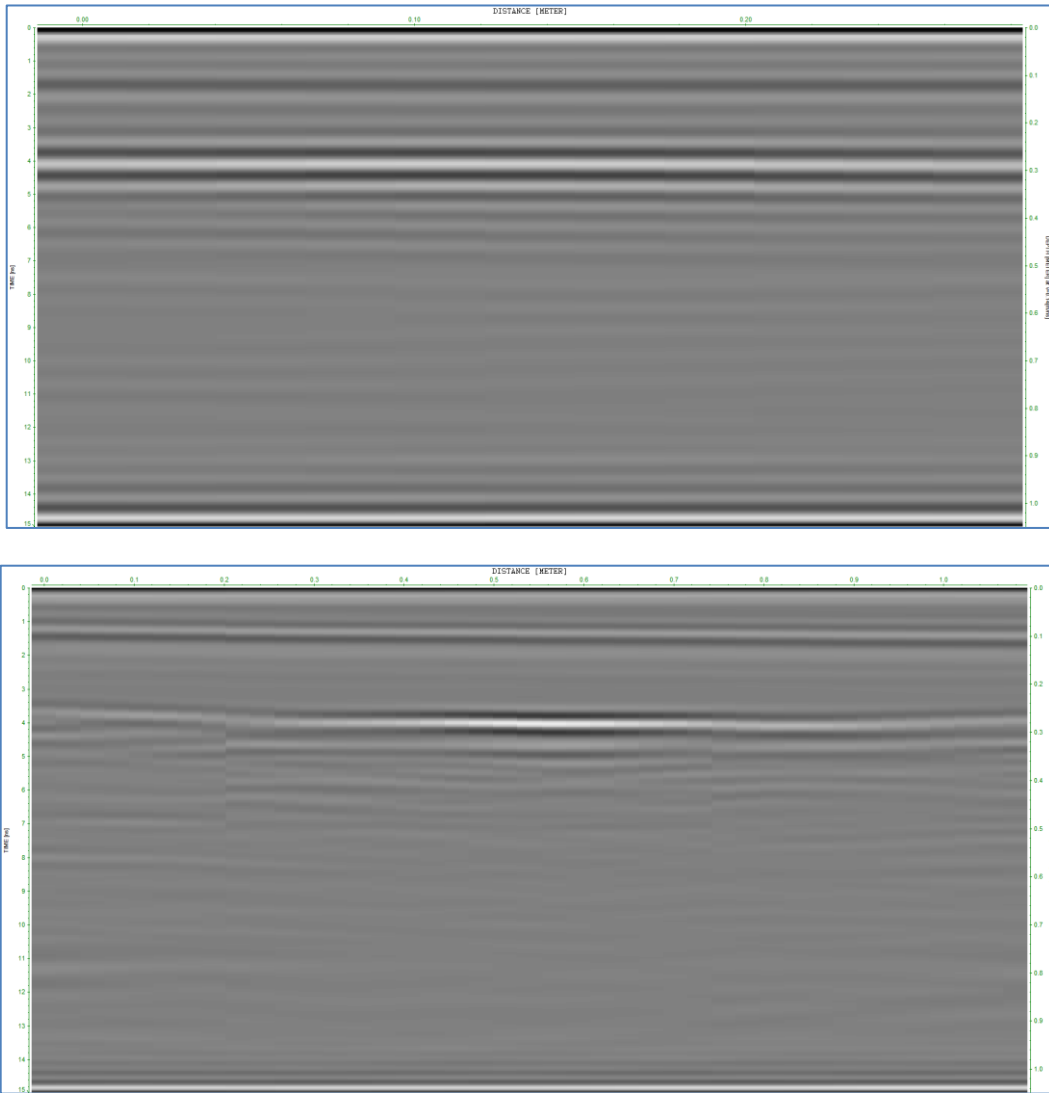
Figure 7.37. Comparison of radargrams from measurements with 2GHz NA antenna with 1 sleeper case in terms of longitudinal and transverse orientations in fouled ballast

Figure 7.38, Figure 7.39, and Figure 7.40 show the radargrams with 2 horizontal steel rods, with 2 horizontal plus 1 vertical steel rod and without any steel rods to imitate rail effects, respectively. The other parameters are the same for these three figures. 1GHz antenna was used in transverse orientation in fouled ballast condition with two sleepers case.
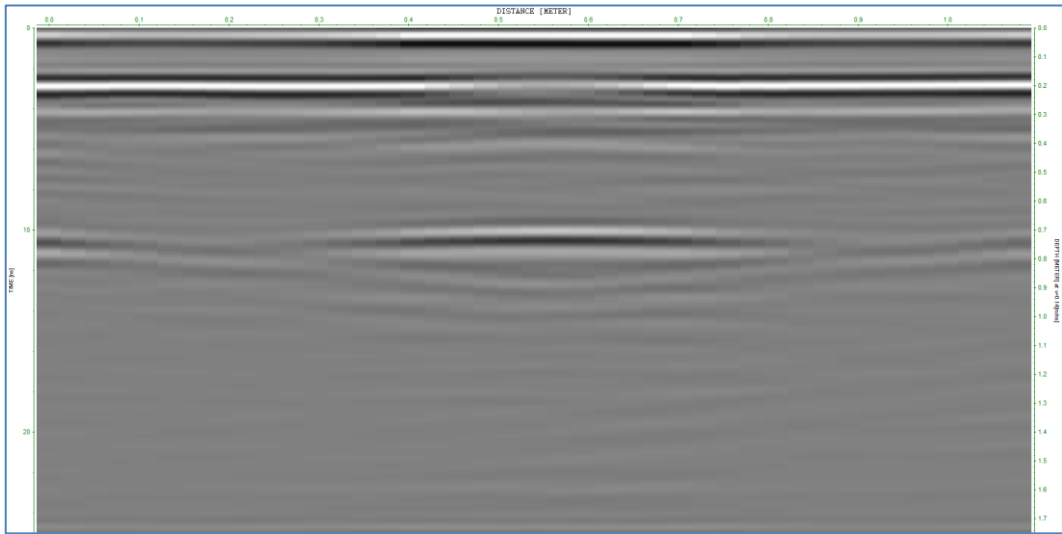
Figure 7.38. 1GHz antenna was used in transverse orientation in fouled ballast condition with two sleepers case: with 2 horizontal steel rods imitating rail effects
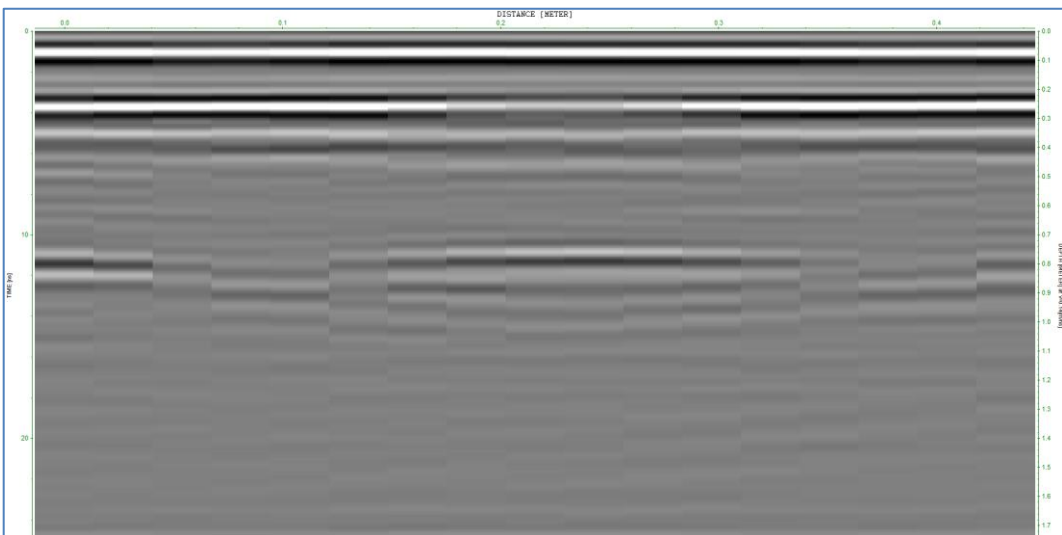
Figure 7.39. 1GHz antenna was used in transverse orientation in fouled ballast condition with two sleepers case: with 2 horizontal and 1 vertical steel rods imitating rail effect
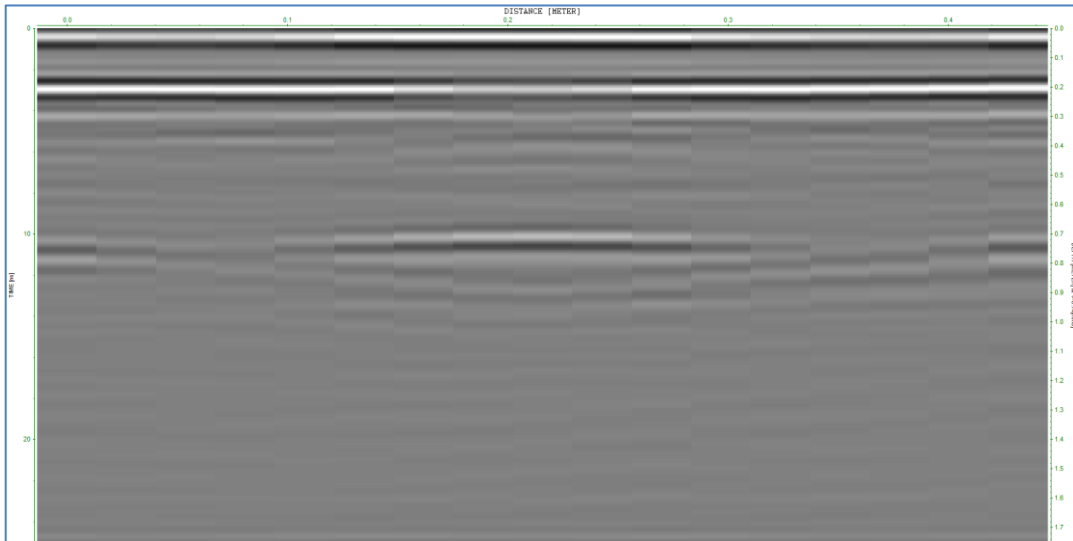
Figure 7.40. 1GHz antenna was used in transverse orientation in fouled ballast condition with two sleepers case: with no steel rods imitating rail effects

As can be seen in Figure 7.38, Figure 7.39, and Figure 7.40, steel rods used to replicate the rails do not pose a discernible, significant difference in the radargrams.

Figure 7.41 below presents the radargrams from 4 antennas in transverse orientation under the same configurations, namely fouled ballast condition with no sleeper and rails. The upper left part is from 1GHz antenna, upper right part is from 1.5GHz VEE antenna, the lower left part is from 2GHz EU antenna and lower right part is from 2GHz NA antenna.
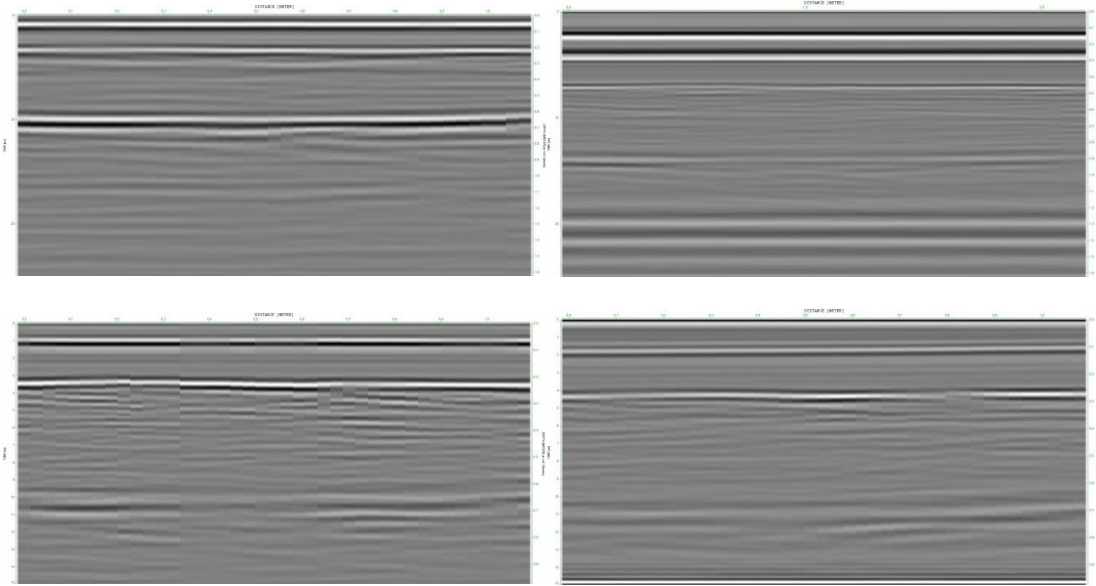
Figure 7.41. Radargrams from 4 antennas in transverse orientation under the same configurations, namely fouled ballast condition with no sleeper and rails: Upper left part: 1GHz antenna, upper right part: 1.5GHz VEE antenna-Lower left part: 2GHz EU antenna lower right part: 2GHz NA antenna

Among all 1.5GHz, VEE type has different character repeating its direct wave in every 20 nanoseconds. Use of 4 antennas proved very beneficial in both calculations of RDP values and interpretations of radargrams. 1GHz antenna provides more discernible layer identification.

For future works and collaboration, different processing steps could be evaluated in order to have better and clearer images, especially under the sleepers. And further comparison combinations could be performed in order to have a better understanding of the parameters tested.

8 CONCLUSION

This dissertation addressed the evaluation of railway infrastructure condition (particularly ballast) by using the non-destructive technology, GPR. The main objective of the dissertation was achieved which was to elaborate the implementation GPR methodology in railway track bed surveys (particularly ballast), through both laboratory and field experiments.

To that effect, the required experience, knowledge and competence with the available GPR software and hardware in order to conduct the experiments, interpret and analyze the results and understand capabilities and the limitations of the GPR methodology was attained.

In summary, EM characteristics of reflected GPR signal from granite (finer and coarser types) and limestone ballast are evaluated and analyzed comparatively under miscellaneous configurations (i.e., as a function of ballast fouling condition – various fouling materials used-, moisture content, type, frequency & orientation of GPR antenna, presence of sleepers and rails, types of sleepers) through laboratory and field experiments.

Laboratory obtained results were validated by theoretical models (by CRIM) and field results.

Results of collected GPR data with different sets of GPR equipment were compared (in terms of brands – IDS: GPR sets owned by University of Pardubice and GSSI: GPR set owned by SŽDC)

Specific objectives of the dissertation as per the experimental sections in Chapter 6 are as follows:

1) In Section 6.1:

Available GPR set owned by the University of Pardubice is evaluated in terms of performance of the equipment through GPR system performance compliance tests. The guidelines, which are still under discussion in view of the threshold values for the performance compliance tests, had been proposed by COST Action TU 1208 members.

4 tests, namely, i) Signal-to-Noise Ratio, ii) Signal Stability, iii) Linearity in the Time Axis and iv) Long-term Stability test were undertaken for 400 MHz, 900 MHz, and 2 GHz central frequencies. The results of 2 GHz antenna were better than the threshold values for Signal-to-Noise Ratio Long-term Stability tests whereas outcomes from 400 MHz and 900 MHz antennas were good to pass Long-term Stability. The guidelines, which are still under discussion in view of the threshold values for the performance compliance tests, had been proposed by COST Action TU 1208 members.

The threshold values, particularly for Signal Stability test are still under discussion, since the average of the results from 9 different antennas from 4 different research teams in 4 different countries (Belgium, Czech Republic, Portugal, Serbia) is 5.52% [112] whereas the criterion dictates that the results should not be higher than 1%. The same applies for also the linearity test, where the average from 5 different antennas is 6% [112] whereas the reference value is 2% (meaning the values should be lower than 2%). It should be noted that all the GPR systems were produced by IDS and GSSI, both of which are among the leading commercial GPR systems commonly used worldwide.

None of them were reported to show signs of malfunctioning. This situation might result in the modification of proposed threshold values, and set new values after having performed further tests to evaluate the performance of GPR systems and the results of those tests with more antennas. Further knowledge and experience in testing could yield the proposal of new threshold values together with modifications of test procedures [112]. For the time being, already new threshold values are proposed in [112] as follows and the results are better comparable with the -proposed threshold values compared to those of ASTM.

2) In Section 6.2:

RDP values of both finer and coarser granite ballast under dry clean and dry fouled conditions by means of various estimation methodologies were estimated. Dry RDP values for both clean ballast types calculated from SRM were much lower than those computed by other two methods.

Comparing three methods for prediction of RDP values, SRM turned out not to suit ballast inspections as also supported by other researchers.

RDP values from other two methods, KHM and CRIM, were in good agreement with each other for both ballast types fouled by all three fouling agents at different times. In other words, experimentally obtained RDP values by means of KHM were verified by the theory-based results computed by CRIM. RDP values for clean and fouled granite ballast values are in good agreement with the published ones by other researchers.

As the fouling level rises, RDP value of the overall system tends to gradually increase which meet the theoretical expectations. The results show how the rise in the fouling levels in case of all three fouling agents leads to an increase in RDP values of both types of ballast and hence a decrease in the EM wave velocity.

Coarser granite ballast was observed to have slightly lower RDP values than finer granite ballast at the same fouling levels when fouled by the same fouling material for all three fouling materials.

For both ballast types, the RDP values of sand fouled ballast were found to be higher than the ones fouled by fine gravel. RDP values for both types of ballast fouled by the mixed material fall into the values between sand fouled ballast and fine gravel fouled ballast.

As a result, for finer ballast, a range of RDP from 3.122 to 5.318 was observed including all three fouling material, while a range of 3.121 to 4.603 was reported for coarser ballast for all three pollutants.

Strong linear trends with the coefficient of determination greater than 0.9 were observed from which RDP values can be predicted for any fouling level.

A baseline for the estimation of the level and type of ballast fouling by correlating the calculated RDP values from GPR acquisitions with fouling percentages based on the ballast materials and fouling agents used in the laboratory experiments was obtained. This is likely to improve the assessment and monitoring efficiency of railway site investigations on the condition that similar ballast types used in these experiments are fouled by similar fouling agents in real track conditions.

3) In Section 6.3:

The influence of moisture (water) in the clean and fouled coarse granite ballast on the GPR signal characteristics are assessed.

RDP values of ballast under wet clean and wet fouled conditions by means of KHM and CRIM were computed. A basis for the prediction of the RDP values of wet clean and wet fouled ballast by comparing the RDP values with the added volumetric percentage of water for a specific fouling level is obtained.

Introducing water into clean and fouled ballast increases RDP value meeting the theoretical expectations since the RDP of water is 81, which is remarkably higher than the ballast and fouling materials. RDP of saturated clean coarse granite ballast was found to be 25.5, whereas the average value of drained ballast (3.152) was observed to have similar values with the dry one (3.090)

For clean ballast and for fouled ballast at each fouling level, increase in the water level resulted in a rise in RDP value of the mixture of ballast and fouling material. RDP values can be estimated for various water contents by the linear relationships observed.

4) In Section 6.4:

Eligibility of GPR surveys on different types of sleepers with various nominal frequencies, types, and orientations of the antenna along a real railway track is evaluated.

Laboratory measured RDP values in Section 6.2 were used for the preliminary analysis of the railway track survey where same type granite ballast was used. The data from GPR surveys and ground truth data matched well which verifies the reliability and the eligibility of using various GPR antenna to image track substructure, identify layers and predict fouling conditions.

Metal sleepers did not allow to image underneath the sleepers due to multiple reflections caused by them. Wooden sleepers did not influence the GPR signal in the test field which enabled imaging the layers under them. Data collected from sections with concrete sleepers were processed and antenna orientation modifications were required to identify layers and fouling.

Air-coupled antennas with 1000 MHz GSSI and 2000 MHz IDS antennas functioned well for layer identification of clean and fouled ballast due to their high

resolutions. Air-coupled antennas are favorable for railway track surveys compared to ground-coupled ones since i) they provide a clearance (air gap of 30-45 cm changing according to the brand and type of air-coupled antenna) resulting in a continuous non-destructive survey at normal traffic speeds free from the obstacles and railway assets, ii) high resolution for identification of clean and fouled ballast layers, and sub-ballast/formation layer in case of 1000 MHz antenna since for 2000 MHz the depth of penetration is not sufficient for detecting sub-ballast/formation layer.

Profiles acquired by both 1000 MHz and 2000 MHz antennas in longitudinal orientations, irrespective of the central frequency, slightly provide more discernible layer identification of clean and fouled ballast layers compared to transverse orientations.

Data collected with longitudinal orientation of 1000 MHz antenna had a distinct reflection from sub-ballast/formation level whereas the transverse orientation of 1000 MHz provided an ambiguous reflection at the same two-way time travel axis.

On the other hand, both air- coupled antennas when oriented transversally are less influenced by the concrete reinforced sleepers.

As for oblique orientation of 2000 MHz antenna, it is noteworthy to state that the noise level under the sleepers is in between the longitudinal and the transverse orientations. In case of limited time and resources, which is the case most of the time, oblique orientation (45 ° with respect to track axis) could be evaluated as an alternative using lower frequency air-coupled antenna (e.g. 1 GHz) to optimize the signal noise ratio under reinforced concrete sleepers hence identification of the ballast/sub-ballast layering and fouling.

5) In Section 6.5:

EM characteristics of limestone ballast material under different configurations of laboratory experiments were assessed. Based on numerous different configurations, it is assessed how and to what extent GPR signal is influenced by the clean and fouled configurations of ballast material with and without the reinforced concrete sleepers and rails by using 4 different air-coupled antennas in two different antenna orientations. Additionally, the variation of RDP values of ballast material caused by fouling were

obtained and compared with the clean ballast. RDP values of obtained clean and fouled limestone ballast matched well with the published ones.

RDP values obtained from 1.5 GHz (VEE type) antenna were slightly different than those values obtained with other antennas. This can be caused by the different nature of this antenna (as told by IDS) compared to other three horn antennas. No obvious variation is observed in the calculated RDP values dependent on the orientation of antenna whether it is longitudinal or transverse. RDP values acquired from processed data tend to have slightly higher values than the ones obtained from raw materials.

Use of sleeper(s) in the tank caused metal plate reflection to be quite masked and barely visible due to the attenuation effect irrespective of clean and fouled condition and irrespective of orientation.

Transverse orientation gave a better imaging, better tracking of the surface reflection variation due to the fact that the antenna is moved along a longer distance (80 cm) compared to the case in longitudinal orientation (20 cm) as explained in detail above in the antenna orientation sub-section.

Among the 4 air-coupled antennas used in Section 6.5 1.5GHz, VEE type has different character repeating its direct wave in every 20 nanoseconds. Use of 4 antennas proved very beneficial in both calculations of RDP values and interpretations of radargrams. 1GHz antenna provides more discernible layer identification.

To conclude, the influences of GPR antenna type, frequency, and orientation together with the effect of presence and type of sleepers on the EM characteristics of ballast have been assessed and analyzed in a comparison-wise manner.

The results and determined relationships apply only to materials and GPR equipment used in this thesis

Overall, upon the results obtained through all the laboratory and field measurements conducted, this dissertation confirms the effectiveness and eligibility of GPR method to diagnose the condition of ballast in terms of fouling level and type, moisture content, and to identify the layering of clean and fouled ballast, hence improving the evaluation and monitoring efficiency of railway infrastructure site investigations.

8.1 Contributions of the Dissertation

Contributions of the dissertation can be summarized as follows:

GPR preliminary signal stability tests have been performed in University of Pardubice parallel with 4 GPR research teams throughout Europe, i.e., i) Université Catholique de Louvain and ii) BRRC, Brussels from Belgium, iii) FTS, Novi Sad from Serbia, and iv) LNEC from Lisbon, Portugal. These preliminary tests contributed to the preparation of the guidelines of GPR Performance Compliance Tests proposed by COST TU1208 Action. There were recommendations on the preliminary results from all 4 research groups at several meetings such as the Working Group Meeting held in Rome, Italy, 6th General Meeting held in Split Croatia, and GPR Roadshow held in Osijek, Croatia, all events within the scope of COST TU 1208 Action. Finally, the discussions on those meetings yielded a better guideline for GPR performance compliance tests which is to be published in 2018 fall with all the results from research teams.

RDP values obtained in this dissertation for clean ballast (granite & limestone) and fouled ballast (granite & limestone) for the fouling materials used (sand, fine gravel, mixture of the first two, and silty sand) might form a preliminary baseline for estimation of RDP values of similar types of ballast in real track field surveys. These values can serve as a basis for future studies in terms of usage and comparison.

Similarly, RDP values attained through moisture tests for wet clean and wet fouled ballast might have the same contribution.

The results obtained from the co-operation and joint field survey with SŽDC along the real railway line next to Rozhovice station might have a good impact for the GPR railway surveys in the Czech Republic. It might draw the interest of other private and/or academical institutions on both GPR measurements and non-destructive assessment of railway infrastructure.

Types, orientations, and frequencies of antennas might pave the way for future studies aiming at the selection of optimized antenna features for specific surveys.

As noted in the Introduction part, Turkish railways lack the non-destructive inspection methods, particularly, GPR evaluation of trackbed. The outcomes acquired

here might influence the other researchers in Turkey in view of the applicability of GPR on Turkish railway infrastructure. The author indeed has the aim of continuing further research on this subject after returning to Turkey and realize this powerful, economical, time-saving and continuous railway infrastructure diagnostic tool as a routine method in Turkey.

Two bachelor students in the Department of Transport Structures, Faculty of Transport Engineering from the University of Pardubice got also involved in the experimental parts of the Sections 6.2 and 6.3 of this study as their bachelor diploma works. The shared knowledge and experience would be encouraging for them to continue their academic career on the same subject for graduate studies which will provide more research on this topic.

8.2 Future Perspectives

At the moment, to improve the use of GPR in railways, the focus is to develop algorithms to enhance data processing and remove the clutter from the GPR signal. Moreover, automation of the overall process from data acquisition to data processing and interpretation is significant to shorten the whole procedure and make it more objective and operator independent. Antenna arrays and GPR with a combination of other NDT methods could be used to improve the efficiency of the GPR technique.

To further advance and build upon the findings of this thesis, several subjects should be explored further, which are mentioned below

My intention is to further study on the guidelines for the GPR performance compliance test in terms of both threshold values and procedures of the tests

I would like to focus on performing specialized surveys on the cribs and in turn on the sleepers in order to further remove the sleeper effect (noise) in an automated way from the GPR data through advanced post-processing schemes.

I plan to work on proposal of guidelines for optimum GPR set configuration (type frequency and orientation of antennas) according to the properties of railway track bed to be surveyed (the expected thickness of ballast, expected condition of ballast,

presence of sub-ballast layer and thickness, overall thickness of the ballast, sub-ballast and subgrade, the type of sleepers, the maintenance information etc.)

It would be very beneficial to incorporate GPR with other non-destructive techniques such as Falling Weight Deflectometer and Lightweight Falling Deflectometer in railway track bed surveys.

I wish to work on the transfer the gained knowledge of GPR methodology on condition assessment of ballast to Turkish Railways infrastructure and further research this challenging subject with the site investigations in Turkish railways.

REFERENCES

[1] W. Shao, A. Bouzerdoum, S.L. Phung, L. Su, B. Indraratna, C. Rujikiatkamjorn, Automatic Classification of Ground-Penetrating-Radar Signals for Railway-Ballast Assessment, IEEE Trans. Geosci. Remote Sens. 49 (2011) 3961–3972. doi:10.1109/TGRS.2011.2128328.

[2] R.C. Agarwal, Advantages and Disadvantages of Railway Transport, http://www.yourarticlelibrary.com/geography/transportation/advantages-and-disadvantages-of-railway-transport/42134/.

[3] G. Santos, Road transport and CO 2 emissions: What are the challenges?, Transp. Policy. 59 (2017) 71–74. doi:10.1016/j.tranpol.2017.06.007.

[4] R. Nålsund, Railway Ballast Characteristics, Selection Criteria and Performance, Norwegian University of Science and Technology (2014).

[5] I.L. Al-Qadi, W. Xie, R. Roberts, Z. Leng, Data analysis techniques for GPR used for assessing railroad ballast in high radio-frequency environment, J. Transp. Eng. 136 (2010) 392–399.

[6] D. Li, D. Read, H. Thompson, T. Sussmann, R. McDaniel, N.S. Railway, V.A. Roanoke, Evaluation of Ground Penetrating Radar Technologies for Assessing Track Substructure Conditions, in American Railway Engineering and Maintenance of Way Association Annual Conference, At Orlando, FL (2010).

[7] T. Lidén, Railway Infrastructure Maintenance - A Survey of Planning Problems and Conducted Research, Transp. Res. Procedia. 10 (2015) 574–583. doi:10.1016/j.trpro.2015.09.011.

[8] J. Hugenschmidt, Railway track inspection using GPR, J. Appl. Geophys. 43 (2000) 147–155.

[9] E.T. Selig, J.M. Waters, Track Geotechnology and Substructure Management,

Thomas Telford (1994).

[10] B. Solomon, Railway Maintenance Equipment: The Men and Machines that

Keep the Railroads Running, Voyageur Press (2001).

[11] M.R. Clark, R. Gillespie, T. Kemp, D.M. McCann, M.C. Forde, Electromagnetic properties of railway ballast, NDT E Int. 34 (2001) 305–311.

[12] J.P. Hyslip, S.S. Smith, G.R. Olhoeft, E.T. Selig, Assessment of railway track substructure condition using ground penetrating radar, in: 2003 Annu. Conf. AREMA (2003).

[13] Rail profile, Wikipedia. (2018). https://en.wikipedia.org/w/index.php?title=Rail_profile&oldid=839675012.

[14] Railroad tie, Wikipedia. (2018). https://en.wikipedia.org/w/index.php?title=Railroad_tie&oldid=840654378.

[15] R.P. De Bold, Non-destructive evaluation of railway trackbed ballast, University of Edinburgh (2011).

[16] F. De Chiara, Improvement of railway track diagnosis using ground penetrating radar, University of Rome "Sapienza" (2014).

[17] TERRAM Rail Geosynthetics | Permanent Way | Track Bed Geotextile, http://www.terram.com/market-sector/railways/.

[18] W.W. Hay, Railroad Engineering, Wiley (1982).

[19] EN 13450:2002/AC:2004 Aggregates for Railway Ballast (2004).

[20] A. Benedetto, F. Tosti, L. Bianchini Ciampoli, A. Calvi, M.G. Brancadoro,

A.M. Alani, Railway ballast condition assessment using ground-penetrating radar – An

experimental, numerical simulation and modeling development, Constr. Build. Mater.

140 (2017) 508–520. doi:10.1016/j.conbuildmat.2017.02.110.

[21] Q. Zhang, J. Gascoyne, A. Eriksen, Characterisation of ballast materials in

trackbed using ground penetrating radar: Part 1, in: Railw. Cond. Monit. Non-Destr.

Test. RCM 2011 5th IET Conf. On, I pp. 1–8. (2011).

[22] P. Anbazhagan, P.S.N. Dixit, T.P. Bharatha, Identification of type and degree of railway ballast fouling using ground coupled GPR antennas, J. Appl. Geophys. 126 (2016) 183–190. doi:10.1016/j.jappgeo.2016.01.018.

[23] P. Anbazhagan, S. Lijun, I. Buddhima, R. Cholachat, Model track studies on fouled ballast using ground penetrating radar and multichannel analysis of surface wave, J. Appl. Geophys. 74 (2011) 175–184. doi:10.1016/j.jappgeo.2011.05.002.

[24] D. Ionescu, Ballast degradation and measurement of ballast fouling, in: Proc. 7th Int. Railw. Eng. Conf., Engineering Technics Press, London, 2004.

[25] P. Anbazhagan, Characterization of Rail Track Ballast Fouling Using Ground Penetration Radar and Field Sampling, (2013).

[26] P.A. Y. Ibrekk, Detecting Anomalies and Water Distribution in Railway Ballast using GPR, Norwegian University of Science and Technology (2015).

[27] R. Jack, P. Jackson, Imaging attributes of railway track formation and ballast using ground probing radar, NDT E Int. 32 (1999) 457–462.

[28] F. De Chiara, S. Fontul, E. Fortunato, GPR Laboratory Tests For Railways Materials Dielectric Properties Assessment, Remote Sens. 6 (2014) 9712–9728. doi:10.3390/rs6109712.

[29] S.S. Artagan, V. Borecky, Applicability of GPR on Turkish Railways, (2016). http://www.ejoir.org/klasik/belge/ozelsayi2015c1/15.pdf.

[30] L. Bianchini Ciampoli, A. Calvi, A. Benedetto, F. Tosti, A.M. Alani, Efficient practices in railway ballast maintenance and quality assessment using GPR, proceedingss of the Aiit International Congress on Transport Infrastructure and Systems (Tis 2017), Rome, Italy (2017).

[31] A. Benedetto, L. Pajewski, eds., Civil Engineering Applications of Ground Penetrating Radar, Springer International Publishing, Cham, (2015).

[32] Maxwell, J.C., On Physical Lines of Force, Philos. Mag. (1861).

[33] Hertz, H.R., Ueber sehr schnelle electrische Schwingungen, Ann. Phys. 7 (1887) 421–448.

[34] Marconi, G., Improvements in Transmitting Electrical Impulses and Signals, and in Apparatus Therefor, 12,039, n.d.

[35] Hülsmeyer, C., Verfahren, um metallische Gegenstände mittels elektrischer Wellen einem Beobachter zu melden, DE165546, n.d.

[36] D.J. Daniels, Ground penetrating radar, The Institution of Electrical Engineers (2004).

[37] H. Löwy, & G. Leimbach, , Eine elektrodynamische Methode zur Erforschung des Erdinneren, Phys. Z. (1910) 697–705.

[38] Invention of radar & the microwave technology - Open Tesla Research, (1917).

[39] Hülsenbeck et al., 489434, (1926).

[40] A. Loulizi, Development of ground penetrating radar signal modeling and implementation for transportation infrastructure assessment, Virginia Polytechnic Institute and State University (2001).

[41] Stern, W., Versuch einer elektrodynamischen Dickenmessung von Gletschereis, Ger Beitr Zur Geophys. (1929) 292–333.

[42] Radar, Wikipedia Free Encycl. (2016). https://en.wikipedia.org/w/index.php?title=Radar&oldid=724446839 (accessed June 14, 2016).

[43] L.B. Conyers, Ground-penetrating radar for archaeology, AltaMira Press, Walnut Creek, CA (2004).

[44] M. A. H. El-said, Geophysical prospection of underground water in the desert by means of electromagnetic interference fringes, in: Proc. IRE (1956) pp. 24–30.

[45] A.P. Annan, GPR—History, trends, and future developments, Subsurf. Sens. Technol. Appl. 3 (2002) 253–270.

[46] J.T. Bailey, S. Evans, G. de Q. Robin, Radio Echo Sounding of Polar Ice Sheets, Nature. 204 (1964) 420–421. doi:10.1038/204420a0.

[47] Bently, C.R., The structure of Antarctica and its ice cover, 2: Solid Earth and Interface Phenomena (1964) 335.

[48] M.E.R. Walford, Radio Echo Sounding Through an Ice Shelf, Nature. 204 (1964) 317–319. doi:10.1038/204317a0.

[49] B. 0. Steenson, Radar methods for the exploration of glaciers, Calif. Inst. Tech (1951).

[50] S. Evans, Radio techniques for the measurement of ice thickness, Polar Rec. (1963) 406–410.

[51] G.R. Olhoeft, Applications and frustrations in using ground penetrating radar, IEEE Aerosp. Electron. Syst. Mag. 17 (2002) 12–20.

[52] S.S. Artagan, V. Borecky, History of using GPR for diagnostics of transport structures in: Proceedings of 6 th International Scientific Conference (2015) pp. 24-30.

[53] a17experiment_sep_en.jpg (JPEG Image, 2810 × 800 pixels) - Scaled (67%), (n.d.). https://www.hq.nasa.gov/alsj/a17/a17experiment_sep_en.jpg (accessed June 21, 2016).

[54] M. Robinson, C. Bristow, J. McKinley and A. Ruffell,Ground Penetrating Radar, Geomorphological Techniques, Part 1, Sec. 5.5 British Society for Geomorphology, (2013).

[55] A. Neal, Ground-penetrating radar and its use in sedimentology: principles, problems and progress, Earth-Sci. Rev. 66 (2004) 261–330. doi:10.1016/j.earscirev.2004.01.004.

[56] T. Saarenketo, Electrical properties of road materials and subgrade soils and the use of Ground Penetrating Radar in traffic infrastructure surveys, University of Oulu (2006).

[57] A.P. Annan, J.L. Davis, Ground penetrating radar—coming of age at last, in: Proc. Explor. (1997) pp. 515–522.

[58] H. B. Thompson II , G. Carr, Ground Penetrating Radar Evaluation and Implementation, Research Results Report, Federal Railroad Administration (2014).

[59] H.M. Jol, ed., Ground penetrating radar: theory and applications, 1. ed, Elsevier Science, Amsterdam (2009).

[60] A. Martinez, A.P. Brynes, Modeling dielectric-constant values of geologic materials: an aid to ground-penetrating radar data collection and interpretation, Kansas Geological Survey (2001).

[61] J.L. Davis, A.P. Annan, Ground-penetrating radar for high-resolution mapping of soil and rock stratigraphy1, Geophys. Prospect. 37 (1989) 531–551. doi:10.1111/j.1365-2478.1989.tb02221.x.

[62] Artagan, Salih Serkan, Borecký, Vladislav, Estimation Methods for Obtaining GPR Signal Velocity, Int. J. Civ. Struct. Eng. 3 (2016) 59–63.

[63] A. Loizos, C. Plati, Ground penetrating radar: A smart sensor for the evaluation of the railway trackbed, in: Instrum. Meas. Technol. Conf. Proc. 2007 IMTC 2007 IEEE (2007) pp. 1–6.

[64] A.P. Annan, 11. Ground-Penetrating Radar, in: -Surf. Geophys., 2012: pp. 357–438. doi:10.1190/1.9781560801719.ch11.

[65] Z. Leng, I. Al-Qadi, Railroad Ballast Evaluation Using Ground-Penetrating Radar: Laboratory Investigation and Field Validation, Transp. Res. Rec. J. Transp. Res. Board. 2159 (2010) 110–117. doi:10.3141/2159-14.

[66] V. Borecky, Implementace technologie GPR do soucasnych metod diagnostiky, University of Pardubice (2017).

[67] K. R. Maser, Condition Assessment of Transportation Infrastructure Using Ground-Penetrating Radar, J. Infrastruct. Syst., 2 (1996) pp. 94–101.

[68] R. Roberts, J. Rudy, S. GSSI, Railroad ballast fouling detection using ground penetrating radar. A new approach based on scattering from voids, ECNDT 2006–Th 45. 1 (2006).

[69] F. Fernandes, M.Pereira, A. Gomes Correia, P. Lourenço, L.Caldeira, Assessment of layer thickness and uniformity in railway embankments with ground penetrating radar, in: E. Ellis, N. Thom, H.-S. Yu, A. Dawson, G. McDowell (Eds.), Adv. Transp. Geotech., CRC Press (2008) pp. 571–575.

[70] T.R. Sussmann, E.T. Selig, J.P. Hyslip, Railway track condition indicators from ground penetrating radar, NDT E Int. 36 (2003) 157–167.

[71] S. Donohue, K. Gavin, A. Tolooiyan, Geophysical and geotechnical assessment of a railway embankment failure, Surf. Geophys. 9 (2011). doi:10.3997/1873-0604.2010040.

[72] R.M. Narayanan, J.W. Jakub, D. Li, S.E.G. Elias, Railroad track modulus estimation using ground penetrating radar measurements, NDT E Int. 37 (2004) 141–151. doi:10.1016/j.ndteint.2003.05.003.

[73] T. Saarenketo, M. Silvast, J. Noukka, Using GPR on railways to identify frost susceptible areas, Proc. Int. Conf. Exhib. Railw. Eng. 2003 held Lond. UK (2003).

[74] Z. Guo, H. Dong, J. Xiao, Detection of Permafrost Subgrade Using GPR: A Case Examination on Qinghai-Tibet Plateau, J. Geosci. Environ. Prot. 03 (2015) 35–47. doi:10.4236/gep.2015.35005.

[75] A. Nurmikolu, Key aspects on the behaviour of the ballast and substructure of

a modern railway track: research-based practical observations in Finland, J. Zhejiang Univ. Sci. A. 13 (2012) 825–835. doi:10.1631/jzus.A12ISGT1.

[76] L.Z. Du, X.P. Zhang, J.H. Qiu, W.B. Liu, Study on Ground Penetrating Radar in Detecting of Zero-Temperature Boundary under the Railway Bed, Adv. Mater. Res. 255–260 (2011) 3975–3978. doi:10.4028/www.scientific.net/AMR.255-260.3975.

[77] R.M. Maturana, B.D. Bautista, Á.A. Aguacil, M.R. Plaza, S.S. Castaño, Preventive Maintenance of Railway Infrastructures using GPR–Ground Penetrating Radar, in 9 th World Congress on Railway Research (2011).

[78] J. P. Hyslip, Substructure maintenance management – its time has come, in Proceedings of the AREMA Conference, Chicago, 9–12 September 2007.

[79] G.P. Gallagher, Q. Leiper, R. Williamson, M.R. Clark, M.C. Forde, The application of time domain ground penetrating radar to evaluate railway track ballast, NDT E Int. 32 (1999) 463–468.

[80] D. Carpenter, P.. Jackson, A. Jay, Enhancement of the GPR method of railway trackbed investigation by the installation of radar detectable geosynthetics, NDT E Int. 37 (2004) 95–103. doi:10.1016/j.ndteint.2003.06.003.

[81] G.R. Olhoeft, S. Smith, J.P. Hyslip, E.T. Selig, GPR in railroad investigations, in: Ground Penetrating Radar 2004 GPR, 2004 Proc. Tenth Int. Conf. On, IEEE (2004)

[82] I. Al-Qadi, W. Xie, R. Roberts, Optimization of antenna configuration in multiple-frequency ground penetrating radar system for railroad substructure assessment, NDT E Int. 43 (2010) 20–28. doi:10.1016/j.ndteint.2009.08.006.

[83] M. Silvast, M. Levomäki, A. Nurmikolu and J. Noukka, NDT Techniques in Railway Structure Analysis, Proceedings of 7th World Congress on Railway Research, 2006.

[84] I.L. Al-Qadi, W. Xie, R. Roberts, Scattering analysis of ground-penetrating

radar data to quantify railroad ballast contamination, NDT E Int. 41 (2008) 441–447. doi:10.1016/j.ndteint.2008.03.004.

[85] R. Roberts, I.L. Al-Qadi, E. Tutumluer, A. Kathage, Ballast fouling assessment using 2 GHz horn antennas-GPR and ground truth comparison from 238 km of track, in: 9th Int. Railw. Eng. Conf., (2007)

[86] H. Faghihi Kashani, Evaluating the Influence of Breakdown Fouling and Moisture Content on Mechanical and Electromagnetic Properties of Ballasted Railroad Track, University of Massachusetts Amherst (2017).

[87] L.J. Su, C. Rujikiatkamjorn, B. Indraratna, An Evaluation of Fouled Ballast in a Laboratory Model Track Using Ground Penetrating Radar, Geotech. Test. J. 33 (2010) 103045. doi:10.1520/GTJ103045.

[88] I.L. Al-Qadi, W. Xie, R. Roberts, Time-Frequency Approach for Ground Penetrating Radar Data Analysis to Assess Railroad Ballast Condition, Res. Nondestruct. Eval. 19 (2008) 219–237. doi:10.1080/09349840802015107.

[89] R. Roberts, I. Al-Qadi, E. Tutumluer, Track Substructure Characterization Using 500 MHz and 2 GHz Ground Penetrating Radar: Results from over 250 Miles of Track in Wyoming and Alaska, Urbana. 51 (n.d.) 61801.

[90] H.F. Kashani, C.L. Ho, C.P. Oden, S.S. Smith, Model Track Studies by Ground Penetrating Radar (GPR) on Ballast With Different Fouling and Geotechnical Properties, in: ASME, 2015: p. V001T01A006. doi:10.1115/JRC2015-5643.

[91] C. Göbel, R. Hellmann, H. Petzold, Georadar-model and in-situ investigations for inspection of railway tracks, in: 1994.

[92] R. Jack, P. Jackson, Imaging attributes of railway track formation and ballast using ground probing radar, NDT E Int. 32 (1999) 457–462.

[93] A. Lalagüe, Use of Ground Penetrating Radar for Transportation Infrastructure

Maintenance, Norwegian University of Science and Technology (2015).

[94] T.R. Sussman, Application of ground penetrating radar to railway track substructure maintenance management, University ofMassachusetts Amherst (1999).

[95] M. Clark, M. Gordon, M.C. Forde, Issues over high-speed non-invasive monitoring of railway trackbed, NDT E Int. 37 (2004) 131–139. doi:10.1016/j.ndteint.2003.05.002.

[96] Z. Khakiev, V. Shapovalov, A. Kruglikov, V. Yavna, GPR determination of physical parameters of railway structural layers, J. Appl. Geophys. 106 (2014) 139–145. doi:10.1016/j.jappgeo.2014.04.017.

[97] Z. Khakiev, V. Shapovalov, A. Kruglikov, A. Morozov, V. Yavna, Investigation of long term moisture changes in trackbeds using GPR, J. Appl. Geophys. 110 (2014) 1–4. doi:10.1016/j.jappgeo.2014.08.014.

[98] S. Shihab, O. Zahran, W. Al-Nuaimy, Time-frequency characteristics of ground penetrating radar reflections from railway ballast and plant, in: IEEE (2002) p. 8. doi:10.1109/HFPSC.2002.1088424

[99]   L. Bianchini Ciampoli, F. Tosti, M.G. Brancadoro, F. D'Amico, A.M. Alani, A. Benedetto, A spectral analysis of ground-penetrating radar data for the assessment of the railway ballast geometric properties, NDT E Int. 90 (2017) 39–47. doi:10.1016/j.ndteint.2017.05.005.

[100]   Benedetto, A., L. Bianchini Ciampoli., M.G. Brancadoro., A.M. Alani. and F. Tosti, (2017). A novel computer-aided model for the simulation of railway ballast by random sequential adsorption process, Computer- Aided Civil and Infrastructure Engineering - An International Journal.

[101]   M.G. Brancadoro, L.B. Ciampoli, C. Ferrante, A. Benedetto, F. Tosti, A.M. Alani, An Investigation into the railway ballast grading using GPR and image analysis,

in: Adv. Ground Penetrating Radar IWAGPR 2017 9th Int. Workshop On, IEEE, 2017: pp. 1–4.

[102]   L. Bianchini Ciampoli, F. Tosti, M.G. Brancadoro, F. D'Amico, A.M. Alani, A. Benedetto, A spectral analysis of ground-penetrating radar data for the assessment of the railway ballast geometric properties, NDT E Int. 90 (2017) 39–47. doi:10.1016/j.ndteint.2017.05.005.

[103]   G. R. Olhoeft, E. T. Selig, Ground-penetrating radar evaluation of railway track substructure conditions, in: 2002: pp. 4758–6. https://doi.org/10.1117/12.462264.

[104]   G. Manacorda, D. Morandi, A. Sarri, G. Staccone, Customized GPR system for railroad track verification, in: Ninth Int. Conf. Ground Penetrating Radar GPR2002, International Society for Optics and Photonics, (2002) pp. 719–723

[105]   A. Eriksen, B. Venables, J. Gascoyne, S. Bandyopadhyay, Benefits of high speed GPR to manage trackbed assets and renewal strategies, in: PWI Conf. (2006).

[106]   J.P. Xiao, Y.Q. Wang, L.B.Liu, "A Multiband-Pass Filter Method to Suppress Sleeper Noise in Railway Subgrade Vehicle-Mounted GPR Data, 16 th International Conference on Gr Penetrating Radar (GPR),Bruxelles, Belgium (2014).

[107]   S. Geraads, B. Charachon, O. Loeffler, G. Omnes, Applying a wavenumber notch filter to remove interferences caused by railway sleepers from a GPR section, in: Proc. SPIE - Int. Soc. Opt. Eng., (2002) pp. 715–718. doi:10.1117/12.462262.

[108]   L. Liao, X. Yang, P. Du, Processing GPR Detection Data of Railway Subgrade, China Railw. Sci. 03 (2008).

[109]   D.B. Zhu, J.N. Geng, M. Huang, Algorithm for suppressing sleeper interferences in railway subgrade GPR signals, J. China Railw. Soc. 5 (2013) 75–79. doi:10.3969/j.issn.1001-8360.2013.05.012.

[110]   K2 Fast Wave Software Data Acquisition User's Guide, IDS (2008)

[111] K.J. Sandmeier, Windows^{TM} 9x/NT/2000/XP/7-program for the processing of seismic, acoustic or electromagnetic reflection, refraction and transmission data, (1998).

[112] L. Pajewski, X. Derobert, S. Lambot, M. Vrtunski, Ž. Bugarinović, A. Ristić, M. Govedarica, C. Van Geem, A. van der Wielen, C. Grégoire, V. Borecky, S.S. Artagan, S. Fontul, V. Marecos, GPR system performance compliance, (2017).

[113] ASTM D6087-08, Standard Test Method for Evaluating Asphalt-Covered Concrete Bridge Decks Using Ground Penetrating Radar, ASTM International, West Conshohocken, PA 2008 ,http://dx.doi.org/10.1520/D6087-08 〈www. astm.org〉., (2008).

[114] ASTM D4748-10, Standard Test Method for Determining the Thickness of Bound Pavement Layers Using Short-Pulse Radar, ASTM International, West Conshohocken, PA 2010 ,http://dx.doi.org/10.1520/D4748-10 〈www.astm.org〉., (2010).

[115] ASTM D6432-11, Standard Guide for Using the Surface Ground Penetrating Radar Method for Subsurface Investigation, ASTM International, West Conshohocken, PA 2011 ,http://dx.doi.org/10.1520/D6432-11 〈www.astm.org〉., (2011).

[116] F. Benedetto, F. Tosti, A signal processing methodology for assessing the performance of ASTM standard test methods for GPR systems, Signal Process. 132 (2017) 327–337. doi:10.1016/j.sigpro.2016.06.030.

[117] EN 13242:2002+A1:2007 Aggregates for unbound and hydraulically bound materials for use in civil engineering work and road construction, (2002).

[118] E.Tutumluer, W. Dombrow, H. Huang, Laboratory Characterization of Coal Dust Fouled Ballast Behavior, AREMA2008 Annual Conference & Exposition September 21-24, (2008), Salt Lake City, UT (2008).

[119] Halabe, U. B., Sotoodehnia, A., Maser, K. R., Kausel, E., Modeling the Electromagnetic Properties of Concrete, ACI Mater. J. 90 (1993) 552–563.

[120] T.R. Sussmann, K.R. O'Hara, E.T. Selig, Development of material properties for railway application of ground-penetrating radar, in: Ninth Int. Conf. Ground Penetrating Radar, International Society for Optics and Photonics, 2002: pp. 42–48.

[121] Keogh, T, Keegan, T. R., "An integrated system for accurate tie and ballast condition assessment, in: 2006.

[122] Weather History for Pardubice, Czech Republic | Weather Underground, https://www.wunderground.com/history/airport/LKPD/2017/12/4/DailyHistory.html?req_city=Pardubice&req_state=PA&req_statename=%C3%87ek+Cumhuriyeti&reqdb.zip=00000&reqdb.magic=192&reqdb.wmo=11652.

[123] L. Le Pen, G. Watson, W. Powrie, G. Yeo, P. Weston, C. Roberts, The behaviour of railway level crossings: Insights through field monitoring, Transp. Geotech. 1 (2014) 201–213. doi:10.1016/j.trgeo.2014.05.002.

[124] J. G. Rose, The Behaviour of Railway Level Crossings: Insights Through Field Monitoring., Kentucky Transportation Center, College of Engineering, University of Kentucky, Lexington, KY 40506-0281, 2009.

[125] F. Tosti, A. Benedetto, A. Calvi, L. Bianchini Ciampoli, Laboratory investigations for the electromagnetic characterization of railway ballast through GPR, Conference: 2016 16th International Conference on Ground Penetrating Radar (GPR) (2016) doi 10.1109/ICGPR.2016.7572605

PUBLICATIONS OF THE PHD STUDENT ON THE DISSERTATION SUBJECT

Artagan S.S., Borecký V., "History of Using GPR for Diagnostics of Transport Structures", Proceedings of 6th International Scientific Conference, Pardubice, September 3rd – 4th, 2015.

Artagan S.S., Borecký V., "Applicability of GPR in Turkish Railways", Electronic Journal of Occupational Improvement and Research, Special Issue (pp.162-174), November 2015.

Artagan S.S., Borecký V., "Estimation Methods for Obtaining GPR Signal Velocity", International Journal of Civil and Structural Engineering, Vol: 3, Issue 1 (pp.59-63), 2016.

Artagan S.S., Borecký V., Incorporation of Materials' Attenuation Effect into the Relative Permittivity Calculations Using GPR, European Geosciences Union General Assembly 2017 EGU 2017), Geophysical Research Abstracts Vol. 19, EGU2017-2229, 23-28 April, 2017.

Pajewski L., Derobert X., Lambot S., Vrtunski M., Bugarinović Ž. Ristić A., Govedarica M., Van Geem C., van der Wielen A., Grégoire C., Borecky V., Artagan S.S., Fontul S, Marecos V., GPR system performance compliance, The Final Conference of COST Action TU1208 Action, Warsaw, Poland: 25th - 27th September, 2017.

Artagan S.S., Benedetto A., STSM 6: GPR Assessment of Railway Ballast in Pajewski L., (Ed.), Rodriguez-Abad, I. (Ed.), Marciniak M., (Ed.), Cost Action TU1208 civil engineering applications of ground penetrating radar: Short-Term Scientific Missions: Years 4 & 5 (pp. 51-85), TU1208 GPR Association, ISBN 9788888173085; DOI (ISBN-A): 10.978.8888173/085, Rome, Italy, January 2018.

Artagan S.S., Borecký V., Bartos J., Kurel R., Laboratory Determination of Variations in the Relative Permittivity Values of Railway Ballast under Various Fouling Levels Using 2 GHz GPR Horn Antenna, European Geosciences Union General Assembly 2018 (EGU 2018), Geophysical Research Abstracts Vol. 20, EGU2018-6286, 2018, 8–13 April 2018.

Bianchini Ciampoli L., Calvi A., Artagan S.S., Tosti F., Alani A.M., A GPR investigation of railway ballast for signal noise filtering of railway sleepers effects, European Geosciences Union General Assembly 2018 (EGU 2018), Geophysical Research Abstracts Vol. 20, EGU2018-15900, 2018, 8–13 April 2018.

Bianchini Ciampoli L., Artagan S.S., Tosti F., Alani, A.M., Benedetto, A., A Comparative Investigation of the Effects of Concrete Sleepers on the GPR Signal for the Assessment of Railway Ballast, 17th International Conference on Ground Penetrating Radar (GPR2018), during June 18–21, 2018 in Rapperswil, Switzerland (to be published on June 2018).

Bianchini Ciampoli, L., Artagan S.S., Tosti F., Calvi A., Alani A.M., Benedetto, A., A GPR spectral-based filtering for minimisation of concrete sleepers effects in railway ballast investigations, 41st International Conference on Telecommunications and Signal Processing (TSP – IEEE Conference Record #43564), during July 4-6, 2018 in Athens, Greece (to be published on July, 2018).

Borecky V., Frantisek H., Artagan S.S., Routil L., Analysis of GPR and FWD Data Dependency Based on Road Test Field Surveys, Materials Evaluation, (ISSN:0025-5327), ASNT American Society for Nondestructive Testing. (Under 2nd round of Review)

APPENDIX 1 Technical Sheet for Fine and Coarse Ballast

PROHLÁŠENÍ O VLASTNOSTECH

Podle nařízení evropského parlamentu a rady EU č. 305/2011 a zákona č. 22/1997 Sb. v platném znění

ϵ

1020

Výrobce
Granita s.r.o. V. Svobody 695
539 73 Skuteč, IČO 45270741
Provozovna : **CHVALETICE**
Systém posuzování a ověřování vlastností : 2+

13

1020-CPD-050012121

EN 13242+A1
Kamenivo pro nestmelené směsi a směsi stmelené
hydraulickými pojivy pro inženýrské stavby a pozemní komunikace

Článek	Základní charakteristiky	Vyjádření	Kategorie/ hodnota
4.2	Frakce kameniva	Označení d/D	**0/32 D**
4.3	Zrnitost	Tolerance/kategorie	G_A80
4.3.2	Mezní hodnoty a tolerance pro zrnitost HK	Kategorie	NPD
4.3.3	Tolerance pro typickou zrnitost DK a směsi	Kategorie	GT_A20
4.4	Tvar zrn hrubého kameniva	Kategorie	NPD
4.5	Podíl ostrohranných a oblých zrn v HK	Kategorie	NPD
4.6	Obsah jemných částic	Kategorie	f_{12}
5.2	Odolnost proti drcení hrubého kameniva	Kategorie	LA_{50}
5.3	Odolnost hrubého kameniva proti otěru	Kategorie	NPD
5.4	Objemová hmotnost	Deklarovaná hodnota	2,63 Mg/m³
-	Stanovení sypné hmotnosti	Deklarovaná hodnota	1,55 Mg/m³
5.5	Nasákavost	Deklarovaná hodnota	$WA_{24} \leq 2$ % hm.
6.2	Sírany rozpustné v kyselině	Kategorie	$AS_{0,2}$
6.3	Celková síra	Kategorie	S_1
6.5.1	Obsah humusovitých částic	Vyhovuje/nevyhovuje	Vyhovuje
7.3	Odolnost proti zmrazování a rozmrazování	Kategorie	F_4
9.1	Druh kameniva	Petrografický název	Žula
8.2	Obsah přírodních radionuklidů	Vyhovuje/nevyhovuje	Vyhovuje

Ve Skutči dne 1.července 2013 GRANITA s.r.o.
Villibalda Svobody 695
539 73 SKUTEČ ⑧
DIČ: CZ45270741

Ing. František Flídr
jednatel společnosti

ES PROHLÁŠENÍ O SHODĚ

$C\epsilon$

1020

Granita s.r.o. V. Svobody 695
539 73 Skuteč, IČO 45270741
Provozovna : **ŽUMBERK**

13
1020-CPD-050012127
EN 13242+A1
Kamenivo pro nestmelené směsi a směsi stmelené
hydraulickými pojivy pro inženýrské stavby a pozemní komunikace

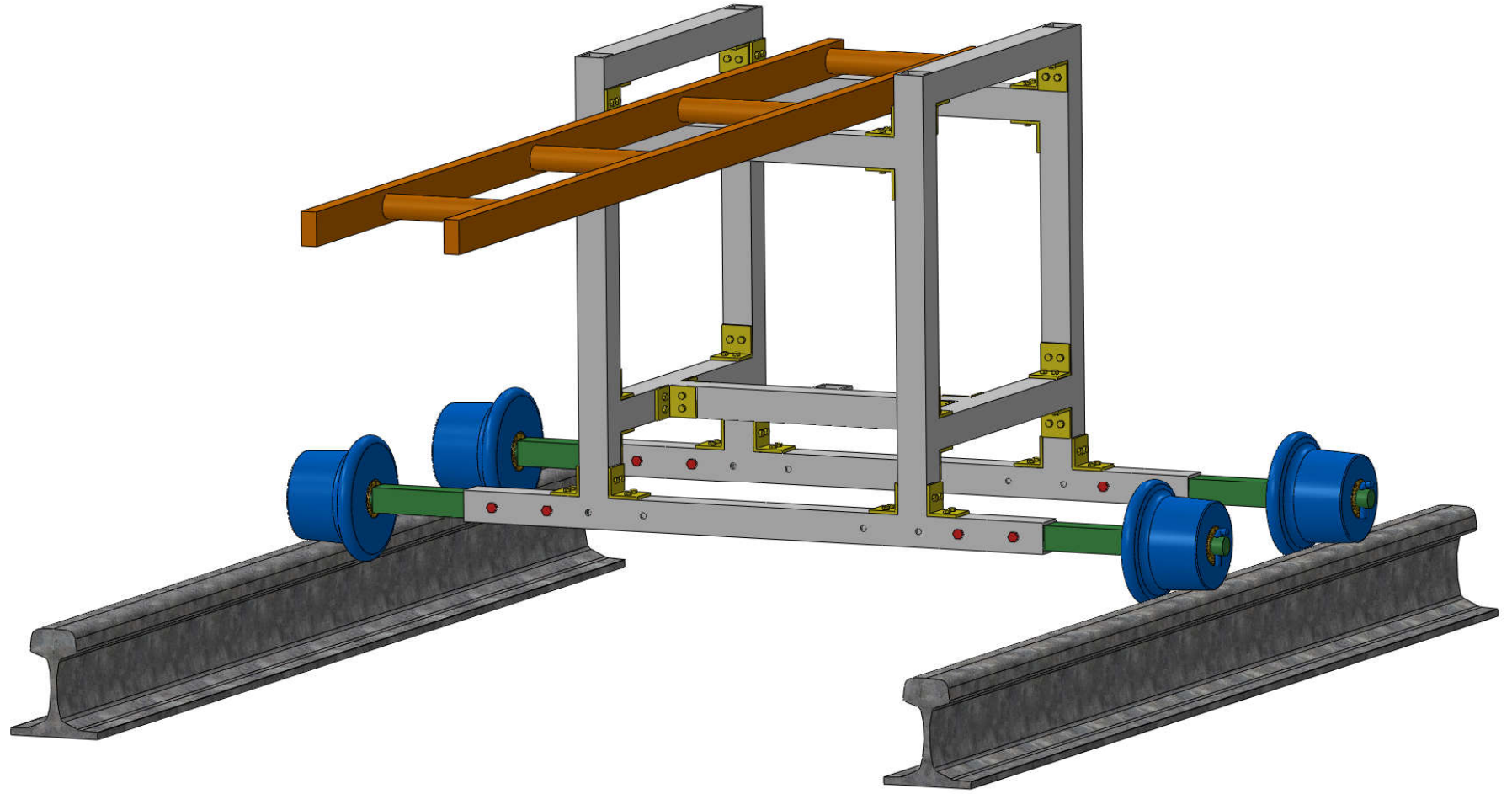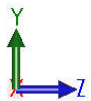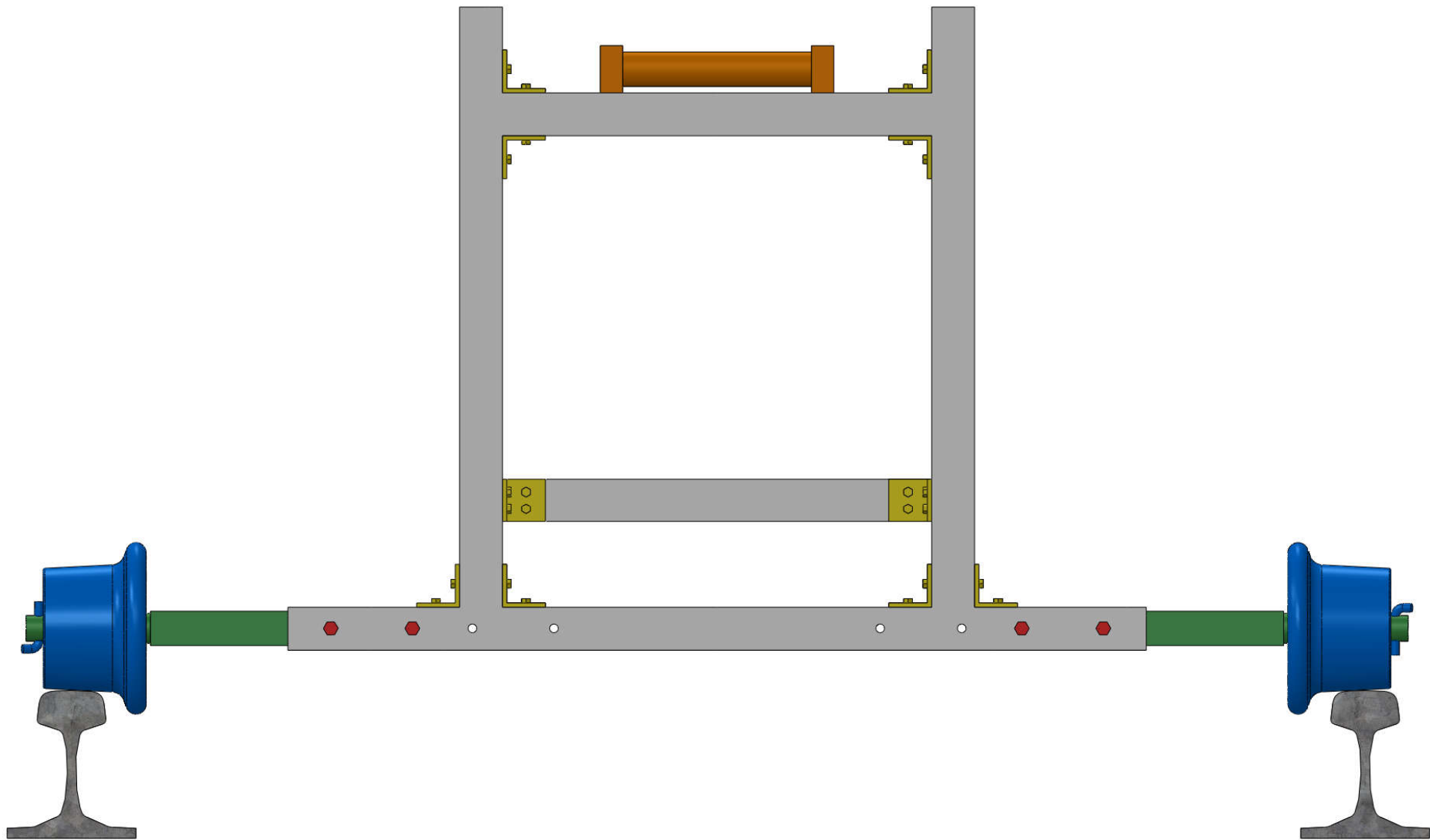| Článek	Základní charakteristiky	Vyjádření	Kategorie/hodnota
4.2	Frakce kameniva	Označení d/D	**32/63 C**
4.3	Zrnitost	Tolerance/kategorie	G_c85-15
4.3.2	Mezní hodnoty a tolerance pro zrnitost HK	Kategorie	$G_{TC}25/15$
4.3.3	Tolerance pro typickou zrnitost DK a směsi	Kategorie	NPD
4.4	Tvar zrn hrubého kameniva	Kategorie	SI_{40}
4.5	Podíl ostrohranných a oblých zrn v HK	Kategorie	NPD
4.6	Obsah jemných částic	Kategorie	f_4
5.2	Odolnost proti drcení hrubého kameniva	Kategorie	LA_{30}
5.3	Odolnost hrubého kameniva proti otěru	Kategorie	NPD
5.4	Objemová hmotnost	Deklarovaná hodnota	$2,75\ Mg/m^3$
-	Stanovení sypné hmotnosti	Deklarovaná hodnota	$1,29\ Mg/m^3$
5.5	Nasákavost	Deklarovaná hodnota	WA_{24}
6.2	Sírany rozpustné v kyselině	Kategorie	$AS_{0,2}$
6.3	Celková síra	Kategorie	S_1
6.5.1	Obsah humusovitých částic	Vyhovuje/nevyhovuje	NPD
7.3	Odolnost proti zmrazování a rozmrazování	Kategorie	F_2
9.1	Druh kameniva	Petrografický název	Žula
8.2	Obsah přírodních radionuklidů	Vyhovuje/nevyhovuje	Vyhovuje

Výrobek splňuje základní požadavky podle NV č. 190 / 2002 Sb. ve znění pozdějších předpisů.

GRANITA s.r.o.
Vilibalda Svobody 695
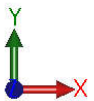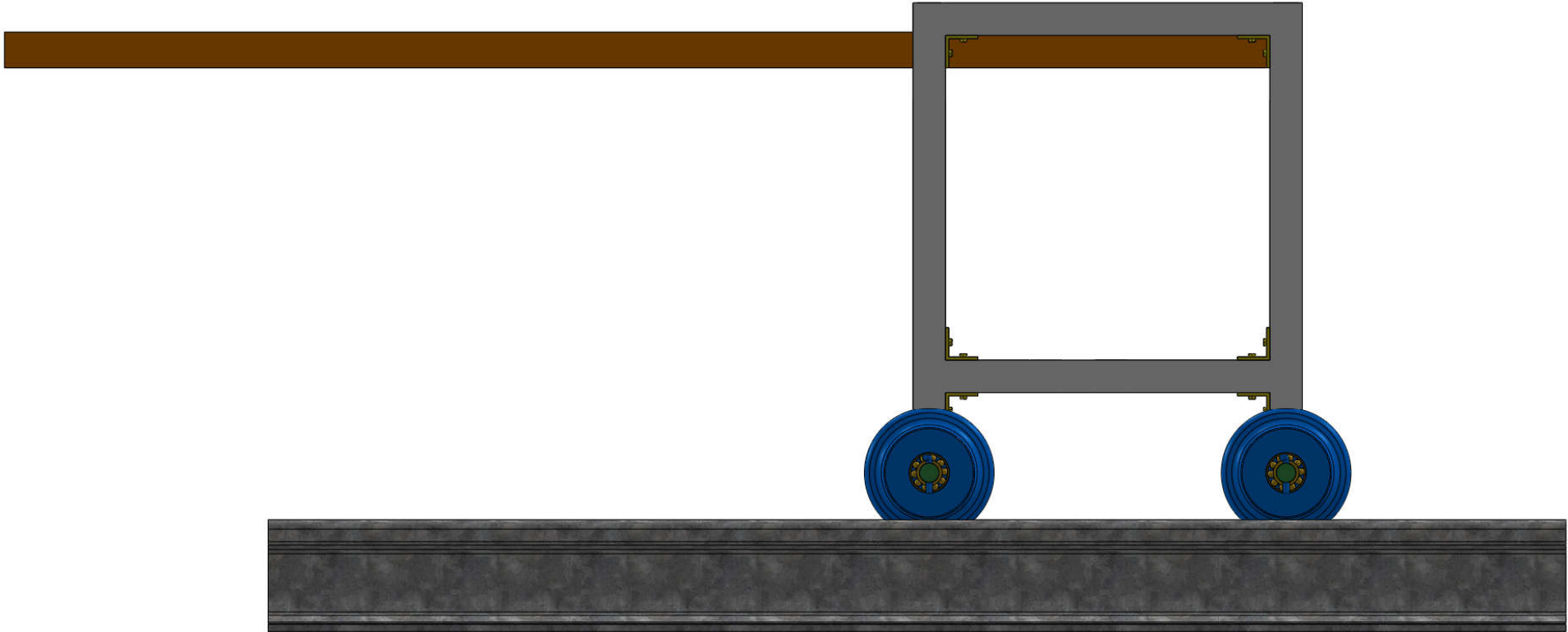539 73 S K U T E Č ③
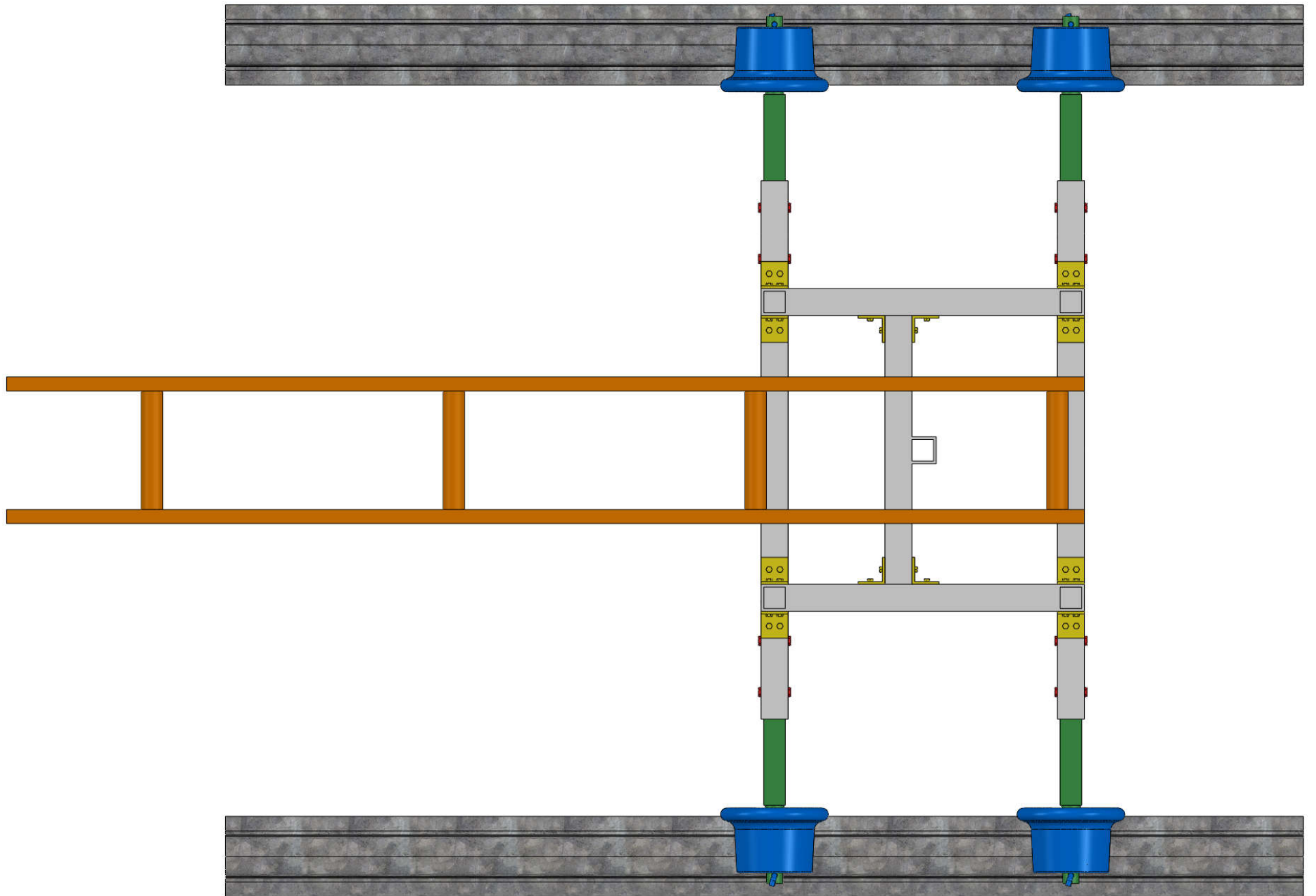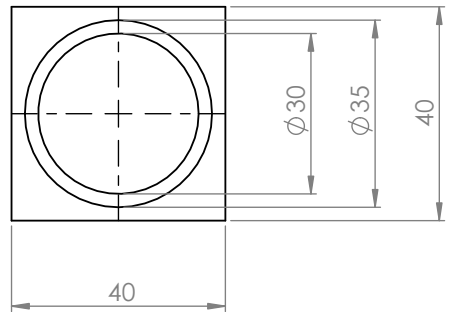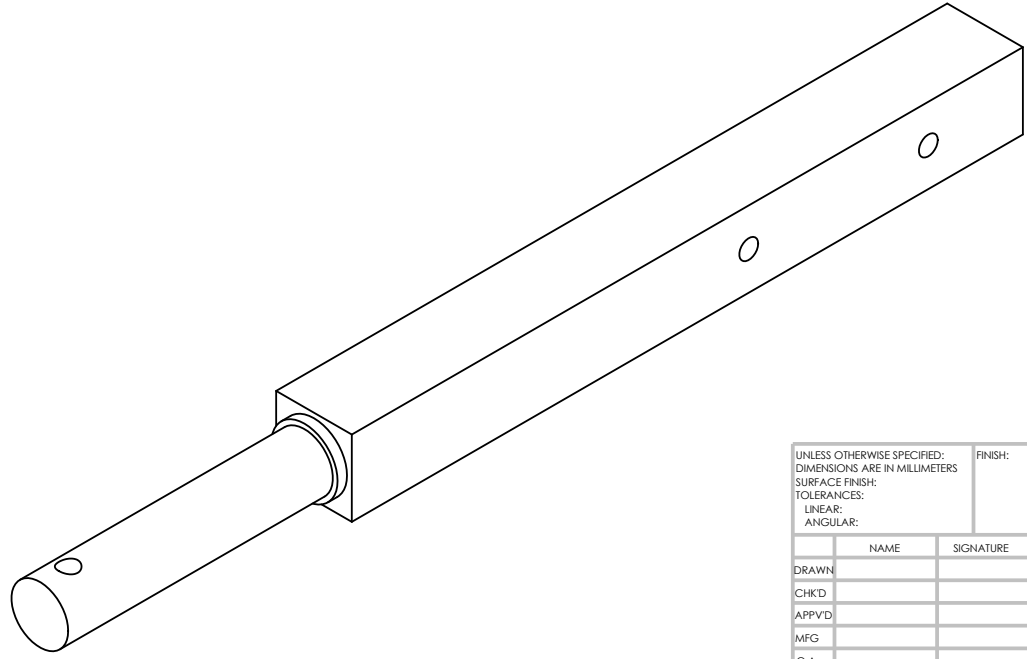DIČ: CZ45270741

Ing. František Flídr
jednatel společnosti

Skuteč 10.1.2013

APPENDIX 2 The detailed design drawings of Railway Cart Constructed for Field Surveys

95

50

Ø35
Ø30

40

5

355

500

Ø10

Ø30
Ø35

40

40

	NAME	SIGNATURE	DATE				TITLE:	
DRAWN								
CHK'D								
APPV'D								
MFG								
Q.A				MATERIAL:			DWG NO.	

wheel shaft

A3

WEIGHT:

SCALE:1:2

SHEET 1 OF 1

APPENDIX 3 The Core Data File used in ReflexW

CORE 1 - dist.dim: METER, vel.dim: m/ns

54.25 0.00 0.00

1 0.31 1 0.1675 0.1675

CORE 2 - dist.dim: METER, vel.dim: m/ns

65.67 0.00 0.00

1 0.28 1 0.1675 0.1675

CORE 3 - dist.dim: METER, vel.dim: m/ns

70.48 0.00 0.00

1 0.30 1 0.1675 0.1675

2 0.24 1 0.16 0.16

CORE 4 - dist.dim: METER, vel.dim: m/ns

75.01 0.00 0.00

1 0.29 1 0.1675 0.1675

2 0.23 1 0.16 0.16

CORE 5 - dist.dim: METER, vel.dim: m/ns

92.84 0.00 0.00

1 0.28 1 0.1675 0.1675

2 0.23 1 0.16 0.16

3 0.21 1 0.150 0.150

CORE 6 - dist.dim: METER, vel.dim: m/ns

98.40 0.00 0.00

1 0.27 1 0.1675 0.1675

2 0.26 1 0.16 0.16

CORE 7 - dist.dim: METER, vel.dim: m/ns

106.20 0.00 0.00

1 0.30 1 0.1675 0.1675

CORE 8 - dist.dim: METER, vel.dim: m/ns

117.05 0.00 0.00

1 0.28 1 0.1675 0.1675

CORE 9 - dist.dim: METER, vel.dim: m/ns

124.20 0.00 0.00

1 0.39 1 0.145 0.145